2024-03-28

The Effect of Oxygen Treatment in the EAE Mouse Model

Ohaezukosi, Uche Joan

UNIVERSITY OF CALGARY

The Effect of Oxygen Treatment in the EAE Mouse Model

by

Uche Joan Ohaezukosi

A THESIS
SUBMITTED TO THE FACULTY OF GRADUATE STUDIES
IN PARTIAL FULFILMENT OF THE REQUIREMENTS FOR THE
DEGREE OF MASTER OF SCIENCE

GRADUATE PROGRAM IN NEUROSCIENCE
CALGARY, ALBERTA

MARCH, 2024

ABSTRACT

Multiple sclerosis (MS) is a lifelong disease that affects over two million people worldwide. MS disease has been linked to inflammation, which results in an autoimmune response. This can result in symptoms that drastically reduce the quality of life and independence of people with this disease. Symptoms can include vision problems, cognitive decline, fatigue, and difficulties with physical movement. Hypoxia has been reported in some people living with MS. This condition occurs when oxygen levels are relatively low and might negatively affect brain function. Hypoxia can worsen inflammation, leading to a vicious cycle of damage. This study highlighted the potential of MRI techniques such as ASL, T_2*, and QSM to evaluate the effects of NBOT on MS and emphasize the importance of clinical scores in evaluating the effects of treatments on MS. This thesis employed a 6-hour duration of normobaric (100%) oxygen treatment (NBOT) for 5 days and investigated its effect on cerebral blood flow, hypoxia markers, and disease clinical score in the EAE MS mouse model using an in vivo Magnetic Resonance Imaging and open-field test. A 15-point clinical grading scale was used to track disability progressions. While NBOT didn't improve CBF and hypoxia, the clinical score was significantly improved in the treated EAE. This is promising and needs further investigation. This study suggests that NBOT may positively affect clinical scores in the EAE. This is consistent with previous research that demonstrated the effects of NBOT in reducing neurological deficits in the EAE spinal cord. The study also added to the growing body of research on the use of MRI techniques in brain disorders. Further research is needed to confirm these findings and to determine the optimal treatment approach. evaluate the effects of NBOT on MS. It emphasized the importance of clinical scores in evaluating the effects of treatments on MS. The results of this study may have implications for developing new treatments for MS and other neurological conditions.

ACKNOWLEDGMENTS

I extend my deepest gratitude to my supervisor, Dr. Jefferey Dunn. His expertise, dedication, and patience throughout this journey have been remarkable. His feedback and constructive criticism have immensely enriched the quality of this thesis.

I am also thankful to the members of my thesis committee; Dr. Bruce Pike and Dr. Hedwich Kuipers. Their contributions and insights improved the quality of this project. Also, I extend my gratitude to my examiner, Dr. Carlos Camara-Lemarroy.

To Dunn lab members; Dr. Ying Wu, Dr. Dami Adingupu, Dr. Mada Hashem, Joel Burma, Ibukun Oni, Ty Makarowski, Aty Soroush, Racheal Steele, Qandeel Shafqat, Abby Palset; our MRI guys, Dave Rushforth and Tad Foniok. Not left out are Rania Muhammed and Rehman Tarig. All your support was felt and appreciated.

Lastly, to my family; my dad, my husband, my only sister Nneka, and friends; Janet, Margret, Kabirat, and Ijeoma for their love, support, and encouragement.

TABLE OF CONTENTS

PREFACE

Chapter 1: Provides a general introduction and literature review. Topics include multiple sclerosis (MS), experimental autoimmune encephalomyelitis (EAE) animal models of MS, magnetic resonance imaging (MRI), and oxygen treatment in the EAE and MS.

Chapter 2: Experimental method and data chapter investigating the effect of oxygen treatment on cerebral blood flow (CBF) in the EAE model.

Chapter 3: Experimental method and data chapter investigating the effect of oxygen treatment on hypoxia in the EAE model.

Chapter 4: Experimental data chapter investigating the effect of oxygen treatment on EAE disease score and motor function in the EAE model.

Chapter 5: General discussion chapter. This chapter describes the progression of this thesis and major findings, as well as limitations and future directions.

LIST OF FIGURES

FIGURE NO. DESCRIPTION OF FIGURES PAGE

LIST OF TABLES

LIST OF ABBREVIATIONS

Abbreviations	Definitions
ASL	Arterial Spin Labeling
BBB	Blood-Brain Barrier
CBF	Cerebral Blood Flow
CFA	Complete Freund's adjuvant
CIS	Clinically Isolated Syndrome
CNS	Central Nervous System
EAE	Experimental Autoimmune Encephalomyelitis
GM	Gray Matter
HBOT	Hyperbaric Oxygen Therapy
MOG	Myelin Oligodendrocyte Glycoprotein
MRI	Magnetic Resonance Imaging
MS	Multiple Sclerosis
NBOT	Normobaric Oxygen Therapy
pwMS	People with Multiple sclerosis
PTX	Pertussis toxin
QSM	Quantitative Susceptibility Mapping
RRMS	Relapsing-remitting Multiple Sclerosis
SPMS	Secondary Progressive Multiple Sclerosis
R_2*	Relaxation Rate
T_2*	Transverse Relaxation

CHAPTER ONE:
INTRODUCTION AND LITERATURE REVIEW

1.1 Multiple Sclerosis

Multiple sclerosis (MS) is a chronic inflammatory disorder affecting the central nervous system (CNS) (Filippi et al., 2018; McGinley et al., 2021). It was estimated that, in 2011, 97,300 Canadians had MS (Gilmour et al., 2018). MS has been proposed to affect more women than men (McGinley et al., 2021). In 2018, the prevalence in Canada was reported to be 159 in men and 418 in women per 100,000 population (Gilmour et al., 2018). Motor, sensory, visual, and autonomic systems are impacted by this disease (Doshi & Chataway, 2016). The decreased motor function in MS was associated with a decrease in sensory function (Alenazy et al., 2021). People with MS (pwMS) experience a wide range of significant and disabling symptoms, such as fatigue, cognitive impairment, bladder dysfunction, pain, and spasticity (Almuklass et al., 2020; Doshi & Chataway, 2016). The early symptoms of this disease include unilateral optic neuritis, partial myelitis, sensory disruptions, or brainstem syndromes like internuclear ophthalmoplegia (McGinley et al., 2021). However, the sequence of events that initiate the disease remains unclear (Noseworthy et al., 2000).

The diagnosis of MS involves the use of the 2017 McDonald criteria, which require evidence of damage to the CNS that is disseminated in time and space (Thompson et al., 2018). Early diagnosis of MS involves the combination of clinical isolated syndrome (CIS), MRI scans, and cerebrospinal fluid analysis (McGinley et al., 2021). The key requirements for a diagnosis of MS include evidence of lesions disseminated in both time and space. Dissemination in "space" requires the presence of clinical evidence of at least two lesions, or a lesion with evidence of a prior attack in the CNS which can be demonstrated by the presence of two or more attacks and corresponding

MRI findings, or by a minimum of one-year disease progression with at least two specific indicators. The concept of "dissemination in time" in the 2017 McDonald criteria involves the presence of at least two attacks separated by a period of at least one month, the simultaneous presence of gadolinium-enhancing and non-enhancing lesions at any time, the appearance of a new T2/gadolinium-enhancing lesion on follow-up MRI, and CSF oligoclonal bands analysis (Thompson et al., 2018). Diagnosis may be indicated by the individual patient symptoms and the temporal progression of the clinical findings (Noseworthy et al., 2000). Early detection of this illness is crucial, especially considering the emergence of new disease-modifying drugs (McGinley et al., 2021), that offer potential neuroprotective benefits (O'Riordan et al., 1998).

Research findings have shown that pwMS experience poor quality of life due to comorbidity, which can lead to a significantly shorter life expectancy (Chou et al., 2020; Marrie et al., 2015). This could be due to a lack of basic understanding of how to protect the brain from additional injury after an immunological response (Dore-Duffy et al., 2011). Thus, using knowledge of MS pathophysiology, either from preclinical or clinical studies could guide research into novel treatments (Criste et al., 2014), that will help improve the quality of life in pwMS.

1.2 MS Disease Course

There is a wide range of variability for the onset of MS across individuals. The majority of pwMS experience an acute episode of CNS dysfunction, involving optic nerve injury, and brainstem impairment (O'Riordan et al., 1998). Some individuals who experience these symptoms subsequently develop additional episodes that align with the CIS (O'Riordan et al., 1998) pwMS experience CIS as their first episode and have a higher likelihood of experiencing repeated

occurrences of the same illness within a period of ten years (O'Riordan et al., 1998). This increased risk is associated with the development of a second demyelinating event within the first year of the initial episode (Mowry et al., 2009).

MS occurs as one of four main traditional phenotypes which include, CIS, relapsing-remitting, primary progressive, and secondary progressive (Lublin, 2014; Stys et al., 2012). CIS refers to the first episode of neurological symptoms caused by inflammation and demyelination. Relapsing-remitting MS (RRMS) is the most common MS phenotype (**Figure 1**) characterized by a disease onset at the beginning, followed by a relapse, marked with neurological disability (Lublin et al., 2003). Secondary progressive MS (SPMS) is marked by a continuous increase in neurological disability after a relapse phase, accompanied by evidence of ongoing inflammatory activity (McGinley et al., 2021).

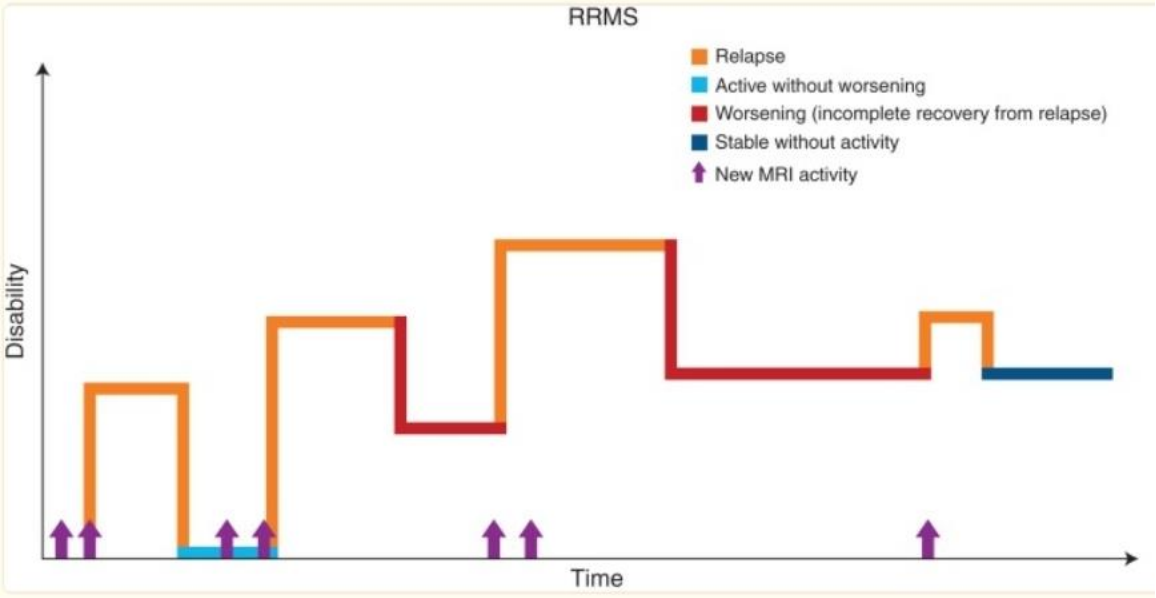

Figure 1: Disease course of relapsing-remitting MS.

Adapted from (Lublin et al., 2003).

Approximately 90% of RRMS progress into SPMS 20 years after disease onset (Rovaris et al., 2006). The mechanism underlying this transition toward a progressive phase remains unclear (Rovaris et al., 2006). Neuroimaging and immunology studies revealed that it may be due to neurodegeneration triggered by inflammation (Rovaris et al., 2006). This phase may involve the infiltration of pro-inflammatory cells in the CNS, initiating a clinical attack (Weiner, 2008). SPMS (**Figure 2**) involves a certain level of ongoing inflammation, although not as pronounced as in RRMS, along with neurodegeneration triggered by mitochondrial dysfunction and axonal insult (Klineova & Lublin, 2018). The peripheral innate immune cells such as dendritic cells, macrophages, and natural killer cells, are recognized to play an important role in mediating the progressive phase. Irregularities in the activation or maturation of dendritic cells and the release of interleukin-12 from dendritic cells, a component of the innate immune system, might be responsible for a shift towards RRMS to SPMS (Weiner, 2008).

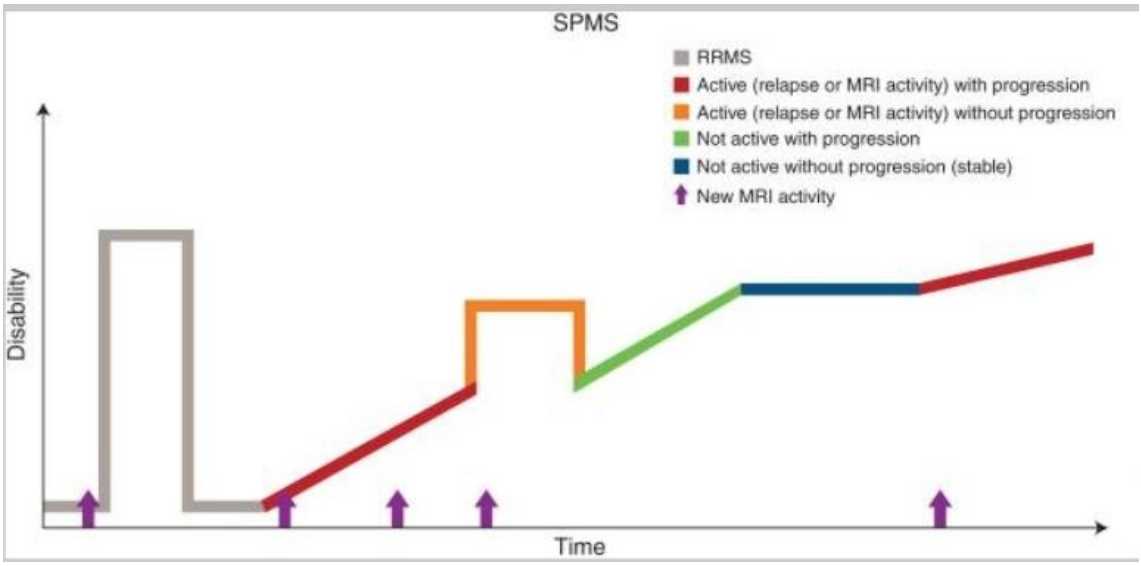

Figure 2: Disease course of secondary progressive MS.

Adapted from (Lublin et al., 2003).

In primary progressive MS (PPMS), about 10-20% of pwMS will develop this phenotype. PPMS is marked by the absence of the initial relapsing-remitting phase and a continuous progression from the disease onset (**Figure 3**) (Lublin et al., 2003). Also, the PPMS phenotype experiences a progressive increase in disability in the early phase due to spinal cord involvement (Weiner, 2008).

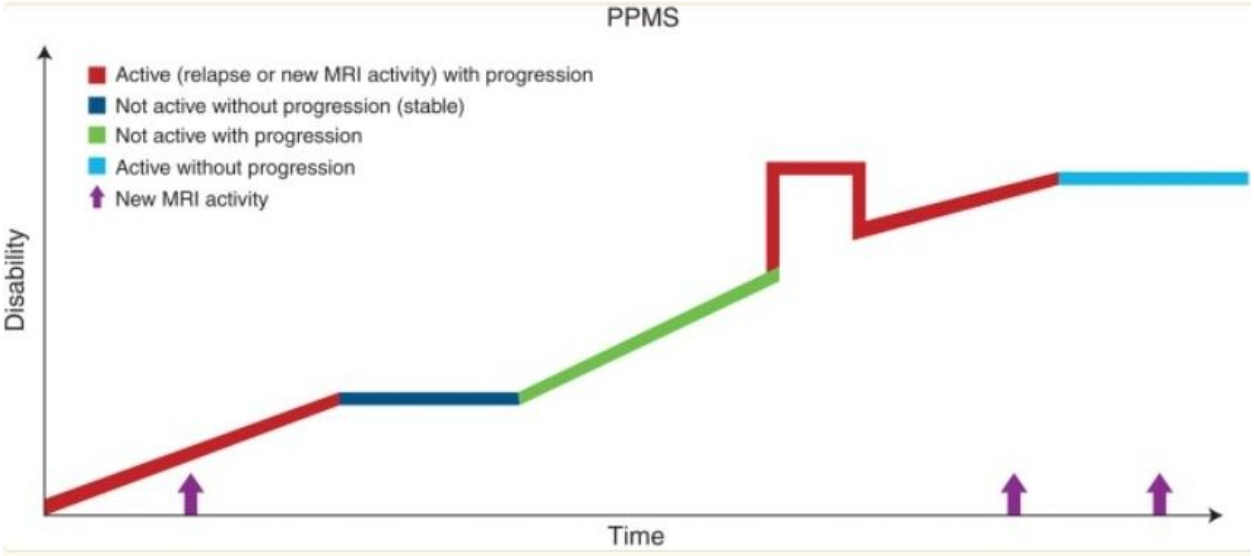

Figure 3: Disease course of primary progressive MS.

Adapted from (Lublin et al., 2003).

MS can be further classified as either active or inactive. Active MS is defined as clinical relapse or the appearance of new MRI lesions. This characterization is based on the rate of clinical relapse and image findings (Lublin, 2014). Also, radiologically isolated syndrome (RIS) is characterized by demyelination with the absence of clinical episode (Barboza et al., 2021), and cannot be considered a distinct MS phenotype (Barboza et al., 2021; Lublin, 2014). However, the CIS mentioned earlier is an established MS disease course (Klineova & Lublin, 2018).

1.3 MS Pathology

Studies have shown that both genetic and environmental factors increase the susceptibility to developing MS (Ramagopalan et al., 2010). Human leukocyte antigen has been linked to MS (Naito et al., 1972). In genetic factors, 2 - 4% of siblings of individuals affected by MS have a risk of developing the disease that is 10 to 20 times higher than that of the general population, with monozygotic twins facing an even greater risk of about 30% (Sadovnick & Baird, 1988; Willer et al., 2003). Conversely, the relative risk does not reach 100% even in identical twins, this suggests that factors beyond DNA (deoxyribonucleic acid) sequence identity must also be involved in creating the conditions that cause immune dysregulation associated with MS. While genetic influences are always present in MS patients, they are not sufficient on their own to trigger the disease. Environmental and lifestyle factors that increase the risk of MS include exposure to tobacco smoke, Epstein–Barr virus infection, and obesity (Olsson et al., 2017). These factors can interact with MS risk genes, providing strong evidence of their influence on the disease (Olsson et al., 2017; Waubant et al., 2019).

However, there is more than one pathogenetic mechanism of MS that may contribute to tissue injury due to its clinical, genetic, MRI, and pathological heterogeneity (Noseworthy et al., 2000). MS is characterized by multifocal demyelinating lesions in the CNS, leading to myelin loss and the formation of astrocytic scars (Lassmann, 2013). Demyelination has been proposed to play a role in neurological deficits (Noseworthy et al., 2000). (Noseworthy et al., 2000). Additionally, there are two proposed hypotheses known as “outside-in” and “inside-out” model. The “outside-in” model proposed that the initial trigger of MS is an abnormal immune response against the CNS (McFarland & Martin, 2007). However, the alternate hypothesis; “inside-out” **(Figure 4)** proposed that MS is primarily a degenerative disease caused by the intrinsic degeneration of CNS cells,

which triggers an autoimmune response only as a secondary reaction in predisposed individuals (Stys, 2010).

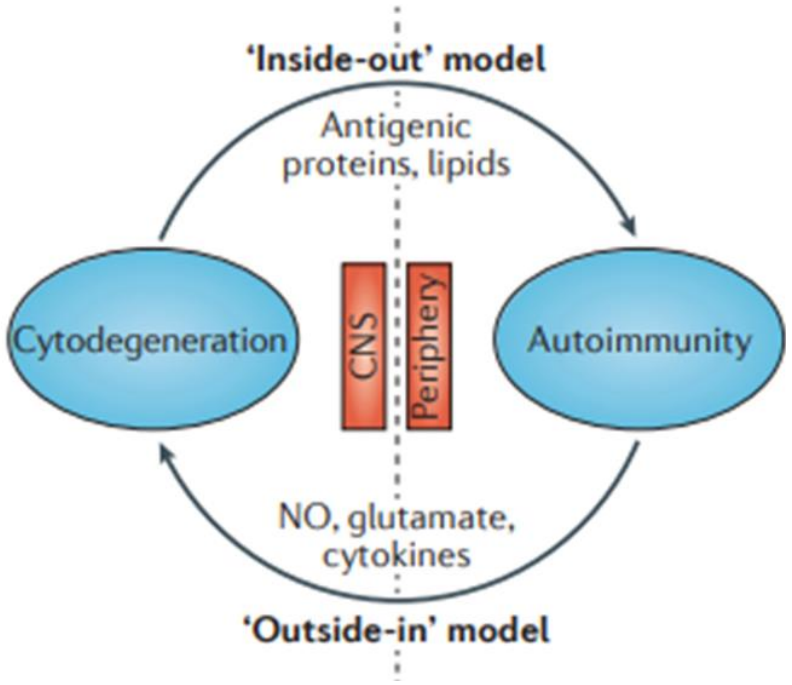

Figure 4: The two competing hypothetical causes of MS.

Adapted from (Stys et al., 2012).

Increasing evidence has shown that the inflammatory nature of MS disease is founded on the premise that the pathophysiology of MS originates from immune dysregulation. This notion aligns with the "outside-in" and “inside-out” model, suggesting that there is a systemic dysfunction of the immune system that specifically targets the CNS (Stys et al., 2012). Two recent studies by (Titus et al., 2020) and (Sen et al., 2020) provided an overview of these models. The first study suggested that both paradigms can occur due to the complex nature of MS disease. This implies

that multiple paradigms may be involved in MS autoimmunity due to its complex nature, while the second study supported the "inside out model" with the cuprizone model as the leading cause of MS autoimmunity.

While the pathologic features of MS, such as extensive axonal loss, cognitive impairment, and white matter plagues, have been well documented, the cause of MS remains unclear, and more effective treatments are needed (Noseworthy et al., 2000).

1.4 Brain Inflammation

Chen et al. (2018) defined brain inflammation as a natural reaction of the immune system that can be initiated by various factors, such as pathogens, injured cells, and harmful substances. Nevertheless, persistent and unregulated inflammation has demonstrated its causational role in tissue damage and has been implicated in the development of chronic diseases (Chen et al., 2018). Additionally, inflammation causes damage to the blood-brain barrier (BBB) and can lead to a detrimental neurological outcome (Candelario-Jalil et al., 2022). The EAE model mimics this form of inflammation resulting from insult in the CNS. This disease model disrupts the cellular integrity of the BBB which triggers immune cells to access the BBB, contributing to disease outcomes (Tietz & Engelhardt, 2019).

1.5 Animal Models of MS

Both neuroinflammation and hypoxia have been demonstrated in the EAE MS model (Johnson et al., 2016). However, the underlying mechanisms of how they originate are not well understood. Various animal models have been developed to study MS; each of these models have their strengths and limitations. The most commonly used animal model for MS is the EAE model,

which involves inducing an autoimmune response in animals with myelin oligodendrocyte glycoprotein (MOG) in complete Freund's adjuvant (CFA). This will cause inflammation in the CNS, similar to what is seen in human MS.

To understand the chronic progressive form of MS, Theiler's murine encephalomyelitis virus (TMEV) model was used (Pike et al., 2022). This model involves infecting rodents with the TMEV virus, causing an immune response that will damage the myelin in the central nervous system. Another alternative way to study demyelination in animals is using the cuprizone model. This involves animals being fed with a diet of cuprizone, a copper-chelating agent that causes demyelination in the CNS. Some researchers also use non-human primate models such as monkeys, to study MS (Kauppinen et al., 2005; t Hart et al., 2004). Primate models allow for more complex behavioral and cognitive testing than is possible with rodents.

This thesis focuses on the inflammation/hypoxia component that occurs in pwMS and the EAE model. EAE has been a useful animal model for studying MS and testing potential treatments because it produces similar pathological features as seen in MS, including inflammation (Cris S. Constantinescu et al., 2011). More so, EAE has been extensively studied and has many protocols available for inducing disease in rodents, making it easy to reproduce in the labs and compare results across studies.

The study of inflammatory and demyelinating encephalopathy models in rodents is targeted toward learning important information about the pathogenic mechanisms of MS. These models are valuable tools for developing and evaluating therapeutic approaches before applying them in human subjects/patients. EAE can be triggered in several animal species, but mice and rats are commonly preferred due to their widespread availability, cost-effectiveness, and ease of genetic manipulation.

1.6 The Use of Experimental Autoimmune Encephalomyelitis in MS Research

The EAE disease manifests as ascending flaccid paralysis, beginning with weakness in the tail, 7-14 days post-induction, and progressing to paralysis of the hind limbs in most susceptible rodent strains. In severe cases, it might prompt forelimb loss of motion and death (Amatruda et al., 2023). EAE is a T-cell-mediated autoimmune disease that causes the CNS myelin to be recognized as an exogenous antigen. The use of this model is common and likely that activated myelin-specific CD4+ T lymphocytes produced following active immunization with myelin-derived proteins trigger an immune cascade (Robinson et al., 2014). This model has been a valuable tool for investigating the pathogenesis of MS and for exploring potential therapeutic strategies. The model's significance lies in its ability to simulate the immune processes involved in MS and to study the effects of various treatment interventions (Mansilla et al., 2021)

EAE is induced either by active or passive induction. Passive EAE is induced via the administration by the adoptive transfer of activated myelin-specific T cells into experimental animals (Amatruda et al., 2023; Stromnes & Goverman, 2006b). On the other hand, active EAE is induced via immunization of myelin antigen in adjuvant priming an autoimmune response in which reactive T-cells enter the CNS, and cause myelin damage (Amatruda et al., 2023; Stromnes & Goverman, 2006a). Many aspects of the acquired immune system play a significant role in active EAE.

More so, the CNS structural damage, including demyelination and degeneration, is frequently accompanied by noticeable inflammation in active EAE (Amatruda et al., 2023). Ascending paralysis of the tail and hind limbs is seen in both passive and active EAE immunization (Mannara et al., 2012). Researchers choose passive EAE when studying the effect of inflammation

in its relative isolation. Its advantages over the active EAE are due to its immunological and pathological simplicity (Amatruda et al., 2023).

Although autoimmune-mediated models of CNS inflammation exist for both active and passive EAE, it is unclear whether these models accurately represent MS (Amatruda et al., 2023). Moreover, preclinical research has demonstrated that active EAE is a complex condition in which the immune-mediated and neurodegenerative mechanisms mimic MS disease pathology, including inflammation, demyelination, axonal loss, and gliosis (Constantinescu et al., 2011). The pathogenesis, sensitivity, and clinical course of EAE can be affected by various factors, including the animal's genetic susceptibility, species, age, and gender, as well as the preparation, dose, and route of administration of the immunogen (Mannie et al., 2009b). However, while no MS animal model reflects the entire human disease pathological spectrum, active EAE exhibits neurological, immunological, and histopathological similarities to MS (Hohlfeld & Wekerle, 2001).

The use of EAE in understanding autoimmune, inflammation, and treatment in MS has been reported (Robinson et al., 2014). Notably, some of the therapeutic interventions for pwMS were developed, examined, and demonstrated on the premise of EAE studies (C. S. Constantinescu et al., 2011). Understanding how inflammation affects the function of the nervous tissue may result in treatment options not only for MS patients but also for other neuroinflammatory disorders (Desai & Smith, 2017; Dore-Duffy et al., 2011).

1.7 The Use of MRI in MS Diagnosis and Monitoring

The use of MRI in MS diagnosis has significantly impacted on understanding and management of the disease (Miller et al., 1998). MRI is a non-invasive tool for diagnosing and monitoring the efficiency of treatments (Miller et al., 1998). It offers data that can be analyzed and examines the progression of pathological features (Miller et al., 1998). This allows for the

identification of the pathology associated with the root cause of MS disease, followed by a histopathology examination (Kramer et al., 2019). MRI is a sensitive imaging modality for detecting inflammatory and demyelinating lesions, which are important for determining a clinical diagnosis of MS and assessing treatment options (Haacke et al., 2021; Prinz et al., 2021). MRI has been utilized to track MS progression as it enabled a quick and sensitive assessment of treatment outcomes, particularly in the early stages of relapsing-remitting and secondary disease (Miller et al., 1998).

MRI is a useful tool in diagnosis and monitoring treatment outcomes, with a focus on identifying regions with T2 (transverse relaxation) signal alterations (Doshi & Chataway, 2016). Studies have shown the use of T2-weighted brain MRI scans to diagnose CIS which is highly predictive of the probability of developing MS (O'Riordan et al., 1998). According to the 2017 changes to the McDonald diagnostic criteria, there may be additional evidence of MS lesion dispersion in time and space, as demonstrated by MRI evidence (Lublin, 2014). However, the rising frequency of this incidental MRI discovery in patients has increased its recognition in MS research (Klineova & Lublin, 2018).

Furthermore, MRI of the EAE mouse model with brain lesions provides new insights into the pathology and progression of CNS lesions and may be useful for the evaluation of novel therapeutic strategies in MS (Nessler et al., 2007). Studies have demonstrated how MRI has been integrated with various animal models to study and understand MS disease mechanisms (Hashem et al., 2022; Nathoo et al., 2015). Understanding how MRI can be effectively utilized in preclinical studies by examining potential MS therapies, would increase the possibility of discovering new treatments for MS condition (Nathoo et al., 2014).

Notably, in 2021, the Magnetic Resonance Imaging in Multiple Sclerosis (MAGNIMS), a consortium of Multiple Sclerosis Centers, and North American Imaging in Multiple Sclerosis Cooperative recommended changes to MRI such as the use of gadolinium-based contrast agents to improve MS diagnosis, prognosis, and monitoring acquisition protocols. Additionally, they expanded on the specific characteristics of progressive MS and extended the guidelines to the use of MRI in pediatric MS, pregnancy, and the postpartum period (Wattjes et al., 2021). These guidelines also offered specific recommendations for MRI protocols in diagnosing and monitoring the disease. The recommendations are based on a comprehensive review of the literature and aim to improve the use of MRI for individuals with MS. However, due to its limited clinical limitations, it is still important to consider clinical evaluations as the definitive determinant of treatment efficacy (Miller et al., 1998). Based on these recommendations, we utilized R_2*, quantitative susceptibility mapping (QSM), and arterial spin labelling (ASL) MRI to evaluate oxygen treatment in the EAE.

1.7.1 R_2* and Quantitative Susceptibility Mapping in Iron Pathology

The MRI parameter R_2* (relaxation rate) is a mathematical inverse of the T_2* (1/ T_2*) called transverse relaxation, which is sensitive to the level of deoxyhemoglobin (dHb)). R_2* increases with dHb. The use of MRI R_2* has found numerous applications in the study of hepatic iron (Wood & Ghugre, 2008; Wood et al., 2014). This relaxation follows an exponential decay, characterized by three distinct time points T_1, T_2, and T_2* or by mathematical inverse R_1, R_2, and R_2*. However, R_2 and R_2* are more powerful in quantifying iron in tissue (Wood et al., 2014). R_2* assesses tissue iron concentration using gradient echo imaging while R_2 uses a spin echo sequence (Wood et al., 2005).

Aside from the use of R_2* to quantify hepatic iron, this technique has also found its usage in brain research. R_2* has been utilized to successfully quantify iron in the brain. Iron overload in basal ganglia was shown to correlate with cognitive impairment in older populations (Ghadery et al., 2015). This proposed iron involvement in neurodegeneration can be mediated in two ways. First, iron was reported to induce oxidative damage by the production of reactive oxygen species which brings about ferroptosis; iron-mediated cell death (Dixon et al., 2012). The second mechanism was more distinct, such as the presence of amyloid plaques, α synuclein, and tau protein, the connection between iron and these proteins increases oxidative capacity and cell death (Masaldan et al., 2019). In addition, this technique has been applied in MS studies to quantify myelin and iron in pwMS and cognition (Bagnato et al., 2018; Ghadery et al., 2015). Furthermore, the combination of high magnetic field MRI (7.0 tesla), and histopathology, validated the use of R_2* to quantify iron in MS (Bagnato et al., 2018).

A newer method: QSM (quantitative susceptibility mapping), can identify iron content due to its pronounced magnetic susceptibility and its capability to signify the degree to which a material becomes magnetized when subjected to an external magnetic field (Ravanfar et al., 2021). Paramagnetic or diamagnetic elements and compounds are classified based on their magnetic susceptibility (Ravanfar et al., 2021). Substances with paramagnetic properties like the biological form of iron and copper exhibit a positive magnetic susceptibility. They are drawn towards an external magnetic field, causing an elevation in the magnetic susceptibility of tissue. Conversely, diamagnetic substances such as water, myelin, and calcifications display a negative magnetic susceptibility. They experience a slight repulsion from an external magnetic field, which reduces tissue magnetic susceptibility (Liu et al., 2019).

This technique uses paramagnetic and diamagnetic elements to provide information on local tissue magnetic susceptibility at the voxel level and extracts the bulk magnetic susceptibility from a single measurement (Deistung et al., 2017). This technique uses a magnetic field shift from a variation of tissue susceptibility (Ravanfar et al., 2021), estimates the total field from MRI data, removes the background field, and inverts susceptibility inversion (Wang & Liu, 2015). QSM detects changes in susceptibility related to changes in iron concentration (Chen et al., 2017). Iron aggregation has been characterized in deep gray matter domain with QSM (Langkammer et al., 2012).

QSM showed that differences in magnetic susceptibility signify iron concentration in the brain (Chen et al., 2017). The accuracy of QSM in iron quantification has been validated in post-mortem studies, QSM contrasts correlated with histological assessment of iron (Langkammer et al., 2012; Wang et al., 2020). Overall, QSM has been recognized as a valuable and non-invasive method for measuring and evaluating brain iron, with potential applications in neurodegenerative diseases. Detection of deoxyhemoglobin with R_2* and QSM MRI could provide insight into tissue oxygenation and vascular health.

1.7.2 Arterial Spin Labelling (ASL)

A significant biomarker of an organ's health and activity is the perfusion of blood through it. Adequate blood supply is essential for organs to survive and function properly. When there is insufficient blood flow, organs can suffer damage and eventually worsen a diseased condition. Understanding the importance of blood circulation throughout the body is crucial for developing effective treatments for conditions that affect cerebral blood flow, such as MS.

Arterial spin labelling (ASL) is an MRI parameter that can measure brain perfusion non-invasively at the tissue level. The ability to image perfusion without tracers or other invasive methods has found numerous applications (Hernandez-Garcia et al., 2019). ASL works by magnetically tagging/labeling protons in arterial blood that enter the brain and then imaging the labeled blood as it flows through the brain's blood vessels. ASL was previously challenged by its inherent low noise signal-to-noise ratio (SNR) and slow temporal resolution. However, with the invention of parallel imaging (Blaimer et al., 2004), and the application of pseudo-continuous labelling (Soman et al., 2020) and background suppression scheme (Garcia et al., 2005), ASL images can now be acquired with sufficient speed and quality to be a robust and novel quantitative imaging tool (Hernandez-Garcia et al., 2019).

Investigations of CBF on stroke were among the first applications that focused on vascular disease (Bokkers et al., 2012). ASL has been effectively utilized to assess CBF in ischemic conditions, where there is blood flow restriction to an area (Duong, 2011). More recently, numerous perfusion imaging studies in MS (Berard et al., 2020), and other neurodegenerative disorders, for example, Alzheimer's disease, show impaired blood flow (Binnewijzend et al., 2016; Collij et al., 2016). More so, ASL has also been useful in quantifying CBF in brain lesions, authors argued that low CBF was associated with poor neuromotor outcomes in neonates (Tortora et al., 2017). As a result of this, ASL techniques have developed into a dependable and indispensable tool for clinicians and researchers (Hernandez-Garcia et al., 2019).

Furthermore, in MS clinical research, perfusion MRI has been employed to measure cortical CBF in MS. A decrease in CBF was observed and linked to white matter lesions in MS (Amann et al., 2012). More so, a study demonstrated the precision of utilizing MRI for quantifying cerebral blood flow, this approach could be beneficial for patients who encounter challenges in obtaining

accurate measurements of CBF (Ssali et al., 2018). Considering the wide range of applications of ASL perfusion imaging in both animal and human clinical research, we postulate that ASL MRI could be a valuable tool in measuring CBF in the EAE. Information from CBF will guide us on the amount of blood flow in an area and possibly provide insight into tissue oxygenation.

1.8 Tissue Oxygenation

The mechanism by which the vascular system ensures that every individual cell in the body receives an adequate oxygen supply to carry out its functions and maintain its survival is crucial. This will provide insight into vascular physiology, tissue energy metabolism, and the development of vascular diseases.

August Krogh, a Danish physiologist pioneered the study of oxygen transport in tissue (Larsen et al., 2011). He made a significant observation that the oxygenation benefits arising from increased blood supply are offset by the reduced time blood spends in the capillaries (Larsen et al., 2011). Despite the vast number of capillaries in the human body and their diverse connections to different organs, the assessment of tissue oxygenation has traditionally been based on the characteristics of a single capillary (Renkin, 1985). **Figure 5** demonstrates the relationship between the blood flow in capillaries and the transportation of oxygen between blood and tissues. As the speed of red blood cells increases, the amount of oxygenated blood supplied also increases linearly. However, the time each red blood cell spends within the capillary decreases rapidly. The capillary transit time, which is determined by the ratio of capillary volume to blood flow, determines the duration available for oxygen exchange between blood and tissues before the blood exits the tissue (Ostergaard, 2020).

As a result of these influences, the optimal efficiency of oxygen transport between blood and tissues occurs at capillary erythrocyte velocities. Conversely, when blood velocities are higher, additional increases in velocity have minimal effect on enhancing oxygen availability in the surrounding tissue (Ostergaard, 2020).

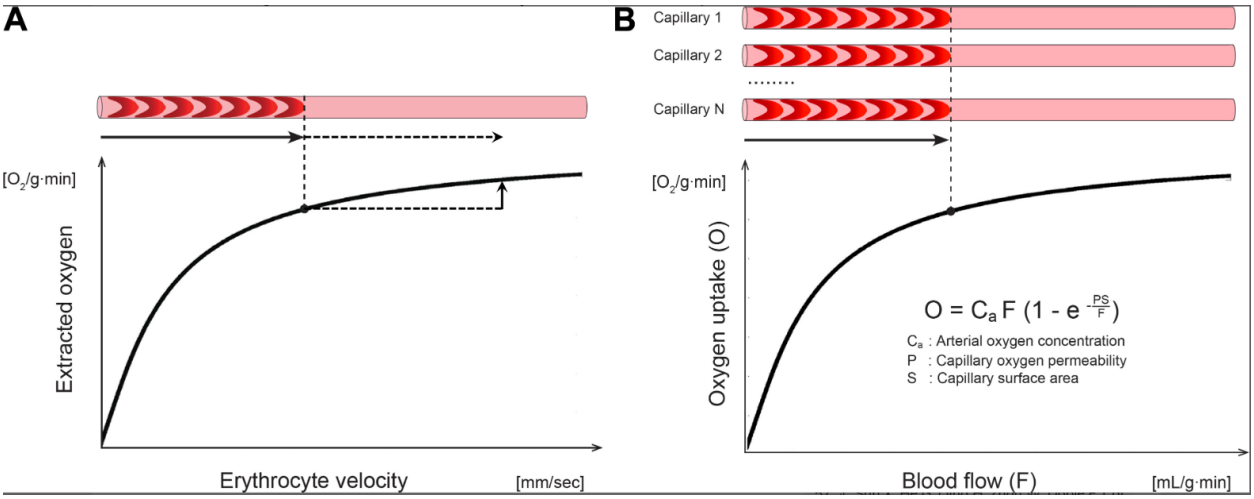

Figure 5: Tissue-enhanced oxygen extraction from capillaries.

Adapted from (Ostergaard, 2020).

A) *The amount of oxygen that can be extracted from a capillary by tissue increases significantly as the flow of erythrocytes through the capillary increases, especially at slower or moderate erythrocyte velocities.* ***B)*** *This relationship applies to tissue volume that contains numerous capillaries with equal length and blood flow. The flow-diffusion equation describes the connection between blood flow (F) and tissue oxygenation (O), which refers to the amount of oxygen that can be continuously taken up by blood flow under normal tissue oxygen levels. In the equation, Ca represents arterial oxygen concentration, P represents the capillary wall permeability to oxygen, and S represents the capillary surface area per unit volume. As blood flow increases significantly, the curve approaches a theoretical maximum. However, across different organs, the orientation, length, and interconnection of capillary segments vary greatly as they adapt to the microscopic organization and metabolism of cells. Consequently, modeling oxygen transport becomes more complex. Quoted directly from (Ostergaard, 2020).*

Furthermore, the homogeneity **(Figure 6)** of blood flow has been reported (Angleys et al., 2015; Jespersen & Ostergaard, 2012), in addition to tissue blood flow.

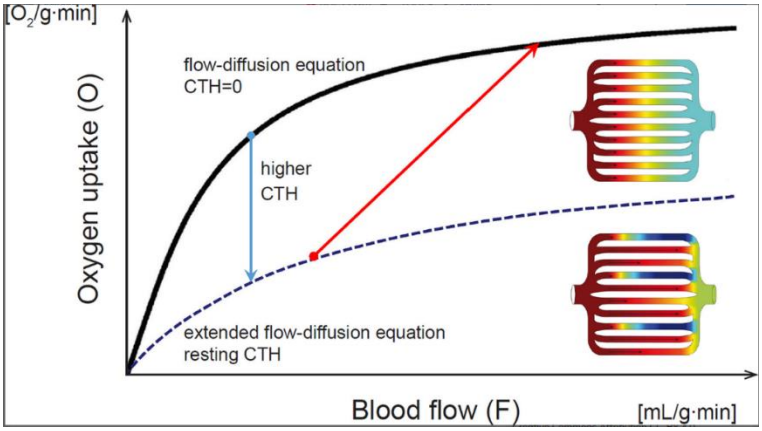

Figure 6: Impact of capillary flow homogeneity on oxygen extraction.

Adapted from (Ostergaard, 2020).

The transport of oxygen across the body heavily relies on the heart, vascular system, and red blood cells, each playing fundamental roles in the process (Crystal & Pagel, 2020; Habler & Messmer, 1997). Once taken up in the lungs, O_2 is transported in the blood through two mechanisms: (1) binding to hemoglobin and (2) physical dissolution in plasma (Dunn et al., 2016; Rhodes et al., 2023). The combined amount of O_2 in these two transport states determines the total oxygen content of the blood (Habler & Messmer, 1997). The O_2 content of arterial blood is the amount of oxygen in each 100 ml of blood and is calculated by the equation: Arterial oxygen content=Hemoglobin bound oxygen + dissolved oxygen (Dunn et al., 2016).

However, the delivery of O_2 to different organs is determined by both cardiac output and arterial O_2 content (Habler & Messmer, 1997). Global oxygen delivery refers to the quantity of oxygen transported to the body's tissues per minute (ml min^{-1}). It is determined by the combined effect of cardiac output, which is the volume of blood pumped by the heart per minute, and arterial O_2 content, which represents the concentration of O_2 in the arterial blood (Dunn et al., 2016).

The constant supply of oxygen to every actively metabolizing cell in the body is vital as it enables the generation of ATP for oxidative phosphorylation (Rhodes et al., 2023). Cerebral oxygenation indicates the balance between the delivery, consumption, and utilization of oxygen by the brain, thus serving as an indicator of the adequacy of cerebral perfusion (Godoy et al., 2023). Factors such as arterial blood pressure, levels of hemoglobin, systemic oxygenation, and the transfer of oxygen from the blood to the cerebral microcirculation can affect brain oxygenation. When there is an impairment between the supply and demand of oxygen in the brain, it leads to cerebral hypoxia/ischemia, which is associated with secondary brain damage and worsened outcomes following acute brain injury (Godoy et al., 2023).

The role of arterial blood flow in tissue oxygenation is crucial in regulating brain function, and any alterations in oxygen supply can lead to hypoxia. Advancing our understanding of tissue oxygenation and devising strategies to optimize oxygen delivery to tissues hold great potential for advancements in medicine, physiology, and critical care. By Prioritizing and optimizing tissue oxygenation, we can work towards enhancing the health and quality of life for individuals with brain disorders involving tissue hypoxia. Next section of this chapter, we discussed how hypoxia can trigger physiological changes in organs, with a specific emphasis on its adverse impact on the brain.

1.9 The Role of Hypoxia in MS

Hypoxia is a state of low tissue oxygenation and has been implicated in MS and EAE disease. This condition can arise from various factors such as a diminished capacity of the blood to carry oxygen (e.g., anemia), difficulties in unloading oxygen from hemoglobin to target tissues (e.g., carbon monoxide toxicity), or a restriction in blood supply (Rhodes et al., 2023). When the body experiences hypoxia, it can lead to irreversible damage to tissues which may contribute to the development of neurodegenerative diseases (Rhodes et al., 2023).

The presence of hypoxia has been validated in various ways such as using an intravenous immunohistochemical probe (Zanelli et al., 2006) or utilizing a finely tuned oxygen-sensitive optical probe inserted directly into the regions under investigation (Johnson et al., 2016). Neuropathological and MRI studies have demonstrated that MS lesions can exhibit hypoxia (Aboul-Enein et al., 2003; Graumann et al., 2003; Yang & Dunn, 2015). MRI and frequency-domain near-infrared spectroscopy (fdNIRS) studies from the Dunn laboratory have confirmed hypoxia in both preclinical (Johnson et al., 2016; Nathoo et al., 2013) and clinical studies (Adingupu et al., 2023). An animal study revealed demyelinating lesions in EAE using susceptibility-weighted imaging (SWI), and increased levels of deoxyhemoglobin (i.e., poorly oxygenated blood) in the EAE spinal cord and cerebellum (Nathoo et al., 2013). Similarly, a clinical post-covid study revealed evidence of brain hypoxia using fdNIRS, and this can prompt an adverse outcome and reduce life expectancy in these individuals (Adingupu et al., 2023). In addition, microvascular hemoglobin oxygen saturation (StO2) in the cerebral cortex of pwMS exhibited a reduction, which is associated with clinical disability (Yang & Dunn, 2019).

Hypoxia can also induce changes in iron susceptibility (Chen et al., 2017), and has been shown to impair mitochondrial oxygen consumption by reducing ATP-utilizing metabolic demand

(Papandreou et al., 2006). Mitochondrial dysfunction leads to energy failure (Desai & Smith, 2017) and can hinder the production of ATP, as observed in both acute (Mahad et al., 2008), and chronic lesions (Mahad et al., 2009; Witte et al., 2009), as well as in axon degeneration in pwMS (Dutta et al., 2006). Axon susceptibility to excitotoxic injury is exacerbated by this energy failure (Abramov & Duchen, 2010). This can also have notable impacts on mitochondrial movement, velocity, and morphology (Desai & Smith, 2017). Smaller diameter fibers, which have a lower mitochondrial density relative to their surface area, may be more susceptible to energy failure and degeneration (Stys, 2005). Additionally, other mechanisms like enormous variability in impulse conduction involving the mitochondria may also contribute to this process (Sajic et al., 2013).

The balance between metabolic demand and oxygen delivery in the brain is measured by brain oxygenation, and there is evidence that hypoxia and inflammation are interconnected (Johnson et al., 2016; Yang & Dunn, 2019). Neuropathology and imaging studies showed that inflammation-induced hypoxia can cause lesions in MS (Aboul-Enein et al., 2003; Graumann et al., 2003; Yang & Dunn, 2015). Additionally, surgically placed pO_2 sensors in EAE mice have demonstrated a strong relationship between gray matter inflammation and hypoxia (Johnson et al., 2016). These findings support the idea that hypoxia can contribute to disease activity. The inflammation/hypoxia cycle proposed that inflammation brings about the release of infiltrating leukocytes, which in turn causes the release of reactive oxygen species, which then can cause damage to the vascular endothelium (Yang & Dunn, 2019). This injury can impair the oxygen delivery to brain tissues. More so, leukocytes have a high energy demand and could result in less oxygen availability to brain tissues leading to cerebral hypoxia (Yang & Dunn, 2019).

Understanding the relationship between hypoxia and increased symptomology emphasizes the need for further research and interventions to address this concern. In recent findings, hypoxia

has emerged as a critical factor in the development of pattern III demyelinating lesions, observed in the EAE animal model (Desai et al., 2016). Thus, by investigating brain hypoxia and its underlying causes, we can strive to improve outcomes and enhance the overall well-being of affected individuals. A greater understanding of how inflammation affects tissue energy balance may lead to novel and effective therapeutic strategies that ultimately will benefit not only people affected by MS but also people affected by the wide range of other neurological disorders in which neuroinflammation plays an important role (Desai & Smith, 2017). However, it remains uncertain whether tissue hypoxia is directly contributing to the pathogenesis of MS disease (Desai & Smith, 2017). A study carried out in the rat EAE model demonstrated the presence of severe tissue hypoxia. This study revealed a quantitative, spatial, and temporal correlation between neurological deficits and hypoxia in both the white and grey matter of the spinal cord (Davies et al., 2013).

The health impact of hypoxia as mentioned in the paragraphs above suggests the potential consideration of oxygen therapy for MS disease. Notably, the limitations posed by deficient mitochondrial respiratory chain enzymes and impaired mitochondrial transport within neurons may restrict the therapeutic effectiveness of oxygen therapy. An anti-inflammatory environment results in several endogenous adaptations triggered by acclimatization to mild hypoxia. However, the hypoxia-inflammation cycle seen in MS cannot be ignored. Through the prolyl hydroxylase pathway, hypoxia can aggravate inflammation. Inflammation can also cause hypoxia by destroying mitochondria and endothelial cells, causing impaired blood flow which can contribute to disease progression (Yang & Dunn, 2019). For this reason, a more profound understanding of these mechanisms could reveal potential new therapeutic targets for neurodegenerative diseases (Esen et al., 2016). Interestingly, the administration of oxygen supplementation (30% then 100%) to EAE

mice resulted in the disappearance of susceptibility-weighted image (SWI) lesions (Nathoo et al., 2015).

Experimental studies have provided evidence of the use of oxygen in rodents (Amatruda et al., 2023; Dore-Duffy et al., 2011). When animals were exposed to chronic moderate hypoxia (10% oxygen), this caused enhanced vascular density, and the clinical onset of EAE disease severity was greatly delayed (Dore-Duffy et al., 2011). When earlier clinical symptoms were seen, animals exposed to hypoxia showed a reduced inflammatory response and spinal cord disorder. While the recovery process is unclear, this study suggests that hypoxia could be used as a treatment target for EAE (Dore-Duffy et al., 2011). Exploring the role of brain hypoxia will provide insight into tissue oxygenation and the potential consideration of oxygen therapy.

1.10 The Use of Oxygen Treatment in Neurological Disorders

Oxygen therapy is a treatment that provides one with supplemental oxygen to breathe in. It is usually delivered in humans through nasal oxygen cannula and in rodents via inhalation in oxygen-enriched cages. The use of oxygen treatment in medical intervention is to increase oxygen levels in a patient's bloodstream, which leads to better breathing and improvement in body oxygenation. This form of therapy plays a vital role in clinical settings for individuals who experience respiratory conditions such as hypoxia, and other condition which cause insufficient oxygen supply to the body.

Oxygen treatment has been attempted in MS clinical trials (Bennett & Heard, 2010). A study argued that oxygen treatment was not useful in treating MS as there was no clinical benefit (Bennett & Heard, 2010). However, it may be effective in a subset of individuals who are not part of the trials (Bennett & Heard, 2010). It's considered prudent to administer oxygen only to hypoxic

individuals in clinical settings. In addition to that, it is unclear whether the patients who underwent these trials experienced hypoxia, which may explain the non-plausible benefit of oxygen treatment in MS. This study used the EAE mouse model of MS, which has been reported by our research team with evidence of hypoxia using MRI. Moreover, an oxygen probe study in the EAE has demonstrated hypoxia in the cortex and cerebellum (Johnson et al., 2016). Interestingly, a study in rats discovered that the administration of normobaric oxygen (80%) for a two-day duration mitigated demyelination in the spinal dorsal column (Desai et al., 2016).

1.10.1 Hyperbaric Oxygen Treatment (HBOT)

HBOT involves the administration of pure oxygen at elevated pressure levels (typically 2 atmospheres), which results in increased concentrations of oxygen in both the blood and tissues (Ortega et al., 2021). A study proposed that hyperbaric oxygen therapy (HBOT) may have the potential to either halt or reverse the progression of MS disease (Bennett & Heard, 2004).

The efficiency of HBOT has been evaluated in large clinical trials, (Bennett & Heard, 2004, 2010; Fischer et al., 1983; Jacoby, 2001; Lambrou et al., 1987; Maillard et al., 1987; Moore et al., 2020; Perrins & James, 2002; Taylor & Webster, 1987). Interestingly, some trials reported beneficial effects in patients but these effects of HBOT were transient (Barnes et al., 1987; Fischer et al., 1983). Also, HBOT effects were shown to attenuate EAE in the initial stage by modulating the T-cell responses (Chiou et al., 2021).

However, the use of HBOT in treating MS requires extreme caution (Lambrou et al., 1987) and is not recommended based on its no plausible benefits in the clinical course (Bennett & Heard, 2010; Fischer et al., 1983). Failure of HBOT in MS clinical trials may be attributed to factors such as administering therapy at an advanced disease stage, short-term exposure to oxygen, insufficient

patient numbers in the trials, and the potential exacerbation of oxidative damage caused by pressurized-inspired oxygen-enriched air (Amatruda et al., 2023). To overcome these limitations, a study proposed that normobaric oxygen therapy may be a more promising treatment option for MS (Amatruda et al., 2023).

It has been shown that extended periods (≥ 24 hours) of normobaric oxygen therapy can improve neurological deficits without apparent adverse effects, particularly when administered during the early stages of the disease (Amatruda et al., 2023).

1.10.2 Normobaric Oxygen Treatment (NBOT)

Normobaric oxygen treatment is a non-invasive medical procedure that delivers oxygen to patients at normal atmospheric pressure (760 mm Hg). NBOT has gained popularity in recent years for its potential to treat various medical conditions such as hypoxia, stroke, traumatic brain injury, and altitude sickness. NBO as a neuroprotective measure in rodents has been reported (Amatruda et al., 2023), and in humans (Tolias et al., 2009). The neuroprotective role of normobaric hyperoxia (excess oxygen delivery) is found to be promising, and further research is needed (Tolias et al., 2009).

The use of oxygen in clinical treatments has been studied (Dixon & Jones, 2017; Dodd, 2000; Forster et al., 2016; McDonald et al., 2016), and in rodents (Yuan et al., 2014) as well as its effect (Nishino et al., 2021). Neurological studies showed that stroke patients who received hyperoxia treatment demonstrated a notable enhancement at the 24 hours, while baseline scores were similar and showed a tendency to improve at 4 hours (during therapy) and 1 week (Singhal et al., 2005). Furthermore, NBO was found to temporarily ameliorate clinical deficits and MRI abnormalities in specific patients diagnosed with acute ischemic stroke (Singhal et al., 2005).

Moreover, NBO may also increase the safety of tissue plasma activator thrombolysis (Hadjiev & Mineva, 2009) in stroke. In the traumatic brain injury (TBI) model, immediate administration of NBO following fluid percussion injury (FPI) holds promise as a viable therapeutic strategy to minimize neuronal damage (Muthuraju et al., 2013).

Additionally, based on the currently available data on oxygen treatment for stroke, it appears that NBO could be a promising therapeutic approach for treating neurological disorders, including MS. As a result, it's possible that normobaric oxygen treatment could be safe for individuals with MS (Singhal et al., 2005). Similarly, the application of NBO in the spinal cord of MS animal models has been demonstrated (**Figure 7**) (Amatruda et al., 2023). Oxygen is useful in hypoxia, and proper administration and monitoring of oxygen therapy can have significant impacts on patient outcomes. However, the amount of oxygen administered to a patient depends on various factors, including the underlying condition, oxygen saturation levels, and the patient's respiratory status.

It is important to administer the appropriate oxygen dose, as both under-dosing and over-dosing of oxygen can have adverse effects on patients' health. Under-dosing of oxygen can lead to inadequate tissue oxygenation, thus contributing to organ failure. Conversely, over-dosing of oxygen can result in oxygen toxicity, which can damage lung tissue and other organs. Therefore, careful monitoring of oxygen saturation levels and regular adjustment of oxygen therapy are essential to optimize outcomes.

Nevertheless, the relationship between treatment outcome and NBO duration was examined in cerebral ischemia (Yuan et al., 2014). Among the different durations of NBO treatment (2 hours, 4 hours, and 8 hours), it was found that 8 hours of NBO was effective after 24 hours. Based on the experimental conditions, a longer duration of NBO treatment showed greater benefits in rats with

cerebral ischemia-reperfusion (Yuan et al., 2014). These previous studies have provided evidence for considering the duration of oxygen treatment in neurological diseases.

Research on acute ischemic stroke also showed that longer durations of high-flow oxygen therapy resulted in more significant improvements in clinical deficits and MRI abnormalities (Singhal et al., 2005). In another study examining the effects of NBO treatment on cerebral ischemia-reperfusion in rats, it was observed that longer durations of NBO treatment yielded greater benefits, including reduced infarction volume, attenuated oxidative stress markers, and alleviated apoptosis markers (Yuan et al., 2014). Similarly, In MS pre-clinical study, 24, and 48, hours duration of NBO was shown to have a therapeutic benefit in the spinal cord of the EAE (Amatruda et al., 2023). With these findings, we proposed that enhancing the oxygen supply to areas affected by inflammation in the brain may have therapeutic benefits in MS. This thesis investigated the effects of administering 100% normobaric oxygen-enriched air for 6 hours daily for 5 days in the EAE MS model.

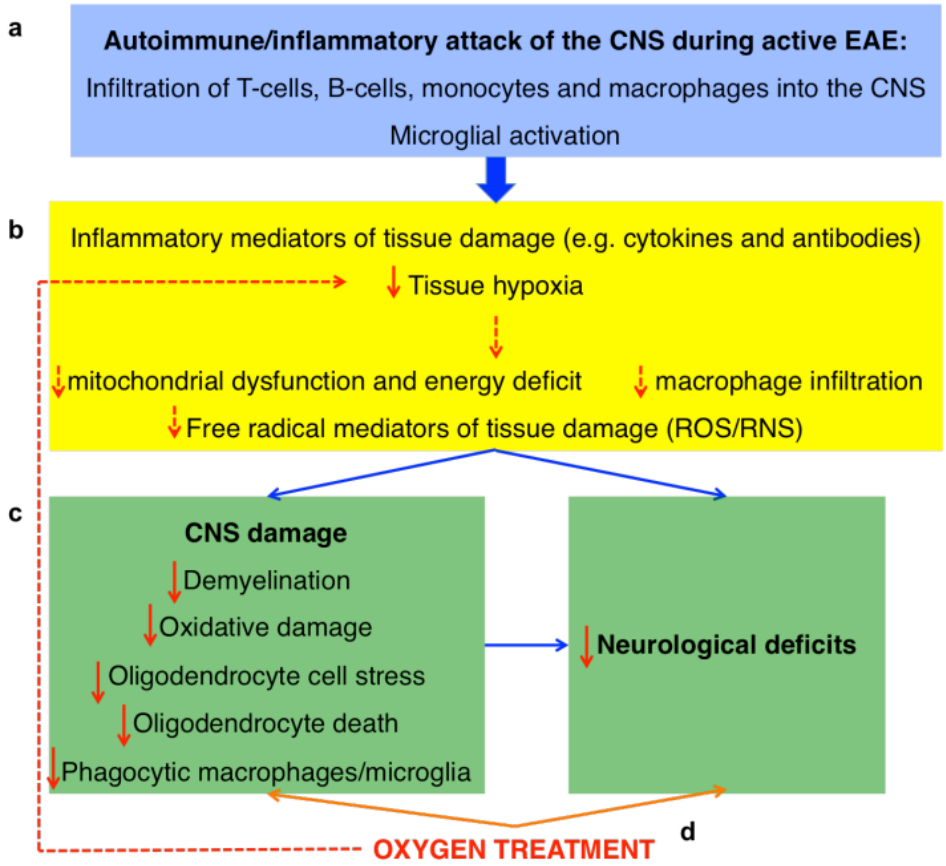

Figure 7: The effect of normobaric oxygen treatment in the EAE mice.

Adapted from (Amatruda et al., 2023).

An overview of the effects of oxygen therapy (administered at 75% concentration for 72 hours after the onset of neurological deficits) in rats with active EAE. ***a****) Inducing active EAE in rats through immunization with MOG triggers an autoimmune/inflammatory response characterized by the infiltration of T-cells, B-cells, monocytes/macrophages, and activation of resident microglia in the CNS.* ***b****) This inflammatory response in the CNS parenchyma results in the release of inflammatory mediators, activation of cytotoxic pathways, tissue hypoxia, generation of reactive oxygen/nitrogen species (ROS/RNS), mitochondrial dysfunction, and energy depletion.* ***c****) Inflammatory response to the CNS causes damage, including demyelination, oxidative damage, phagocytosis, stress, and death of oligodendrocytes, leading to neurological deficits.* ***d****) Administration of oxygen to rats with active EAE alleviates the severity of neurological deficits and reduces several pathological features (indicated by solid red arrows), including*

tissue hypoxia, demyelination, oxidative damage, stress-induced apoptosis in oligodendrocytes, and activation of phagocytic microglia/macrophages. The dashed red arrows indicate a proposed mechanism by which oxygen may attenuate disease severity. It suggests that by reducing tissue hypoxia, oxygen may decrease macrophage infiltration, ROS/RNS production, mitochondrial damage, and energy depletion, thus enhancing the resilience of CNS cells against inflammatory attacks. Adapted from (Amatruda et al., 2023).

1.11 Thesis Aims

Previous studies from Dunn's laboratory have shown that inflammation and hypoxia play a role in the disease progression of MS (Johnson et al., 2016; Yang & Dunn, 2019). This holds implications for the development of new treatments. While disease-modifying therapies target the more advanced progression of the disease, there is a need for therapeutic approaches to target the underlying pathophysiology of MS such as hypoxia. Oxygen treatment shows potential as a treatment intervention for MS due to its ability to increase tissue oxygenation which may reduce inflammation.

However, the impact of oxygen treatment on CBF, hypoxia, and disease severity in MS is poorly understood. We used MRI to evaluate treatment outcomes in the EAE. MRI sequences were designed to image towards T_1 or T_2 relaxation giving different tissue contrasts. Different MRI sequences can be utilized to capture specific aspects of brain anatomy and pathology, allowing for a comprehensive evaluation of various parameters. Spin Echo (SE) and multi-echo gradient echo (MGE) are two distinct MRI sequences that provide valuable information about the brain's anatomy and pathology. The Spin echo sequence is one of the fundamental sequences in MRI. It involves applying a 90-degree radiofrequency pulse to tip the spins of protons in the body from their equilibrium state. This is followed by a 180-degree refocusing pulse, which rephases the spins

that became de-phased due to their different precession frequencies. The rephased spins generate an echo signal that is detected and used to construct the MRI image.

The Spin echo sequence is particularly useful in producing high-resolution anatomical images with excellent tissue contrast. By manipulating the timing parameters, such as the repetition time (TR) and echo time (TE), different contrast weightings can be achieved. For example, short TE values enhance proton density contrast, while longer TE values increase T2 contrast. These contrast variations can help visualize different tissues and identify abnormalities within the brain.

On the other hand, multi-gradient echo (MGE) is a sequence that acquires multiple echoes at different echo times. Instead of using a 180-degree refocusing pulse, MGE sequences rely on the gradient echo created by the spins after the 90-degree excitation pulse. The acquired echoes provide information about the relaxation properties of tissues, particularly the T_2* relaxation time. MGE sequences are advantageous in capturing susceptibility-related effects and tissue microstructure. By acquiring multiple echoes, MGE can detect subtle changes in T_2* relaxation time caused by variations in tissue composition, magnetic susceptibility, or iron content. This makes MGE sequences valuable for investigating cerebral pathologies related to susceptibility changes, such as microbleeds, iron deposition, or hemorrhagic strokes.

More so, MGE sequences can be used to generate susceptibility-weighted imaging (SWI), which enhances the visualization of veins, small vessels, and hemorrhagic lesions. SWI combines information from the phase and magnitude images, producing high contrast between tissues with different susceptibilities. However, Studies have proposed that cognition and sensory information are implicated in MS (Rae-Grant et al., 1999; Sumowski et al., 2018) in addition to cortical hypoxia in the brain (Manole et al., 2014). Hippocampus dysfunction is associated with cognitive decline in MS (Rocca et al., 2018). Reduction in CBF has been reported in the cortex (de la Pena et al.,

2019), and thalamus (Ota et al., 2013) of pwMS and in EAE (Desai et al., 2020). For these reasons mentioned above, we explored the impact of oxygen treatment in the cortex, hippocampus, and thalamus brain regions, due to their involvement in cognition and sensory function in MS. We employed the 3-dimensional MGE sequence for its ability to provide information about tissue susceptibility effects.

This study aims to provide valuable insight into the potential effect of hypoxia and oxygen treatment on MS. The three aims of this thesis are discussed in **Chapters 2, 3,** and **4**.

Aim 1. Used ASL MRI by combining four perfusion images and the T1 map to quantify cerebral blood flow in the EAE mouse model.

Aim 2. Used QSM MRI with regularized enabled sophisticated harmonic artifact reduction on T_2* phase data (RESHARP) for background field removal and utilized R_2* MRI by inverting T_2* values to quantify brain hypoxia in the EAE mouse model.

Aim 3. Used a 15-point clinical grading scale to score EAE symptoms, and an open-field test to assess disease severity in the EAE mouse model.

CHAPTER TWO:
ASSESSING THE EFFECT OF OXYGEN TREATMENT ON CEREBRAL BLOOD FLOW IN THE EAE

2.1 Introduction to Cerebral Blood Flow

The brain has a remarkable ability to regulate its blood flow within a certain homeostatic range despite changes in blood pressure. This autoregulatory mechanism helps to maintain the dilation or constriction of blood vessels in response to changes in metabolic demands. There are 3 competing hypotheses behind cerebral autoregulation. The first proposed idea is the neurogenic hypothesis which argues that nerves connected to blood vessel walls are responsible for their control (van Beek et al., 2008). Another theory is the myogenic hypothesis which posits that the smooth muscle cells within cerebral vessels can detect pressure changes both inside and outside the vessel walls. In response, these cells contract or dilate the vessel wall to regulate blood flow (van Beek et al., 2008). In contrast, the metabolic hypothesis proposes that variations in concentrations of oxygen, carbon dioxide (CO_2), adenosine, and other metabolites resulting from high neuronal activity led to changes in cerebral blood flow (CBF).

Variations in oxygen and carbon dioxide levels within the blood will impact blood flow. For example, individuals suffering from hypercapnia (excess carbon dioxide) and hypoxia (low oxygen) will experience vasodilation in systemic arteries, increasing CBF which ensures sufficient oxygen supply to the brain. Through neurogenic processes, the brain controls its blood flow. In response to neuronal activity, nerve cells in the brain can produce vasoactive chemicals that modify the width of blood vessels, thereby enhancing CBF (Silverman & Petersen, 2023).

2.2 Neurodegenerative Disease's Impact on Cerebral Flood Flow

The brain consumes about 20% of the body's oxygen and glucose but has limited energy reserves, so continuous blood flow and oxygen are crucial. Cerebral blood flow (CBF) is defined as the blood volume that flows per unit tissue mass per unit time in the brain and is usually expressed in units of ml $_{blood}$ ·$(100g_{tissue})^{-1}$ min^{-1}. Changes in CBF have been associated with a variety of neurological conditions, including stroke (Fan et al., 2022), TBI (Sankar et al., 2019), Alzheimer's (Binnewijzend et al., 2016), and MS (Hostenbach et al., 2020). Therefore, measuring and monitoring CBF can provide valuable insight into brain health and potential disease progression. There is an established relationship between systemic arterial blood flow (SABF) and cerebral perfusion measures in MS patients. The observed correlation between systemic and CBF in patients with progressive multiple sclerosis (PMS) could indicate impaired cerebrovascular reactivity mechanisms and inadequate perfusion regulation (Jakimovski et al., 2022).

Consequently, CBF in progressive MS may rely more on the SABF due to the direct connection between systemic and CBF which may explain cerebrovascular regulation and impaired perfusion control (Jakimovski et al., 2022). Furthermore, hypoperfusion in capillaries has been linked to a reduction in microstructural integrity of white matter in patients with RRMS, as demonstrated by the decreased lesion perfusion observed at both the global and capillary levels (Sisco et al., 2021). The associations between cortical and deep gray matter perfusion vs. physical and cognitive performance in patients with MS have been investigated (Jakimovski et al., 2020). Findings revealed that decreased perfusion in gray matter (GM) and deep GM is associated with worse MS outcomes. However, there was no correlation between the presence of cardiovascular disease (CVD) and reduced GM and deep GM perfusion (Jakimovski et al., 2020).

White matter hyperintensities (WMHs) refer to areas of increased signal intensity in the white matter of the brain, often observed on MRI scans. On the other hand, CBF refers to the blood supply to the brain tissue, which is vital for metabolic needs. Research has shown that WMH is associated with reduced CBF (Stewart et al., 2021), indicating that the blood flow to the areas affected by WMH may be compromised. White matter hyperintensities (WMHs), were shown to be associated with cerebrovascular risk (Bahrani et al., 2017). It represents the amount of tissue damage (Wardlaw et al., 2015) and is closely linked to stroke (Wardlaw et al., 2015), and cognitive decline (Huang et al., 2021). It has been suggested that vascular inflammation plays a role in the development of WMHs, potentially affecting CBF throughout the brain; however, WMH pathogenesis remains unclear and needs further investigation (Huang et al., 2021).

Furthermore, a reduction in pericyte coverage leads to blood-brain barrier dysfunction via endothelial transcytosis following chronic cerebral hypoperfusion has been studied (Sun et al., 2021). Consequently, restoring BBB function could hold promise as a potential treatment strategy for CSVD (Sun et al., 2021). The objective of this chapter was to examine the impact of oxygen treatment on CBF in the EAE model and provide insights into the effects of oxygen treatment in the cortex, hippocampus, and thalamus of EAE mice.

2.3 Methods

2.3.1. Study Ethics

All experimental procedures were performed by the guidelines of the Canadian Council of Animal Care. This study was approved by the Animal Care Committee, University of Calgary (AC19-0036).

2.3.2. Animal

Female C57BL/6 mice aged (8-10 weeks old) were purchased from Charles Rivers laboratory. The animals were housed five mice per cage under standard environmental conditions, in the animal halfway house facility. All mice groups, (EAE, n = 20, CFA/PTX, n = 10, and naïve, n = 10) were subjected to the same handling, disease clinical scoring, open-field (OF) test, and MRI.

2.3.3. EAE Induction

EAE induction was performed on the day after the first CBF MRI/OF for baseline measurement. EAE and CFA/PTX mice were anesthetized with a mild dose of ketamine/xylazine. This was followed by subcutaneous injection with 50µl myelin oligodendrocyte glycoprotein $(MOG)_{33-55}$ mixed in complete Freund's adjuvant (CFA), comprised of 10 mg/ml of mycobacterium tuberculosis into each side of flank which triggered an autoimmune response. This was followed by intraperitoneal (ip) administration of 200ml of pertussis toxin (PTX) (300ng PTX in 200µl of PBS (phosphate buffer saline) on day 0 and day 2. CFA/PTX mice were induced with only PTX on day 0. Naive mice received no injection.

2.3.4. Post-Induction

Animals were monitored from 6 - 14 days post-induction to check for symptoms. At the onset of symptoms, days 14 - 17, EAE clinical score was assessed daily, and recorded from 14 - 21 days post-induction. The total number of the EAE mice was n = 20 before induction. However, following induction two mice didn't show sickness symptoms, this may be attributable to induction failure. Therefore, for this study, 18 EAE mice were used for data collection, processing, and

analysis. EAE treated (n=9) and untreated (n=9) and CFA/PTX treated (n=5) and untreated (n=5) and naïve treated (n=5) and untreated (n=5) groups before, and post-oxygen treatment. The second OF test was performed before oxygen treatment, and the last OF was carried out a day after oxygen treatment, which was compared to the OF baseline (before induction). All control mice (CFA/PTX and naive) were randomly grouped into two treatment groups (e.g., CFA/PTX and naïve treated and untreated). At the onset of symptoms, EAE mice were split into treated and untreated groups **(Table 1)** after disease scoring. This was necessary to avoid potential bias and helped control for an even distribution of EAE disease severity in each group. The last CBF MRI/OF was done a day after oxygen treatment. No imaging was done before treatment.

Table 1: Table showing study sample size.

Animal group	Treated	Untreated
EAE	n = 9	n = 9
CFA/PTX	n = 5	n = 5
Naïve	n = 5	n = 5

2.3.5. Oxygen Administration

At the onset of symptoms, normobaric oxygen (100%) was administered to the treatment groups of experimental animals for 6 hours (9:30 am - 3:30 pm) duration for 5 days. Treatment was administered by placing the mice in an oxygen chamber connected to an oxygen tank (5 mice per cage). Mice without treatment were placed in a similar chamber (21% room air). Mice were monitored throughout the duration of treatment. An overview of the study method is shown in **Figure 8.**

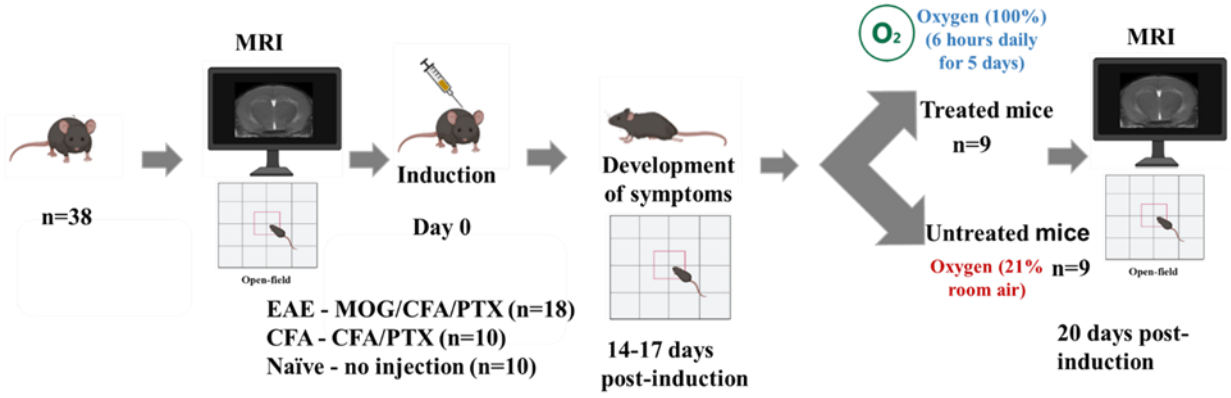

Figure 8: An overview of the study method and EAE induction.

Images from biorender.com.

2.3.6. Animal MRI Imaging

It was challenging to get animals to remain still when inside an MRI coil. However, this was overcome using with 2.0 - 2.5% isoflurane via inhalation to achieve anesthesia in 30% oxygen and 70% nitrogen. To minimize the effect of anesthesia in experimental animals, we imaged twice, at baseline (day 0, before induction) and 6 days post oxygen treatment (19 - 20 days post-induction).

MRI was performed using a 9.4T MRI Bruker Avance Console with a 33mm quadrature volume coil. Hypoxia was quantified with R_2*, and QSM, based on changes to iron susceptibility respectively. The images were obtained from the MRI RAREVTR sequence (TR=100, 500, 1000, 3000, 7500 ms, TE = 10 ms). We measured CBF using ASL MRI to determine the effect of oxygen treatment on blood flow. This was compared between the treated and untreated mice, before induction and after oxygen treatment. Thus, we applied MRI parameters two times in these selected ROIs (**Figure 9**); before induction and post-oxygen treatment. Before analysis, we carefully paired

each mouse in the treated and untreated groups to their baseline MRI measures (CBF, R_2*, and QSM).

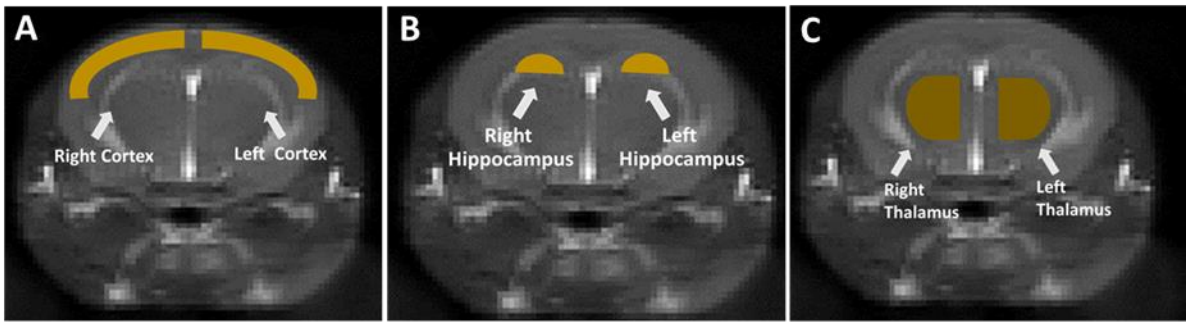

Figure 9: Brain regions of interest selected for MRI data analysis.

Anatomical brain MRI scan from a naive mouse showing the brain regions selected for analysis of CBF, QSM, and R_2. A) left and right cortex. B) left and right hippocampus, and C) left and right thalamus. Manual delineation of regions of interest (ROIs) was performed to draw boundaries on the image for MRI analysis. For data analysis, the mean values of each region in individual mice were calculated by averaging the values from both the right and left sides and treating them as a single region rather than distinguishing between left and right.*

2.3.7. Data Processing and Statistical Analysis

A custom MATLAB script was utilized to generate a perfusion map by combining four perfusion images and the T1 map. This map calculated the CBF on a voxel-by-voxel basis using the provided equation ($f = \frac{1}{T_1'} \frac{\lambda}{2\alpha} (\frac{M_c - M_L}{M_c})$ (Hashem et al., 2020). Tissue perfusion (f) in milliliters per 100 grams per minute (ml/100g/min) was calculated using the equation, considering various factors. The blood-brain partition coefficient (λ) was set to 0.9. The average signal of the two control images (M_c) and the average signal of the two tagged images (M_L) were used. The spin-

labelling efficiency (α) was determined to be 0.675 ± 0.044. The T1 value (T'1) in each voxel was incorporated into the calculation. Perfusion maps were calculated on an individual basis for each animal in the study. To create a region of interest (ROI), a tagged image with enhanced contrast was utilized. For each mouse, regions of interest (ROIs) were delineated manually on the tagged perfusion scans. These ROIs were then applied to the perfusion map to calculate the mean CBF of all voxels within the ROIs.

All statistical analyses and graph generation were conducted using GraphPad Prism (version 10.0.1). Graphs represent mean ± S.E.M. (standard error of the mean). All statistical analyses were considered significant when $p < 0.05$. One-way analysis of variance (ANOVA) test was used to compare multiple groups (e.g., EAE, CFA/PTX, and naïve) at a time point. Mixed-model ANOVA was used to compare groups at two-time points (pre vs. post-CBF) for treated and untreated groups. Tukey multiple comparison was used to determine the statistical significance for all possible pairwise comparisons between groups. Relationships between parameters were determined by correlating CBF vs. disease clinical score, CBF vs. total distance travelled in OF test, and CBF vs. R_2*. This was determined using the Pearson correlation coefficient in GraphPad prism.

2.4 Results

2.4.1 Oxygen Treatment in Improving CBF in the Cortex of EAE Mice.

First, to rule out the possibility that any group differences are due to differences in mice before induction, CBF was quantified in the naïve, CFA/PTX, and EAE groups before induction (baseline). CBF in each ROI was compared for all groups; treated and untreated. For example, we compared EAE treated vs. untreated, CFA/PTX treated vs. untreated, and naïve treated vs. untreated using one-way ANOVA at baseline (before induction).

Following statistical analysis with one-way ANOVA and Tukey multiple comparisons, at baseline, there was no statistically significant difference in the CBF cortex, as expected for all mice groups; EAE (untreated 219 ± 10.5 ml·100g^{-1}·min^{-1}, treated 226 ± 9.5 ml·100g^{-1}·min^{-1}), CFA/PTX (untreated 220 ± 14.6 ml·100g^{-1}·min^{-1}, treated 221 ±11.7 ml·100g^{-1}·min^{-1}), and naïve (untreated 222 ±18.9 ml·100g^{-1}·min^{-1}, treated 231 ±15.4 ml·100g^{-1}·min^{-1}); ($F(5,32) = 0.75$, $p = 0.59$) **(Figure 10)**.

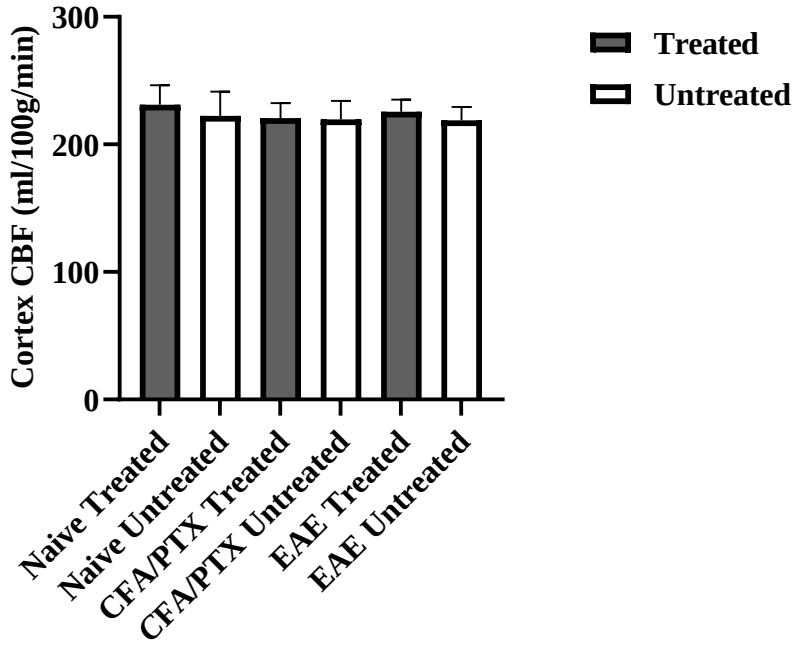

Figure 10: Baseline mean CBF measured in the cortex of all mice.

CBF cortex is represented as the mean±SD measured in the treated and untreated mice. Animals analyzed at baseline in the cortex region were EAE, CFA/PTX, and naïve. Mean±SD for each groups were; EAE cortex (untreated 219 ± 10.5 ml·100g^{-1}·min^{-1}, treated 226 ± 9.5 ml·100g^{-1}·min^{-1}), CFA/PTX cortex (untreated 220 ± 14.6 ml·100g^{-1}·min^{-1}, treated 221 ±11.7 ml·100g^{-1}·min^{-1}), and naïve cortex (untreated 222 ±18.9 ml·100g^{-1}·min^{-1}, treated 231 ±15.4 ml·100g^{-1}·min^{-1}). No significant difference was observed at baseline; $p>0.05$. Dark gray bars represent untreated mice and white bars represent treated mice. Bars represent standard deviation.

The next question we addressed was, whether were there group differences without treatment. In this case, we compared the CBF for all mice in the untreated group factoring in the pre and post-induction CBF. Then, we employed a mix-model ANOVA and Tukey multiple group comparisons. There were reductions in CBF of the EAE and CFA/PTX **(Figure 11A)** untreated groups compared to CBF observed in the naïve mice. More so, we found a significant difference in CBF between the untreated EAE vs. controls (naïve and CFA/PTX); $p<0.05$, ($F(2,32) = 8.547$, $^{**}p < 0.01$) **(Figure 11A)**. CFA/PTX vs. naïve post-induction CBF $^{**}p \leq 0.01$, and untreated EAE pre-induction CBF vs. post ** $p < 0.0$. Post-induction mean±SD CBF cortex of the EAE (166 ± 39.1 $ml \cdot 100g^{-1} \cdot min^{-1}$), CFA/PTX (190 ± 38.2 $ml \cdot 100g^{-1} \cdot min^{-1}$), and naïve (254 ± 8.1 $ml \cdot 100g^{-1} \cdot min^{-1}$) were showed in **Table 2**.

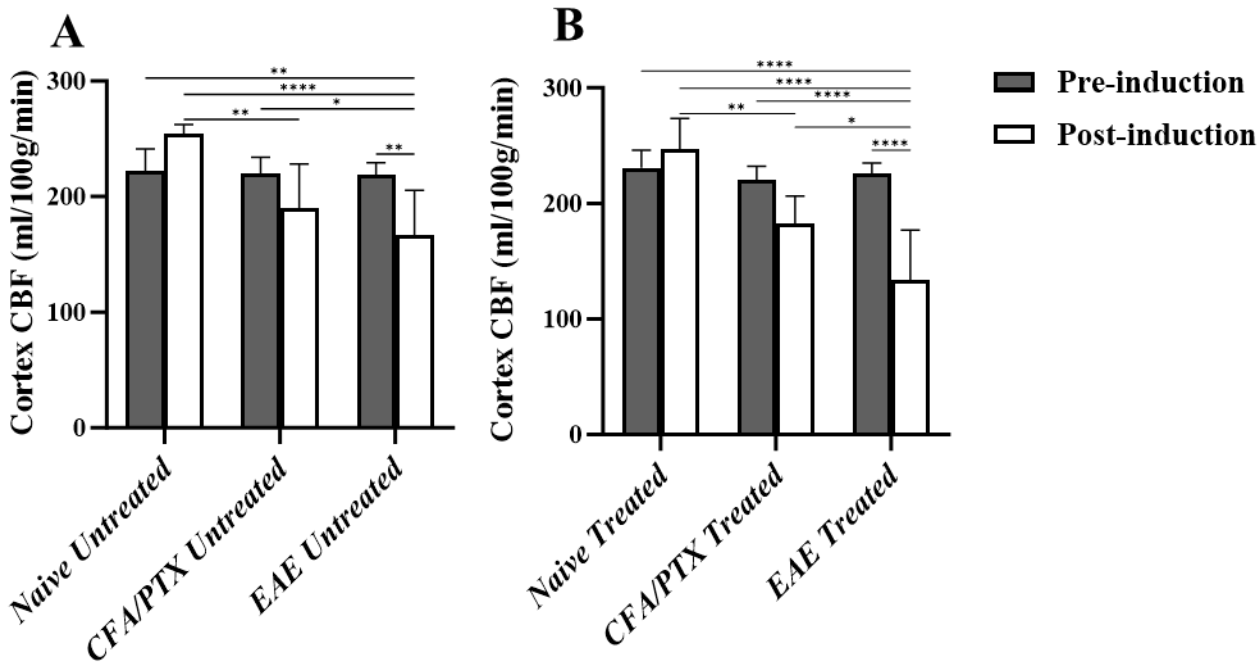

Figure 11: Mean CBF measured in the cortex of untreated (A) and treated mice (B).

*Animals analyzed in the cortex region were EAE, CFA/PTX, and naïve each for both groups. Pre-induction (Figure 10) and post-induction mean±SD for each groups were CBF EAE (166 ± 39.1 ml·100g^{-1}·min^{-1}), CFA/PTX (190 ± 38.2 ml·100g^{-1}·min^{-1}), and naïve (254 ± 8.1 ml·100g^{-1}·min^{-1}) for untreated (A) and EAE (134 ± 42.9 ml·100g^{-1}·min^{-1}), CFA/PTX (183 ±23.8 ml·100g^{-1}·min^{-1}), and naïve (247 ± 26.1 ml·100g^{-1}·min^{-1}) for treated group (B). Significant difference was observed among groups; ****p<0.0001, **p<0.01, *p<0.05. Dark gray bars represent cortex pre-induction CBF while white bars represent post-induction CBF in untreated mice (A) and treated mice (B). Bars represent standard deviation.*

After oxygen treatment, we found a decrease in CFA/PTX and EAE compared to naïve CBF. We then determined the effect of oxygen treatment in the CBF of treated mice factoring pre- and post-induction CBF. In the EAE cortex, mixed-model ANOVA result revealed a significant difference between the treated controls (naïve and CFA/PTX) and EAE; $p<0.05$; ($F(2,32) = 13.99$, ****$p<0.0001$) (**Figure 11B**). Mean EAE (134 ± 42.9 ml·100g^{-1}·min^{-1}), CFA/PTX (183 ±23.8 ml·100g^{-1}·min^{-1}), and naïve (247 ± 26.1 ml·100g^{-1}·min^{-1}) treated groups were shown in **Table 2**.

Finally, we determined the effects of oxygen treatment. Here we used two types of comparisons. We calculated the change in parameters for each animal in all groups. We subtracted the values of post-induction/treatment from baseline CBF values. This provided a change in parameter. We then computed a one-way ANOVA for all mice. We found a drastic CBF reduction in CFA/PTX and EAE, especially in EAE-treated mice. However, a significant difference was seen between controls (CFA/PTX and naïve) vs. EAE; *p<0.05; F (32) = 11.82, ****p0.0001) (**Figure 12**). After this, we then used a student-paired t-test to compare each group with or without oxygen treatment. There was no significant difference between treated and untreated mice for each group, $p>0.05$ except for EAE treated vs. untreated *$p<0.05$.

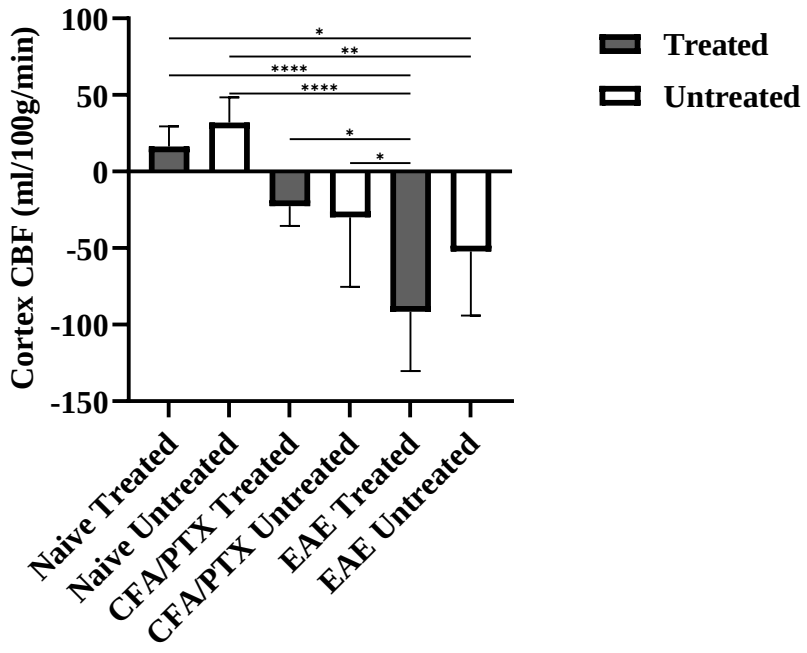

Figure 12: Mean CBF difference measured in the cortex brain region of all mice.

*Animals analyzed in the cortex region were EAE, CFA/PTX, and naïve, each for both groups. Significant difference was observed among groups; ****p<0.0001, **p<0.01, *p<0.05. Mean±SD for each group was -92±36.5 ml·100g^{-1}·min^{-1}, -52±39.5 ml·100g^{-1}·min^{-1} for EAE, -23±11.6 ml·100g^{-1}·min^{-1}, -30±40.7 ml·100g^{-1}·min^{-1} for CFA/PTX, and naïve 16 ± 11.8 ml·100g^{-1}·min^{-1} , 32±14.6ml·100g^{-1}·min^{-1} treated and untreated mice respectively. Dark gray bars represent treated while white bars represent untreated mice. Bars represent standard deviation.*

2.4.2 Oxygen Treatment in Improving CBF in the hippocampus of EAE Mice.

In the hippocampus, at baseline, no significant difference was found for all groups ($p>0.05$); EAE (188 ± 9.8 ml·100g^{-1}·min^{-1}, 188 ± 10.1 ml·100g^{-1}·min^{-1}), CFA/PTX (192 ± 35.3 ml·100g^{-}

^{1}·min^{-1}, 186 ± 9.3 ml·100g^{-1}·min^{-1}), and naïve (193 ± 13.1 ml·100g^{-1}·min^{-1}, 189 ± 23.9 ml·100g^{-1}·min^{-1},) untreated vs. treated respectively, (F(5,32) = 0.10, p = 0.99) **(Figure 13)**.

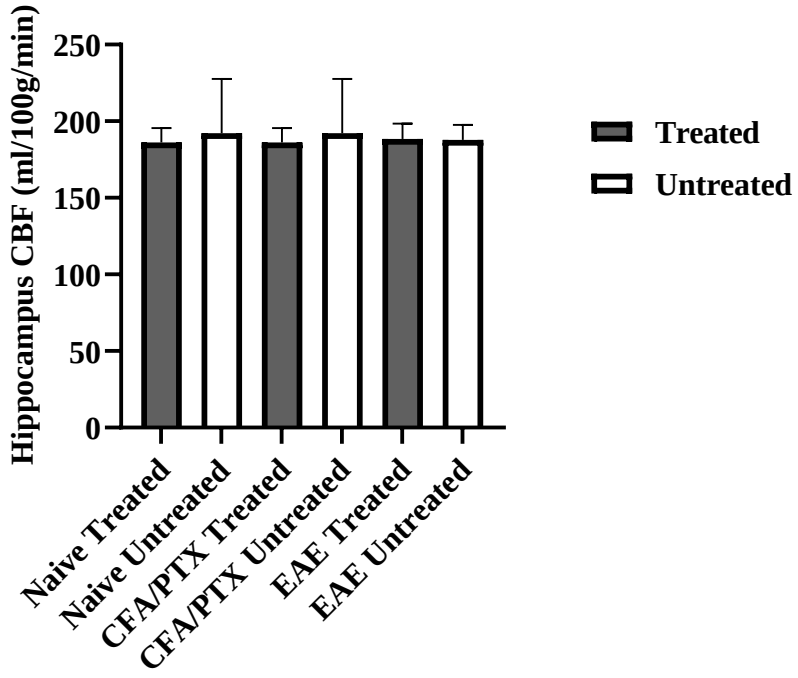

Figure 13: Baseline mean CBF measured in the hippocampus of all mice.

Animals analyzed in the hippocampus region at baseline were EAE, CFA/PTX, and naïve, each for both groups. No significant difference was observed at baseline; p>0.05. CBF mean±SD for each group for EAE was 188 ± 9.8 ml·100g^{-1}·min^{-1}, 188 ± 10.1 ml·100g^{-1}·min^{-1}), CFA/PTX (192 ± 35.3 ml·100g^{-1}·min^{-1}, 186 ± 9.3 ml·100g^{-1}·min^{-1}), and naïve (193 ± 13.1 ml·100g^{-1}·min^{-1}, 189 ± 23.9 ml·100g^{-1}·min^{-1}) untreated and treated respectively. Dark gray bars represent treated while white bars represent untreated mice. Bars represent standard deviation.

Next, we determined if there were group differences after induction in mice without oxygen treatment taking into consideration their baseline CBF. We computed this with a mixed-model ANOVA. We found no significant difference in the CBF hippocampus among untreated groups,

p>0.05. However, we observed no variance in CBF of naïve, CFA/PTX, and EAE after induction; F (2,32) = 0.64, p = 0.5304). (**Figure 14A**).

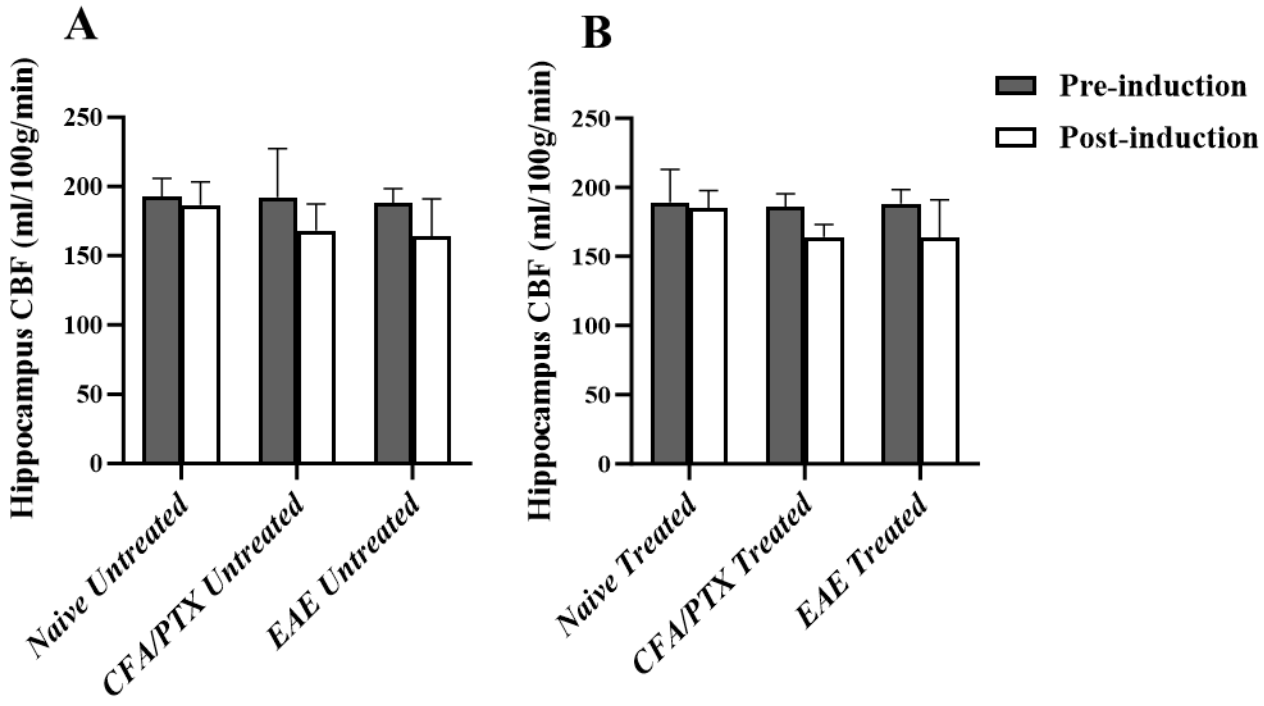

Figure 14: Mean CBF measured in the hippocampus of untreated (A) and treated (B) mice.

Animals analyzed in the hippocampus region were EAE, CFA/PTX, and naïve for each group. No significant difference was observed among groups; p>0.05. CBF pre-induction (Figure 13), and post-induction mean±SD for each EAE group were (164 ± 27.8 ml·100g^{-1}·min^{-1}), CFA/PTX (168 ± 19.0 ml·100g^{-1}·min^{-1}), and naïve (186 ± 16.7 ml·100g^{-1}·min^{-1}) for untreated (A) and EAE (163 ± 27.3 ml·100g-1·min^{-1}), CFA/PTX (164 ± 8.9 ml·100g-1·min^{-1}), and naïve (185 ± 12.7 ml·100g-1·min^{-1}) for treated group (B). Dark gray bars represent hippocampus pre-induction CBF while white bars represent post-induction CBF in untreated mice (A) and treated mice (B). Bars represent standard deviation.

Following oxygen treatment, we then performed a mixed-model ANOVA to compare the mean differences of treated groups with time points. Results revealed no significant difference

(p>0.05) in the EAE hippocampus of treated compared to CFA/PTX and naïve mice; F (2,32) = 1.09, p = 0.3463) (**Figure 14B**). Finally, to further determine the effect of oxygen treatment, we first computed the change in parameter by subtracting the post-treatment CBF of all mice from pre-induction CBF values. We compared the absolute values across groups utilizing a one-way ANOVA, F(5,32) = 0.7216, p = 0.6121). We found no significant difference among groups (**Figure 15**). Following this, we used a paired t-test to compare each group with and without oxygen treatment. We found no significant difference in the hippocampus between treated and untreated mice for each group, p>0.05. However, both EAE and CFA hippocampus-treated mice showed no significant change in CBF notwithstanding oxygen treatment.

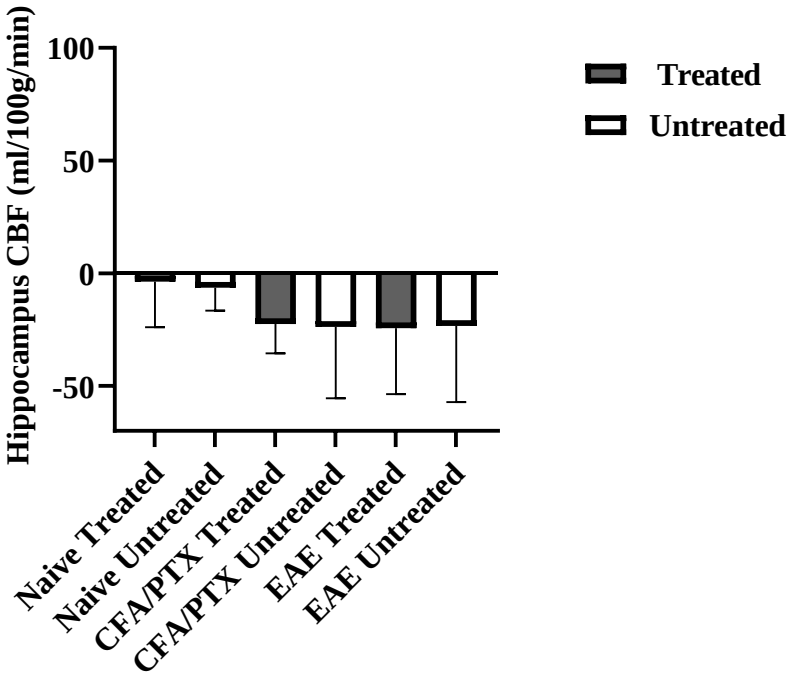

Figure 15: Mean CBF difference measured in the hippocampus of all mice.

Animals analyzed in the cortex region were EAE, CFA/PTX, and naïve, each for both groups. No significant difference was observed among groups; p>0.05. Mean±SD for each group was -24±27.6 ml·100g^{-1}·min^{-1}, -23±31.9 ml·100g^{-1}·min^{-1} for EAE, -23±11.6 ml·100g^{-1}·min^{-1},-24 ±28.3 ml·100g^{-1}·min^{-1} for CFA/PTX, and naïve -4±18.1 ml·100g^{-1}·min^{-1}, -6 ±9.2ml·100g^{-1}·min^{-1} treated and untreated mice

respectively. Dark gray bars represent treated while white bars represent untreated mice. Bars represent standard deviation.

2.4.3 Oxygen Treatment in Improving CBF in the Thalamus of EAE Mice.

More so, in the thalamus, we ruled out the possibility that group differences may be due to differences in CBF mice at baseline. Thus, we utilized a one-way ANOVA and found no significant difference across the group at baseline; EAE CBF thalamus (262 ± 7.1 ml·100g^{-1}·min^{-1}, 261 ± 14.3 ml·100g^{-1}·min^{-1}), CFAPTX (255 ± 7.5 ml·100g^{-1}·min^{-1}, 267 ± 7.4 ml·100g^{-1}·min^{-1}), and naïve (257 ± 13.9 ml·100g^{-1}·min^{-1}, 261 ± 7.1 ml·100g^{-1}·min^{-1}) untreated and treated respectively; ($F(5,32) = 0.84$, $p = 0.52$) **(Figure 16)**.

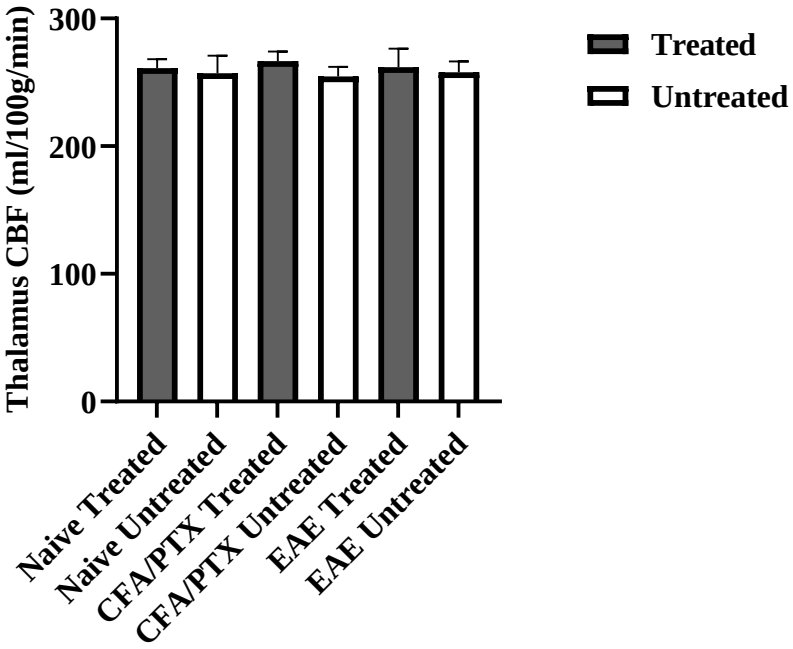

Figure 16: Baseline mean CBF measured in the thalamus of all mice.

Animals analyzed in the thalamus region were EAE, CFA/PTX, and naïve, each for both groups. No significant difference was observed among groups; p>0.05. CBF mean±SD for each group of EAE was

262 ± 7.1 ml·100g^{-1}·min^{-1}, 261 ± 14.3 ml·100g^{-1}·min^{-1}, CFAPTX 255 ± 7.5 ml·100g^{-1}·min^{-1}, 267 ± 7.4 ml·100g^{-1}·min^{-1}, and naïve 257 ± 13.9 ml·100g^{-1}·min^{-1}, 261 ± 7.1 ml·100g^{-1}·min^{-1}; untreated and treated respectively. Dark gray bars represent treated while white bars represent untreated mice. Bars represent standard deviation.

We further determined if there were group differences without oxygen treatment. In this case, we compared the CBF of untreated mice in the thalamus at time points. Using a mixed-model ANOVA, we found a significant difference in the pre and post-induction CBF of naïve and CFA/PTX compared to EAE, ****p<0.0001, ***p = 0.0004, ** p = 0.0032; (F(2,32) = 9.51, ***p = 0.0006). However, pre-induction EAE CBF was significantly different from the post-induction (**Figure 17A**).

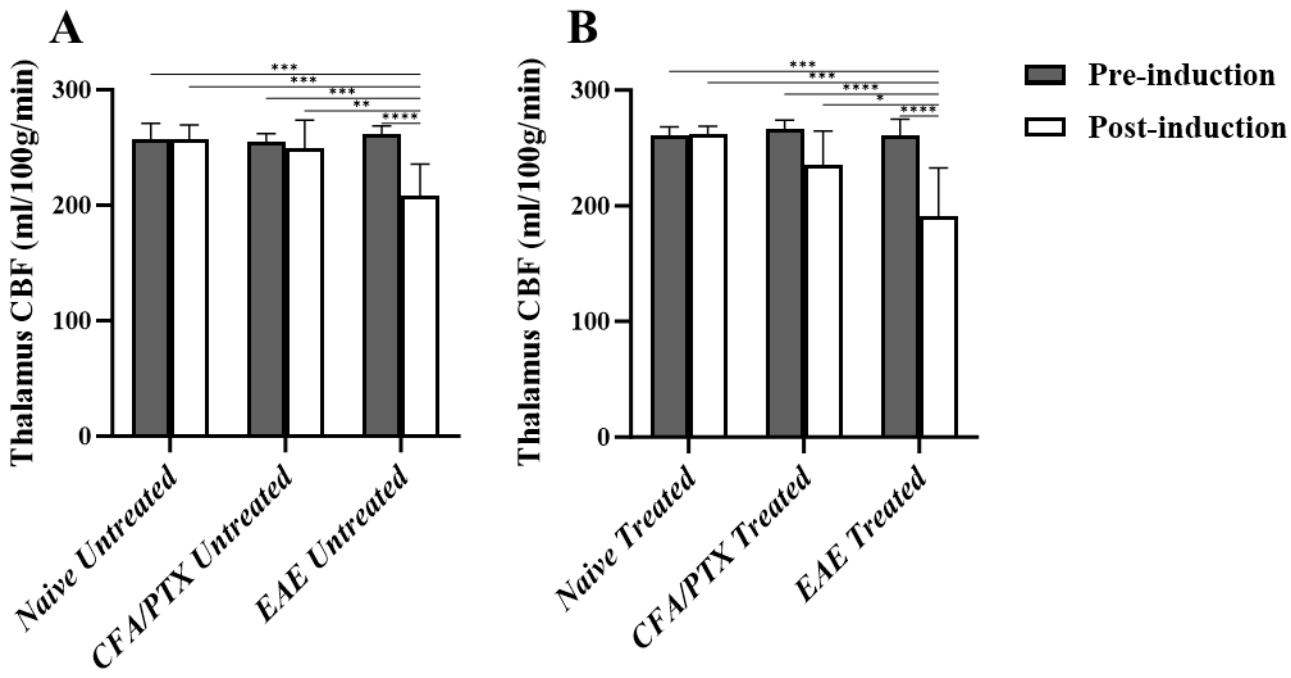

Figure 17: Mean CBF measured in the thalamus of untreated (A) and treated (B) mice.

*Animals analyzed in the thalamus region were EAE, CFA/PTX, and naïve each for both groups. Significant difference was observed among groups; ****p<0.0001, ***p<0.001, **p<0.01, *p<0.05. CBF pre-induction (Figure 16), and post-induction mean±SD for each EAE group was 208 ± 27.4 ml·100g^{-1}·min^{-1}, CFA/PTX (250 ± 24.2ml·100g^{-1}·min^{-1} , and naïve (257 ± 12.2 ml·100g^{-1}·min^{-1}) for untreated (A) and EAE 191 ± 41.8ml·100g^{-1}·min^{-1}), CFA/PTX (235 ± 29.3ml·100g^{-1}·min^{-1}), and naïve (261 ± 7.1ml·100g^{-1}·min^{-1}) for treated group (B). Dark gray bars represent hippocampus pre-induction CBF while white bars represent post-induction CBF in untreated mice (A) and treated mice (B). Bars represent standard deviation.*

After oxygen treatment, we employed a mixed-model ANOVA to determine the effect of treatment in the oxygen-treated mice considering pre-induction CBF **(Figure 17B)**. As reported previously in the cortex and hippocampus, we found a significant difference between the CBF of the controls (naïve and CFA/PTX) and EAE; ****p<0.0001, ***p=0.002, * p=0.0323; ($F(2,32) = 6.76$, **p = 0.036). We also found a significant difference between pre-induction and post-treatment EAE thalamus CBF ****p<0.0001 **(Figure 17B)**. Furthermore, we analyzed the change in thalamus CBF parameters following induction and treatment by subtracting post-induction CBF values from pre-induction values for all mice and computed a one-way ANOVA with Tukey's multiple comparisons **(Figure 18)**. We found a significant difference between the controls and the EAE, **p=0.0013, *p=0.0223;($F(5,32) = 7.60$, ****p< 0.0001). Also, with a paired t-test, no significant difference was seen in each group with or without treatment, p>0.05, except for CFA/PTX treated vs. untreated, p=0.0334. Thalamus mean±SD values are shown in **Table 2**.

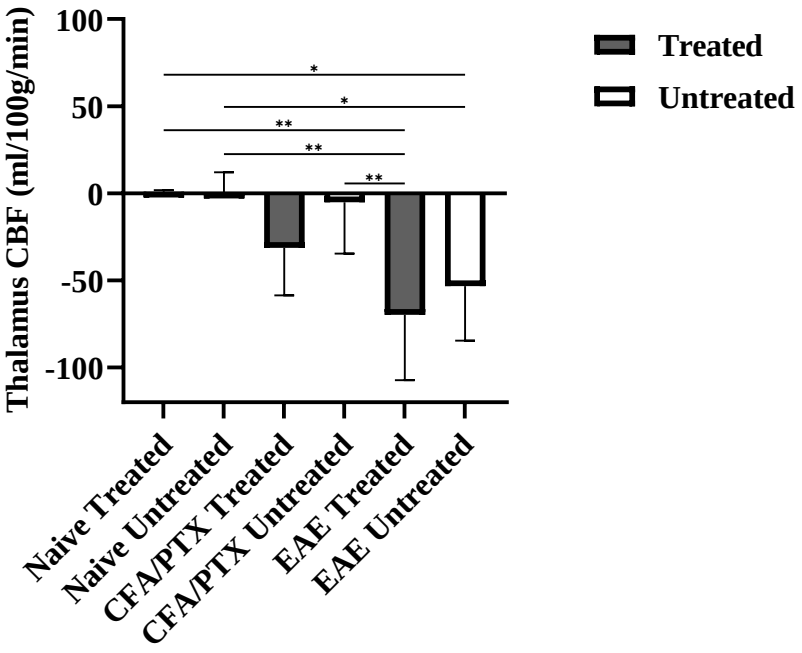

Figure 18: Mean CBF differences measured in the thalamus of all mice.

*Animals analyzed in the thalamus region were EAE, CFA/PTX, and naïve each for each group. A significant difference was observed among groups; **p<0.01, *p<0.05. Mean±SD for each EAE group was -53 ± 28.0 ml·100g^{-1}·min^{-1}, -69.8±24.1 ml·100g^{-1}·min^{-1}, CFA/PTX -31.4 ± 22.2 ml·100g^{-1}·min^{-1} , -5.2± 24.1 ml·100g^{-1}·min^{-1} and naïve 1±0.9 ml·100g^{-1}·min^{-1}, 0±9.5ml·100g^{-1}·min^{-1} treated and untreated mice respectively. Dark gray bars represent treated while white bars represent untreated mice. Bars represent standard deviation.*

Table 2: Mean CBF of different ROIs in all mice after induction/treatment.

Mice groups	Cortex Mean±SD	Hippocampus Mean±SD	Thalamus Mean±SD
EAE untreated	166 ± 39.1	164 ± 27.8	208 ± 27.4
EAE treated	134 ± 42.9	163 ± 27.3	191 ± 41.8
CFA/PTX untreated	190 ± 38.2	168 ± 19.0	250 ± 24.2
CFA/PTX treated	183 ±23.8	164 ± 8.9	235 ± 29.3
Naïve untreated	254 ± 8.1	186 ± 16.7	257 ± 12.2
Naïve treated	247 ± 26.1	185 ± 12.7	261 ± 7.1

2.5 Discussion and Conclusion

This chapter investigated the impact of oxygen treatment on CBF using ASL perfusion MRI. The study hypothesis was that oxygen treatment would improve disease by enhancing CBF and reducing hypoxia in the EAE mice. Our results revealed that systemic immunization with MOG led to a significant decrease ($p<0.05$) in CBF in the cortex and thalamus in both treated and untreated EAE groups compared with naïve controls. Also, CBF in the cortex was reduced in the CFA/PTX control vs. naïve controls. However, significant CBF reductions were observed in the cortex and thalamus of control (naïve, and CFA/PTX) vs. EAE mice with or without treatment, $p<0.05$.

Furthermore, in the cortex and thalamus of EAE-treated mice, there was more CBF reduction compared to the untreated groups, but this variation is not significant. This unexpected occurrence contradicted our initial hypothesis and needs further investigation. More so, we found CBF reduction in the EAE and CFA/PTX **(Figures 12, 15, and 18)** compared to naïve after oxygen treatment. However, we found significant CBF reduction in the EAE-treated cortex and thalamus compared to the control group, **(Figure 12 and Figure 18)** compared to the hippocampus region, and this could be due to disease severity in those regions. In the hippocampus (**Figure 15**), both treated and untreated CFA/PTX and EAE mice showed almost the same CBF reduction, with no observed significant difference across groups. The alterations in CBF in EAE, after MOG administration, may be attributed to inflammation and the potential for hypoxia. Our result demonstrated hypoperfusion in the EAE MS model and is supported by recent literature on the role of low CBF in the pathogenesis of MS (Hostenbach et al., 2020; Jakimovski et al., 2022).

Research has revealed that systemic inflammation impacts CBF on tissues (Murray et al., 2014). It was proposed to be caused by a dysfunction of the BBB (Murray et al., 2014). This explains how systemic inflammation can cause hypoperfusion and impaired treatment recovery (Murray et al., 2014). In addition, hypoperfusion has been linked to brain lesions. Pathological and imaging studies provided evidence of ischemic changes during type III lesions. Also, cognitive impairment in pwMS is correlated with lower white matter perfusion (De Keyser et al., 2008).

However, under pathological conditions, reduced CBF leads to an increased likelihood of having a hypoxic environment, as there may be inadequate blood flow to compensate for hypoxia. This study showed that stimulation of inflammation with CFA/PTX induced hypoperfusion in EAE. It also showed that repeated oxygen treatment had minimal effect on CBF. The insufficient supply of oxygen to brain tissue area resulting from low CBF could have a significant role in disease progression, including cell death. Nonetheless, a recent study utilized NBO in chronic cerebral circulation insufficiency which is characterized by a long-term reduction in CBF (Ding et al., 2019). The study revealed that NBO increased intracranial oxygen partial pressure, stimulated antioxidants, and reduced ROS (Ding et al., 2019). We have demonstrated that neuroinflammation can reduce CBF in EAE and this can worsen disease outcomes and irresponsiveness of NBO oxygen treatment.

To conclude, this study demonstrated that low CBF in the EAE, and CFA/PTX CBF might contribute to disease progression. However, there was a significant difference between the EAE (treated and untreated) and naïve treated vs. untreated $p<0.05$. We also found a decrease in CBF of the treated and untreated CFA/PTX compared to naive mice. Reductions in CBF have also been observed in pwMS (Jakimovski et al., 2020). However, the duration of administered NBO was not

sufficient to improve disease outcomes of EAE mice. We elaborated more on this in the last **Chapter**.

CHAPTER THREE:
ASSESSING THE EFFECT OF OXYGEN TREATMENT ON HYPOXIA IN THE EAE

3.1. Introduction

Cerebral hypoxia is caused by a decrease in the supply of oxygen to the brain tissues. Brain oxygenation is vital for the proper functioning of brain cells. This is essential as the brain requires a good amount of oxygen for various metabolic and neurological functions. Insufficient/reduced blood supply discussed in **Chapter 2,** can give rise to a hypoxic environment. Other conditions such as traumatic brain injury (Hadanny & Efrati, 2015), ischemia (Liu et al., 2023), and stroke (Kossorotoff, 2012) can lead to inadequate oxygen levels in the brain.

Cerebral hypoxia can range from mild to severe brain damage, depending on the duration and severity of oxygen starvation. Therapeutic intervention that restores oxygen supply to the brain and prevents further damage is crucial for recovery. The extent of recovery may depend on the duration of oxygen deprivation, the time and effectiveness of medical intervention, overall individual health status, and the extent of brain damage. This chapter investigated the efficiency of the 6-hour duration of normobaric oxygen in reversing hypoxia in the EAE mouse model.

The transverse relaxation rate (R_2*) is sensitive to deoxyhemoglobin in tissues. Deoxyhemoglobin, being paramagnetic, creates inhomogeneities in the magnetic field, which in turn increases the R_2* value. (Blockley & Stone, 2016). R_2* has been utilized to extract information about deoxyhemoglobin content in brain tissue (Fujita et al., 2003). This means that areas with higher concentrations of deoxyhemoglobin will have higher R_2* values. It has been utilized to examine the oxygenation status of tissues, as it reflects the content of deoxyhemoglobin but can also be influenced by other factors such as field inhomogeneities (Choi et al., 2016).

Quantitative susceptibility mapping (QSM), on the other hand, is a technique that quantifies the magnetic susceptibility of tissue. It is sensitive to paramagnetic (deoxyhemoglobin) and diamagnetic substances (myelin). It has been employed to evaluate myelin (Rahmanzadeh et al., 2022) and iron content in the brain (Langkammer et al., 2012) and in MS (Gillen et al., 2021) by measuring changes in magnetic susceptibility. Increased deoxyhemoglobin will reduce the frequency in quantitative susceptibility mapping. Employing R_2* and QSM can provide more understanding of tissue oxygenation and iron content. Both parameters can be calculated from a single acquisition protocol of multi-gradient echo imaging. For these reasons, we applied R_2* and QSM measurements as an indirect measure of increased deoxyhemoglobin, which is also an indirect measure of hypoxia.

3.2. Methods

3.2.1 Study Ethics

All experimental procedures were performed with the guidelines of the Canadian Council of Animal Care. This study was approved by the Animal Care Committee, University of Calgary (AC19-0036).

3.2.2 Animal

Female C57BL/6 mice aged (8-10 weeks old) were purchased from Charles Rivers Laboratory. The animals were housed under standard environmental conditions, with five mice per cage in the animal halfway house facility. All mice groups (EAE, n = 18, 9 treated, 9 untreated), CFA, n = 10 (5 treated, 5 untreated), Naïve, n = 10 (5 treated, 5 untreated) were subjected to the

same handling, clinical disease scoring, open-field (OF) test, and MRI. These animals were the same as those used in the CBF study.

3.2.3 EAE Induction

EAE induction was performed on the day after the first R_2* MRI and open-field baseline measurement. EAE and CFA mice were anaesthetized with mild ketamine/xylazine anesthesia. This was followed by subcutaneous injection with 50µl myelin oligodendrocyte glycoprotein (MOG)33-55 mixed in complete Freund's adjuvant (CFA), comprised of 10 mg/ml of mycobacterium tuberculosis into each side of flank which triggered an autoimmune response. This was followed by intraperitoneal (ip) administration of 200ml of pertussis toxin (PTX) (300ng PTX in 200µl of PBS (phosphate buffer saline)) on day 0 and day 2. CFA/PTX mice were induced with only PTX on day 0. Naive mice received no injection.

3.2.4 Post-Induction

Following induction, animals were monitored from 6 - 14 days post-induction to check for symptoms. At the onset of symptoms, day 14-17, clinical disease score was assessed daily, and recorded from 14,15 - 20 days post-induction. The second OF test was performed before oxygen treatment, and the last OF was carried out a day after oxygen treatment, which was compared to the OF baseline (before induction). All experimental animals were randomly grouped into two treatment groups (treated and untreated) at symptom onset. Symptomatic EAE mice were further subdivided into treated and untreated groups **(Figure 8).** This helped to control for an even distribution of disease severity. The last R_2* MRI/OF was done a day after oxygen treatment.

3.2.5 Oxygen Administration

Oxygen treatment was the same in Chapter 2 for all mice in the treated groups.

3.2.6 Data Processing and Statistical Analysis

We utilized ImageJ software for R_2* data processing. The MRI analysis calculator plugin was employed to generate a T_2* map. Using the same ROIs employed in the CBF analysis in Chapter 2, the T_2* intensity was measured. To obtain R_2*, the T_2* values in each brain region were inverted, R_2* = 1/ T_2* value. Measurement occurred in the cortex, hippocampus, and the thalamus (**Figure 9**). A 3D multi-gradient echo sequence was used for T_2* (TR = 100ms, TE = 3.1248. 7.1248 11.1248 15.1248 19.1248 ms, echo spacing = 4ms, matrix = 128x106x62 mm, FOV = 19.2x15.9x9.3 mm).

3.3 Results

3.3.1 Oxygen Treatment in Ameliorating Hypoxia in the cortex of EAE Mice.

The number of mice in R_2* data was the same for CBF in **Chapter 2** except for the untreated naïve mice at pre-induction which has n = 4. We couldn't collect data for one mouse due to a respiratory problem that occurred during MRI data collection. A one-way ANOVA test was used to determine variance and compare the mean differences between groups. Each experimental group has treated and an untreated subgroup of EAE (n = 18; 9 treated, 9 untreated), CFA/PTX (n =10; 5 treated, 5 untreated), and naïve (n= 9; 5 treated, 4 untreated at pre-induction, 5 untreated after

induction). At baseline (before induction) we found no significant difference (**Figure 19**) in the EAE (26 ± 1.3 ms^{-1}, 28 ±2.2 ms^{-1}), CFA/PTX (27 ±1.1 ms^{-1}, 27 ± 0.9 ms^{-1}) and naïve (27 ± 0.8 ms^{-1}, 27 ±1.9 ms^{-1}; p>0.05); F(5,31) = 0.74, p = 0.5966), in the untreated and treated cortex respectively.

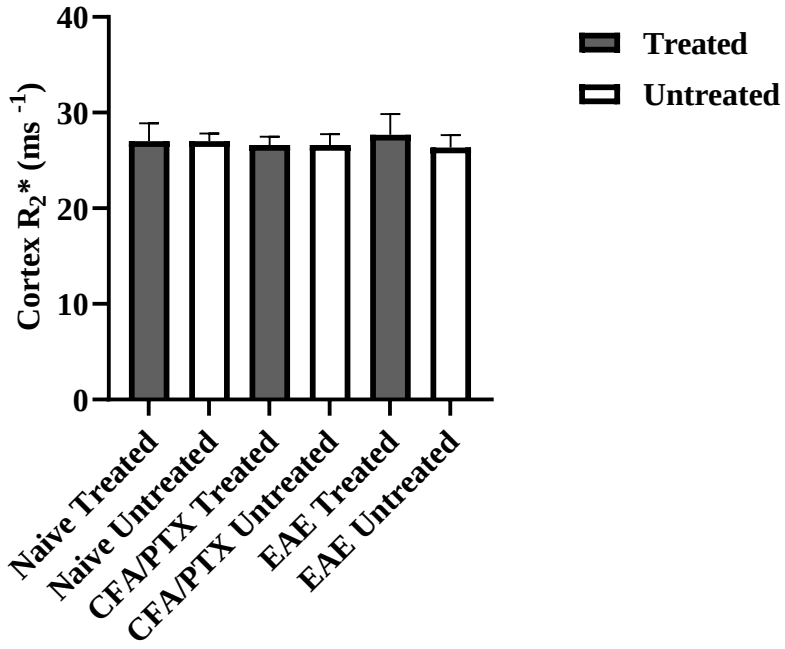

Figure 19: Baseline mean R_2* measured in the cortex of treated and untreated mice.

Transverse relation rate (T_2) measured in the cortex brain region. R_2* is calculated as the inverse of T_2*. Animals analyzed in the cortex region were EAE, CFA/PTX, and naïve, for each group (treated/untreated). No significant difference was observed among groups; p>0.05. Mice mean±SD values were 26 ± 1.3 ms^{-1}, 28 ±2.2 ms^{-1} for EAE, 27 ±1.1 ms^{-1}, 27 ± 0.9 ms^{-1} for CFA/PTX, and naïve, 27 ± 0.8 ms^{-1}, 27 ±1.9 ms^{-1}, untreated and treated mice respectively. Dark gray bars represent treated while white bars represent untreated mice. Bars represent standard deviation.*

Following induction, we asked if there were group differences without oxygen treatment. Here we compared all mice in the untreated groups at the two time points **(Figure 20A)**. Increased R_2* was observed in the untreated EAE (pre 26 ± 1.3 ms^{-1} and post 29 ± 2.7 ms^{-1}). This was not in the controls; CFA/PTX (pre 27 ±1.1 ms^{-1} and post 28 ±1.3 ms^{-1}), and naïve (pre 27 ± 0.8 ms^{-1} and post 26 ± 1.1 ms^{-1}) mean±SD. Using a mixed-model ANOVA, we found a significant difference only in the EAE pre vs. post induction but not in other groups, *p=0.0166; F(2,31) = 3.05, p = 0.0615).

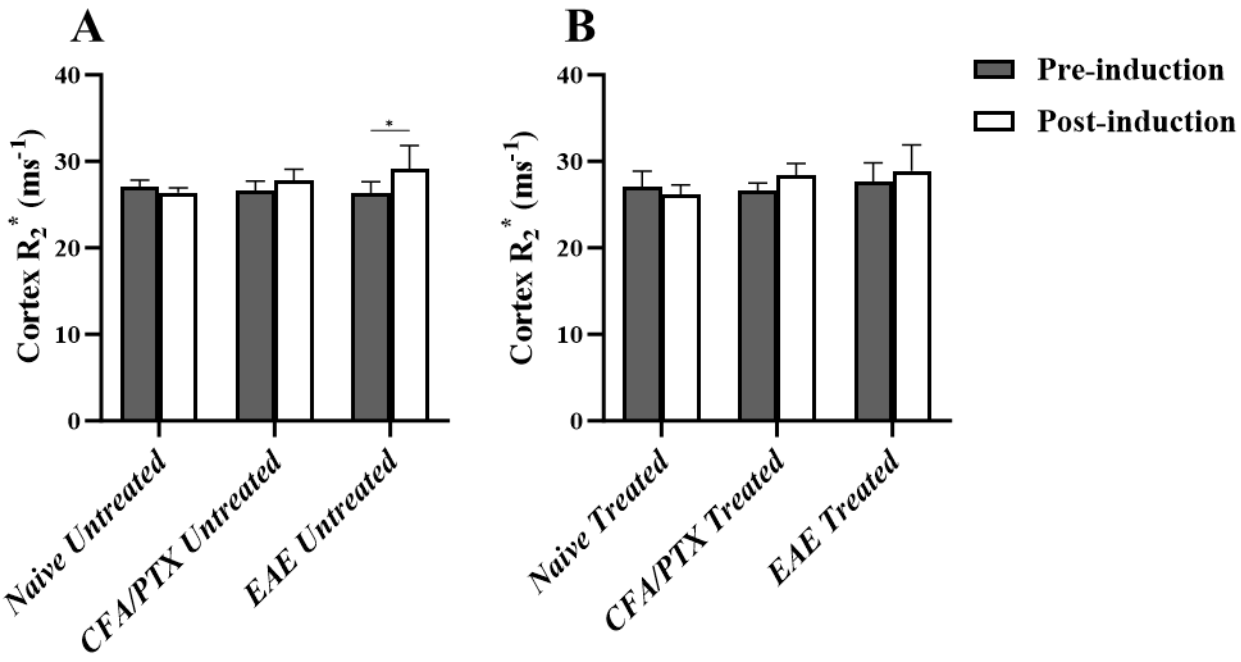

Figure 20: Mean R_2* measured in the cortex of untreated (A) and treated mice (B).

Mice analyzed in the cortex region were EAE, CFA/PTX, and naïve, each for both groups. A significant difference was observed between pre- and post-EAE untreated R_2; *p<0.05. R_2* pre-induction (Figure 19), and post-induction mean±SD for each EAE group was 29 ± 2.7 ms^{-1}, CFA/PTX 28 ±1.3 ms^{-1}, and naïve 26 ± 1.1 ms^{-1} for untreated (A) group, and EAE (29 ± 3.0 ms^{-1}), CFA/PTX (28 ± 1.3 ms^{-1}) and naive (26 ± 0.5 ms^{-1}) for treated group (B). Dark gray bars represent R_2* cortex pre-induction while white bars represent post-induction in untreated mice (A) and treated mice (B). Bars represent standard deviation.*

Following oxygen treatment, R_2* of treated mice was computed with a mixed-model ANOVA. There were no significant differences among the treated group of mice, EAE (29 ± 3.0 ms^{-1}), CFA/PTX (28 ± 1.3 ms^{-1}) and naive (26 ± 0.5 ms^{-1}); ($F(2,32) = 1.10$, $p = 0.3431$) **(Figure 20B)**. More so, we computed the change in the R_2* by subtracting R_2* post-induction/treatment values from pre-induction. Then, we utilized two comparisons, using a student t-test to compare each group with or without treatment and one-way ANOVA to compare across groups in the cortex. T-test revealed no significant difference between treated and untreated mice in each group, $p>0.05$. One-way ANOVA also revealed no significant difference among the groups (treated and untreated), $p>0.05$; ($F(5,30) = 0.9432$, $p = 0.4676$) **(Figure 21)**. Naïve mice employed for R_2* change in parameter calculation was n=4 and for other ROIs.

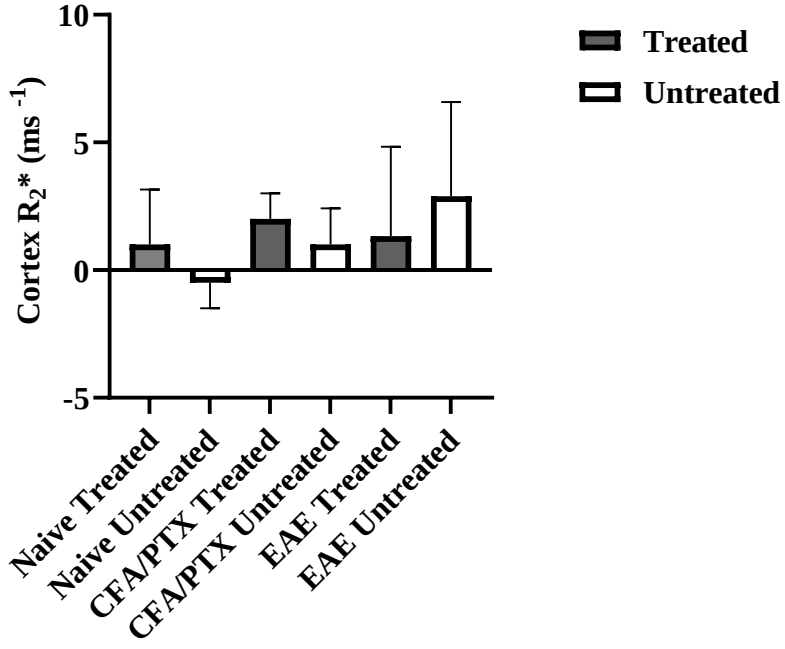

Figure 21: Mean R_2* differences measured in the cortex of all mice.

Mice analyzed in the cortex region were EAE, CFA/PTX, and naive, each for each group. No significant difference was observed among groups; $p>0.05$. R_2 Mean±SD for each group of the EAE was, 1.3 ± 3.3*

ms^{-1}, 2.5 ± 3.5 ms^{-1}, CFA/PTX 2.0 ± 0.9 ms^{-1}, 0.8 ± 1.3 ms^{-1}, and naïve 1.0 ± 1.9 ms^{-1}, -0.5 ± 0.9 ms^{-1} treated and untreated mice respectively. Dark gray bars represent treated while white bars represent untreated mice. Bars represent standard deviation.

3.3.2 Oxygen Treatment in Ameliorating Hypoxia in the Hippocampus of EAE Mice.

At baseline, there were no significant differences in the hippocampus R_2* mean of the EAE (27 ±2.2 ms-1, 29 ± 2.6 ms^{-1}), CFA/PTX (27 ±1.5 ms-1, 28 ± 0.8 ms^{-1}), and naive (28 ± 2.1 ms^{-1}, 28 ± 2.2 ms^{-1}; p>0.05); (F(5,31) = 1.08, p = 0.3870), treated and untreated mice respectively **(Figure 22)**. Following induction, we determined if there were group mean differences without treatment (EAE, 31 ± 2.2 ms^{-1}, 32 ± 3.5 ms^{-1}; CFA/PTX, 28 ± 2.3 ms^{-1}, 27 ± 1.5 ms^{-1}, and naïve 28 ±1.3 ms^{-1}, 27 ±1.8 ms^{-1} untreated and treated respectively).

We compared mice in the untreated group using a mixed-model ANOVA **(Figure 23A)**. We found significant differences between R_2* CFA/PTX pre-induction vs. EAE post-induction and R_2*, EAE pre-induction vs. post-induction, *p=0.0435; while close/no significance was observed in ANOVA (F(2,31) = 2.662, p = 0.0858).

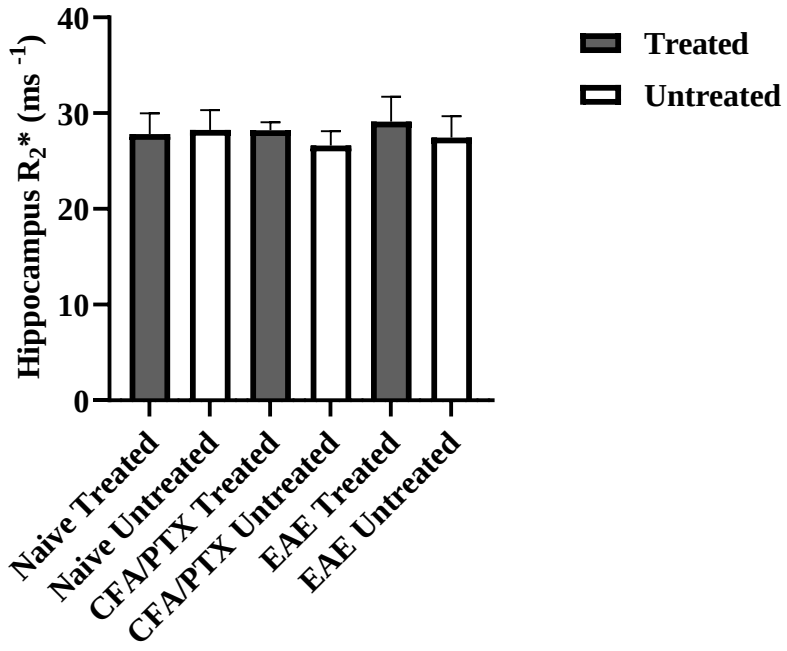

Figure 22: Baseline mean R_2* measured in the hippocampus of treated and untreated mice.

Transverse relation rate (T_2) measured in the hippocampus brain region. R_2* was calculated as the inverse of T_2*. Animals analyzed in this region were EAE, CFA/PTX, and naive, for each group (treated/untreated). No significant difference was observed among groups; $p>0.05$. Mice mean±SD values of the EAE mice were 27 ± 2.2 ms^{-1}, 29 ± 2.6 ms^{-1}, CFA/PTX 27 ± 1.5 ms^{-1}, 28 ± 0.8 ms^{-1}, and naive 28 ± 2.1 ms^{-1}, 28 ± 2.2 ms^{-1} untreated and treated mice respectively. Dark gray bars represent treated while white bars represent untreated mice. Bars represent standard deviation.*

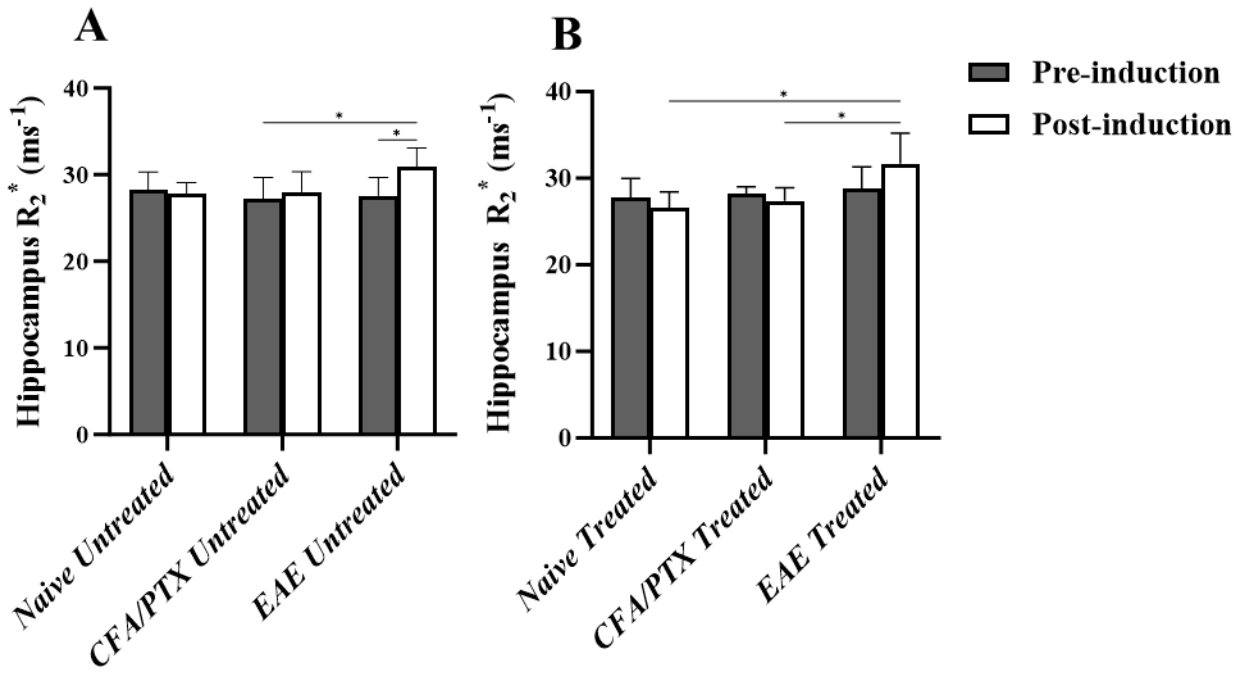

Figure 23: Mean R_2* measured in the hippocampus of untreated (B) and treated (A) mice.

Mice analyzed in the hippocampus region were EAE, CFA/PTX, and naïve, each for both groups. A significant difference was observed between pre (Figure 22) and post-EAE untreated R_2; *p<0.05. R_2* pre-induction (Figure 22), and post-induction mean±SD for each EAE group were, 31 ± 2.2 ms^{-1}, 32 ± 3.5 ms^{-1}; CFA/PTX, 28 ± 2.3 ms^{-1}, 27 ± 1.5 ms^{-1}, and naïve 28 ± 1.3 ms^{-1}, 27 ± 1.8 ms^{-1} untreated (A) and treated respectively (B). Dark gray bars represent R_2* cortex pre-induction while white bars represent post-induction in untreated mice (A) and treated mice (B). Bars represent standard deviation.*

After oxygen treatment, R_2* increased in the EAE treated, compared to CFA/PTX and naïve treated mice. With a mixed-model ANOVA, we found a significant difference between the R_2* of CFA/PTX vs. EAE post-treated, and naïve R_2* vs. EAE post-treated, *p=0.0430 **(Figure 23B)**; however, we observed a close significance in ANOVA ($F(2,32) = 2.947$, $p = 0.0669$). The difference in Tukey comparisons and ANOVA may be due to the statistical power of individual

tests to detect differences from the omnibus in treated and untreated. Next, we subtracted post-treated R_2* values from pre-induction for all mice and then employed two comparisons. We compared the change in parameters for all mice with and without oxygen treatment (**Figure 24**). R_2* increased in CFA/PTX without treatment and EAE (treated and untreated).

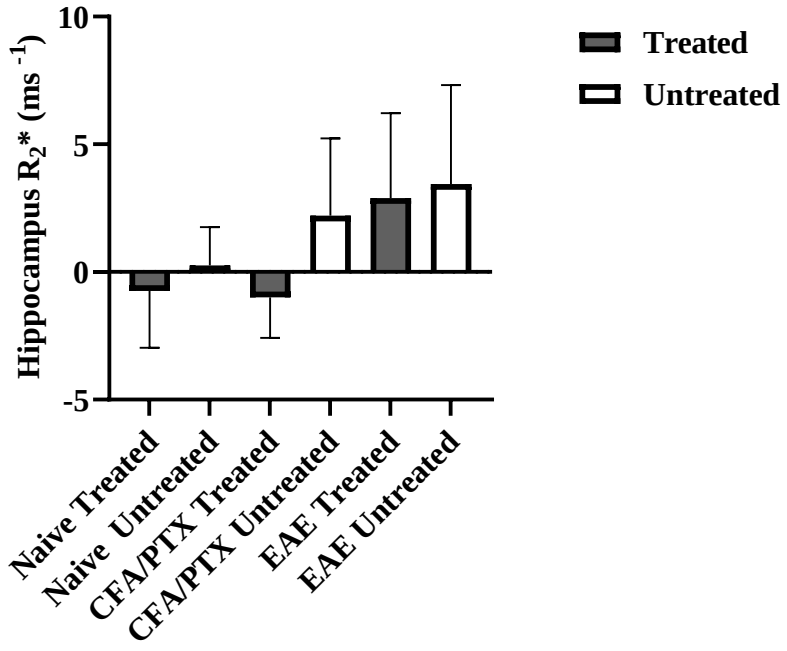

Figure 24: Mean R_2* differences measured in the hippocampus of all mice.

Mice analyzed in the hippocampus region were EAE, CFA/PTX, and naive, each for both. No significant difference was observed among groups; p>0.05. R_2 Mean±SD for each EAE group was 2.9 ± 3.1 ms^{-1}, 3.4 ±3.7 ms^{-1}, CFA/PTX -1.5 ± 1.1 ms^{-1}, 2.5 ± 3.0 ms^{-1}, and naïve -0.8 ± 1.9 ms^{-1}, 0.3 ± 1.3 ms^{-1} treated and untreated mice respectively. Dark gray bars represent treated while white bars represent untreated mice. Bars represent standard deviation.*

No significant differences were found across groups with one-way ANOVA Tukey comparisons; $F(5,30) = 2.384$, $p = 0.0619$). Lastly, we compared between treated and untreated

mice using a paired t-test and found no significant difference in the mean hippocampus of mice with and without oxygen treatment for each group, p>0.05.

3.3.3 Oxygen Treatment in Ameliorating Hypoxia in the Thalamus of EAE Mice.

At baseline, we found no significant differences (**Figure 25**) in the EAE thalamus (29 ±1.2 ms^{-1}, 29 ±1.9 ms^{-1}), CFA/PTX thalamus (29 ±1.1 ms^{-1}, 29 ±1.3 ms^{-1}), and naïve thalamus (29 ±1.0 ms^{-1}, 29 ±1.5 ms^{-1}; p>0.05) between untreated and treated group of experimental animals respectively; (F(5,31) = 0.23, p = 0.9459.

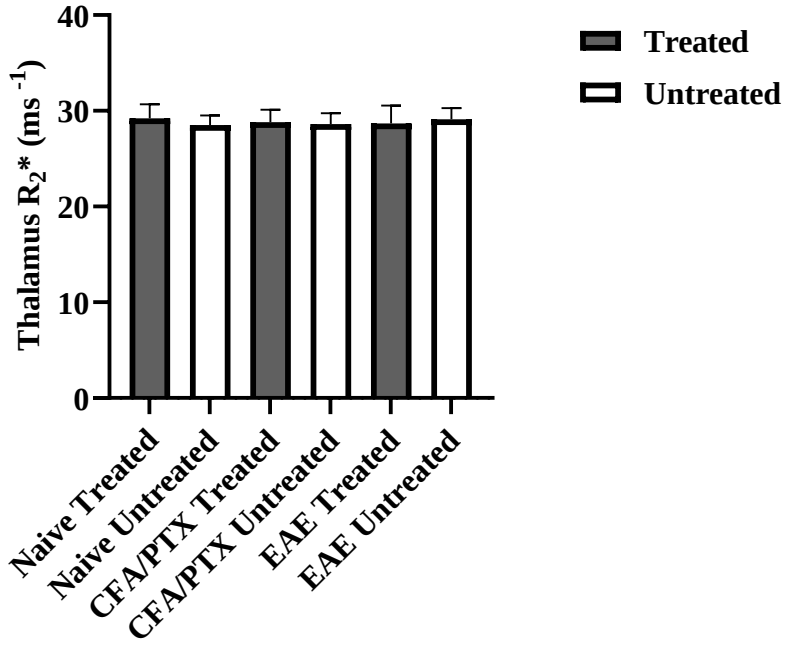

Figure 25: Baseline mean R_2* measured in the thalamus of treated and untreated mice.

Transverse relation) measured in the thalamus brain region. R_2 was calculated as the inverse of T_2*. Animals analyzed in this region were EAE, CFA/PTX, and naive, for each group (treated/untreated). No significant difference was observed among groups; p>0.05. Mice*

mean±SD values for EAE mice were 29 ± 1.2 ms^{-1}, 29 ± 1.9 ms^{-1}, CFA/PTX 29 ± 1.1 ms^{-1}, 29 ± 1.3 ms^{-1}, and naïve 29 ± 1.0 ms^{-1}, 29 ± 1.5 ms^{-1} mice untreated and treated respectively. Dark gray bars represent treated while white bars represent untreated mice. Bars represent standard deviation.

After induction/oxygen treatment, we determined if there were group differences in mice without oxygen treatment. Using a mixed-model ANOVA Tukey comparisons, we found a significant difference only in the post-induction R_2* of EAE vs. naïve untreated, *** p=0.0005; (F(2,31) = 4.025, p =0.0279) **(Figure 26A).** EAE (31 ± 1.6 ms^{-1}, 30 ± 0.7 ms^{-1}; p>0.05), CFA/PTX (30 ± 1.6 ms^{-1}, 29 ± 0.7 ms^{-1}; p>0.05), and naïve (27 ± 2.3 ms^{-1}, 29 ± 1.0 ms^{-1}; p>0.05) of untreated and treated mice respectively.

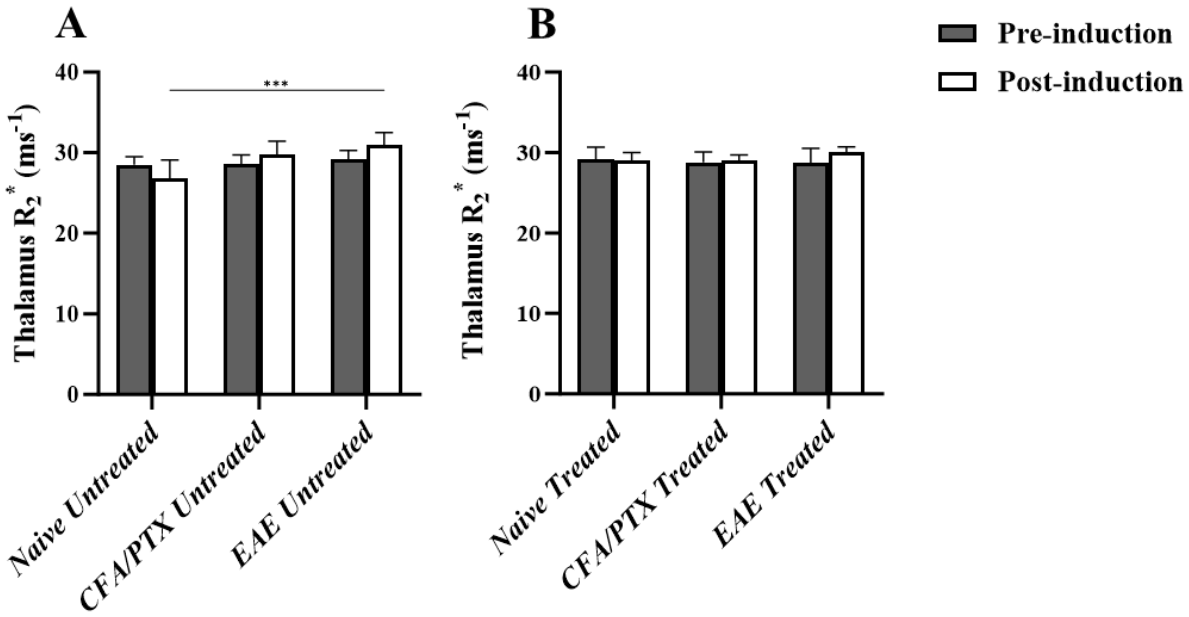

Figure 26: Mean R_2* measured in the thalamus of untreated (A) and treated (B) mice.

Transverse relation rate (T_2) measured in the thalamus brain region. R_2* was calculated as the inverse of T_2*. Animals analyzed in this region were EAE, CFA/PTX, and naive, for each group (treated/untreated). No significant difference was observed among groups except for untreated naïve and EAE post-induction; ***p<0.001. Mice pre-induction (Figure 25) and post-induction mean±SD values for EAE mice were 31±1.6 ms^{-1}, 30±0.7 ms^{-1}, CFA/PTX (30 ± 1.6 ms^{-1}, 29 ± 0.7 ms^{-1}, and naïve 27 ± 2.3 ms^{-1}, 29 ± 1.0 ms^{-1} for untreated and treated mice respectively. Dark gray bars represent treated while white bars represent untreated mice. Bars represent standard deviation.*

In the treated group, we found no significant difference in the R_2* thalamus of the controls (naïve and CFA/PTX), and EAE, p>0.05; (F(2,32) = 1.317, p = 0.2822) **(Figure 26B)**. We then computed the absolute R_2* measurement for all mice by subtracting post-induction/treated R_2* from baseline values and employed one-way ANOVA. We found a positive shift in R_2* of CFA/PTX and EAE (with and without treatment) and the negative shift was observed in the naïve untreated mice (F(5,30) = 1.862, p = 0.138) **(Figure 27)**. However, no significant difference was observed among the groups. Finally, we analyzed each group with or without treatment with a paired t-test and found no significant difference, p>0.05.

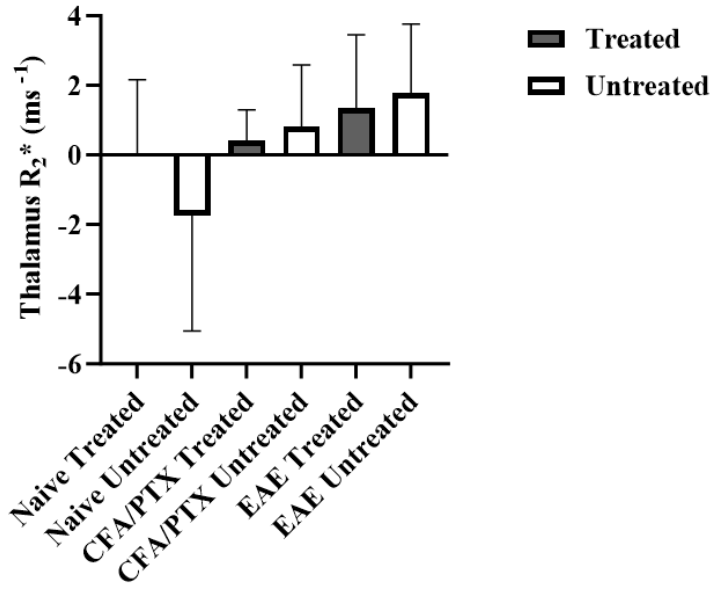

Figure 27: Mean R_2* differences measured in the thalamus of all mice.

Mice analyzed in the hippocampus region were EAE, CFA/PTX, and naïve each for each group. No significant difference was observed among groups; p>0.05. R_2 Mean±SD for each EAE group was 1.3 ± 2.0 ms^{-1}, 1.8 ± 1.9 ms^{-1}, CFA/PTX 0.8 ± 0.3 ms^{-1}, 0 ± 1.3 ms^{-1}, and naïve 0 ± 1.9 ms^{-1}, -1.8 ± 2.9 ms^{-1} treated and untreated mice respectively. Dark gray bars represent treated while white bars represent untreated mice. Bars represent standard deviation.*

To further determine hypoxia with MRI spatial resolution techniques in different ROI we employed QSM. QSM is sensitive to tissue changes, and it is susceptible to iron changes caused by disease. In the ROIs of interest as shown in **Figure 9**. Before induction, using a one-way ANOVA, we found no significant difference in the QSM cortex of treated and untreated mice for all groups, p >0.05. EAE treated .0050 ± .0018 ppm; untreated .0037 ± .0044 ppm, CFA/PTX treated .0030 ± .0018 ppm; untreated .0014 ±.0016 ppm, naive treated .0035 ± .0012 ppm; untreated .0046 ± .0027 ppm; (F(5,31) = 0.4473, p = 0.8119) (**Figure 28A**).

Similarly, in the hippocampus (**Figure 28B**), no statistically significant differences were observed in the EAE and naïve group at baseline; p>0.05 (EAE treated -0.121 ± 0.0035 ppm, untreated -.0109 ± .00033 ppm, CFA/PTX treated -.0077 ± .00037 ppm, untreated -.0049 ± .00032 ppm, naïve treated -.0140 ± .00025 ppm, untreated -.0105 ± .00025 ppm). However, significant difference was observed between CFA/PTX untreated and naïve treated (*p = 0.04); (F(5,31) = 2.847, p = 0.0315), and also in the thalamus, no significant difference was observed among groups at baseline (EAE treated -.0035 ± .0052 ppm, untreated -.0046 ± .0035 ppm; CFA/PTX treated -.0046 ± .0018 ppm, untreated -.0052 ± .0015 ppm; naïve treated -.0057 ± .0010 ppm, untreated -.0048 ± .0026 ppm; (F(5,31) = 0.3151; p = 0.9001) (**Figure 28C**). However, QSM in the hippocampus and thalamus showed a negative shift in susceptibility.

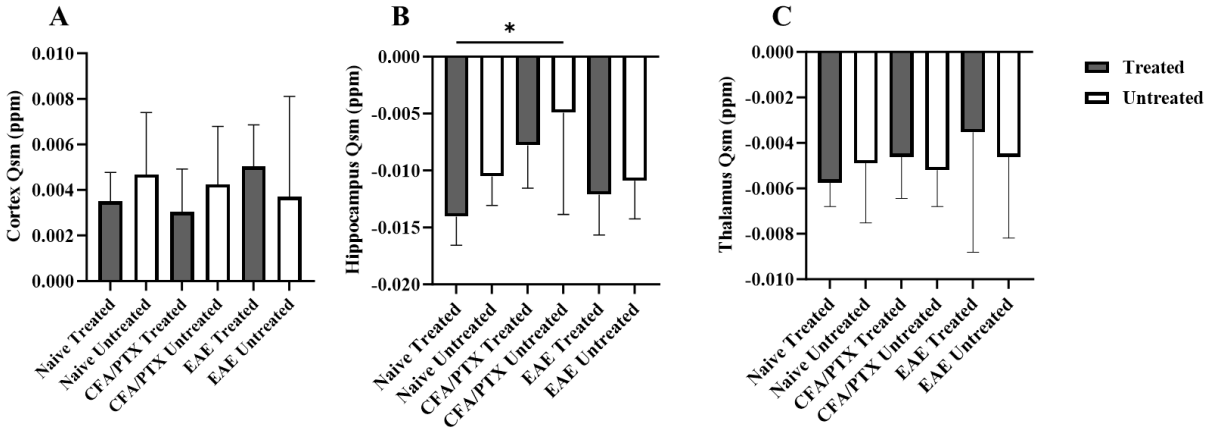

Figure 28: Baseline mean QSM measured in the cortex (A) hippocampus (B) and thalamus (C) of treated and untreated mice.

*Mice were analyzed in the cortex, hippocampus, and thalamus at baseline. No statistically significant differences were observed in each group and different brain regions at baseline except for the comparison between CFA/PTX untreated and naïve treated (*p = 0.04) in the hippocampus. Bars represented as the baseline mean±SD in the QSM cortex (EAE treated .0050 ± .0018 ppm; untreated .0037 ± .0044 ppm, CFA/PTX treated .0030 ± .0018 ppm; untreated .0014 ±.0016 ppm, naive treated .0035 ± .0012 ppm; untreated .0046 ± .0027 ppm), hippocampus (EAE treated -0.121 ± 0.0035 ppm, untreated -.0109 ±*

.00033ppm, CFA/PTX (treated -.0077 ± .00037 ppm, untreated -.0049 ± .00032 ppm, and naïve treated -.0140 ± .00025 ppm, untreated -.0105 ± .00025 ppm), and the thalamus (EAE treated -.0035 ± .0052, untreated -.0046 ± .0035 ppm; CFA/PTX treated -.0046 ± .0018 ppm, untreated -.0052 ± .0015 ppm; naïve treated -.0057 ± .0010 ppm, untreated -.0048 ± .0026 ppm) of all mice.

Next, we addressed whether there were group differences in the QSM cortex, hippocampus, and thalamus of untreated mice pre- and post-induction. We employed a mixed-model ANOVA to compare the mean of untreated groups. Following analysis, we found no significant difference in the cortex ($F(2,31) = 0.2461$, $p = 0.7833$) **(Figure 29A)**, hippocampus ($F(2,31) = 0.0891$, $p = 0.4544$) **(Figure 30A)**, and thalamus ($F(2,31) = 0.7484$, $p = 0.4815$) **(Figure 31A)** of untreated mice.

Following oxygen treatment in the cortex (EAE treated .0030 ± .0029 ppm; untreated .0025 ± .0015 ppm, CFA/PTX treated .0043 ± .0046; untreated -0.0000 ± .0033ppm, naive treated .0030 ± .0013 ppm; untreated .0017 ± .0027 ppm; ($F(5,32) = 1.402$, $p = 0.2499$) **Figure 29B**, hippocampus (EAE treated -.0135 ± .00052 ppm, untreated -.0149 ± .00022 ppm; CFA/PTX treated -0.091 ± .0041 ppm, untreated -0.118 ± .0041 ppm; naïve treated -.0123 ± .00013 ppm, untreated -.0123 ± .00034 ppm ($F(5,32) = 1.402$, $p = 0.1699$) (**Figure 30B)**, and the thalamus, there was no significant difference in the QSM pre-induction and post-oxygen treatment (EAE treated -.0074 ± .0017 ppm, untreated -.0082 ± .0034 ppm; CFA/PTX treated -.0065 ± .0028 ppm, untreated -.0068 ± .0014 ppm; naïve treated -.0062 ± .0026 ppm, untreated -.0059 ± .0023 ppm; ($F(5,32) = 0.7832$; $p = 0.5694$) (**Figure 31B)**.

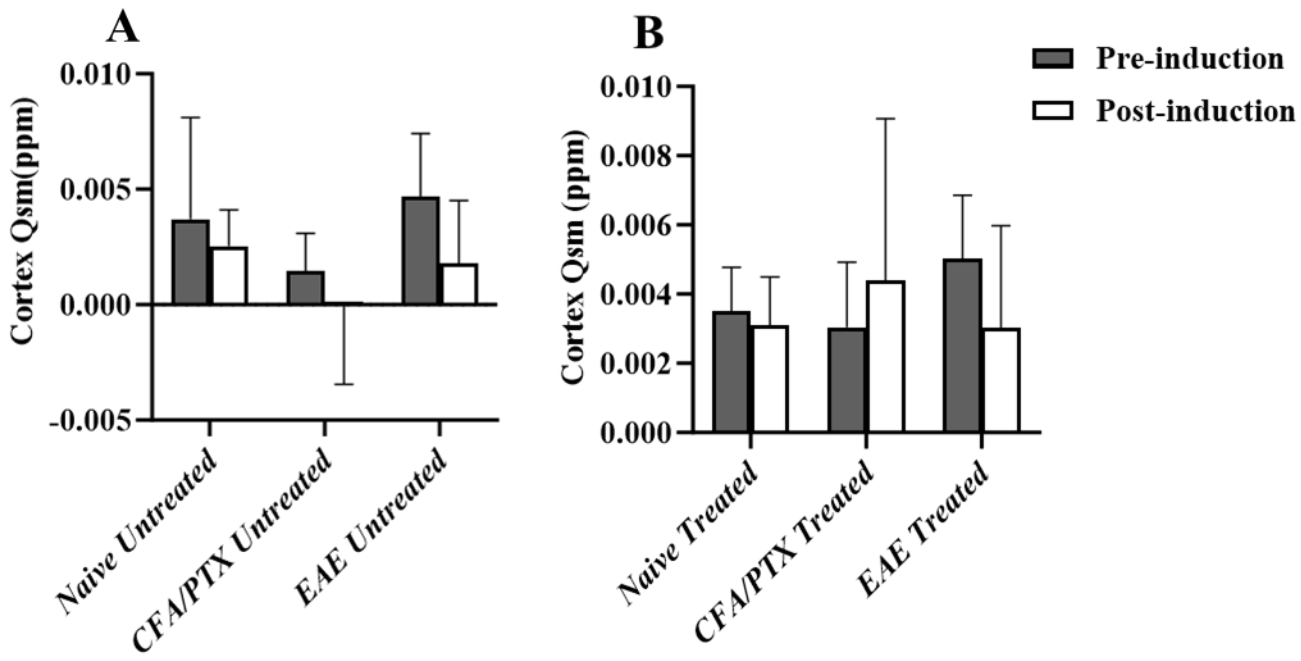

Figure 29: Mean QSM measured in the cortex of untreated (A) and treated (B) mice.

Animals analyzed in the cortex region were EAE, CFA/PTX, and naïve, for each group (treated/untreated). No significant difference was observed among groups; p>0.05. Mice pre-induction (Figure 28A) and post-induction mean±SD values for EAE mice were .0030 ± .0029ppm; .0025 ± .0015 ppm, CFA/PTX .0043 ± .0046 ppm; -0.0000 ± .0033ppm, and naive .0030 ± .0013 ppm; .0017 ± .0027 ppm for treated and untreated mice respectively. Dark gray bars represent treated while white bars represent untreated mice. Bars represent standard deviation.

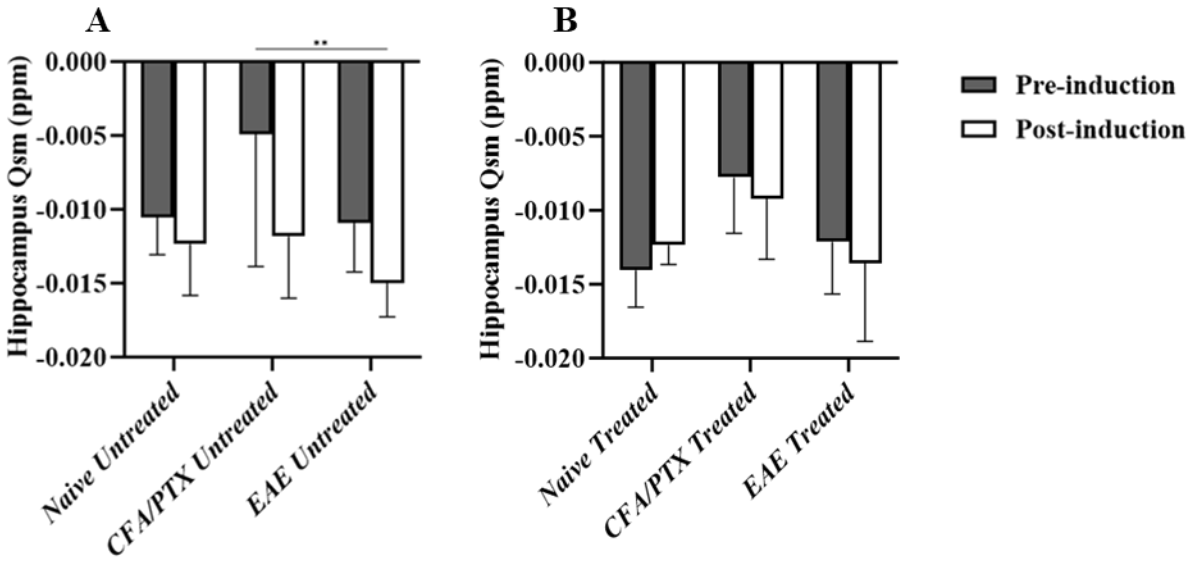

Figure 30: Mean QSM measured in the hippocampus of untreated (A) and treated mice (B).

Animals analyzed in this region were EAE, CFA/PTX, and naive, for each group (treated/untreated). No significant difference was observed among groups; p>0.05. Mice pre-induction (Figure 28B) and post-induction mean±SD values for EAE mice were -.0135 ± .00052 ppm, -.0149 ± .00022 ppm, CFA/PTX -0.091 ± 0.0041 ppm, -0.118 ± 0.0041 ppm, and naïve treated -.0123 ± .00013 ppm, -.0123 ± .00034 ppm for treated and untreated mice respectively. Dark gray bars represent treated while white bars represent untreated mice. Bars represent standard deviation.

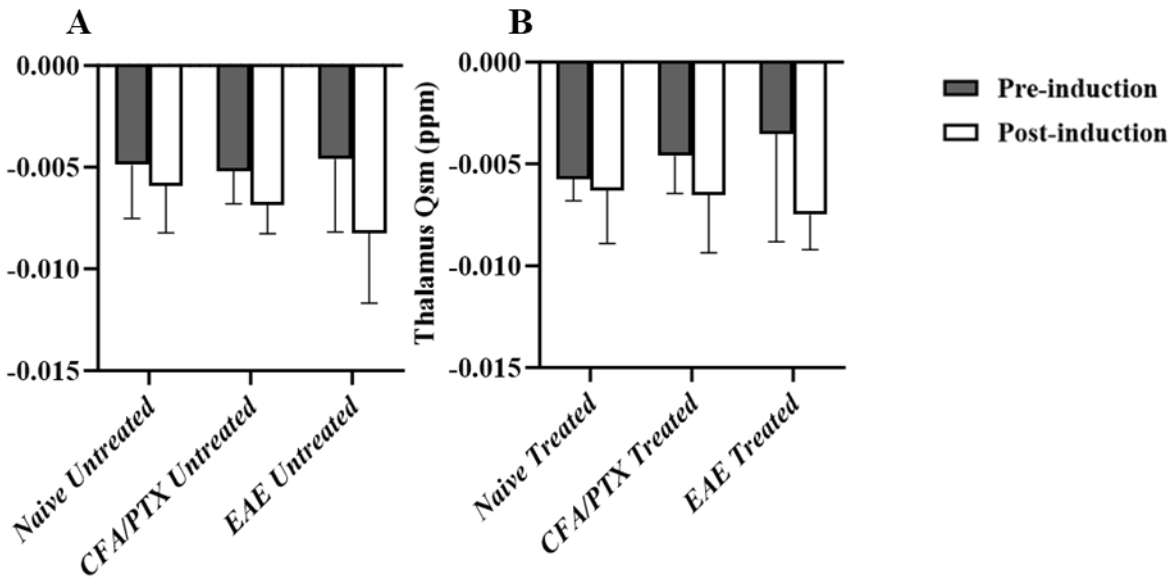

Figure 31: Mean QSM measured in the thalamus of untreated (A) and treated (B) mice.

Animals analyzed in this region were EAE, CFA/PTX, and naive, for each group (treated/untreated). No significant difference was observed among groups; p>0.05. Mice pre-induction (Figure 28C) and post-induction mean±SD values for EAE mice were -.0074 ± .0017 ppm, -.0082 ± .0034 ppm, CFA/PTX -.0065 ± .0028 ppm, -.0068 ± .0014 ppm, and naïve -.0062 ± .0026 ppm, -.0059 ± .0023 ppm for treated and untreated mice respectively. Dark gray bars represent treated while white bars represent untreated mice. Bars represent standard deviation.

We then analyzed the effect of oxygen treatment in the treated group and utilized a mixed-model ANOVA in various ROIs. We found no significant difference in the cortex ($F(2,32) = 1.390$; $p = 0.2638$) (**Figure29A)**, hippocampus ($F(2,32) = 0.76079$; $p = 0.5506$) (**Figure 30A)**, and the thalamus of treated mice ($F(2,32) = 0.9794$; $p = 0.3865$) (**Figure 31A)**.

Next, we calculated the absolute QSM values by subtracting post-induction/treatment values from baseline in all mice. We utilized one-way ANOVA to determine group differences in mean. No significant difference was observed in the cortex ($F(5,30) = 0.5168$; $p = 0.7614$) (**Figure 32A)**, hippocampus ($F(5,30) = 1.086$; $p = 0.3883$) (**Figure 32B)**. and thalamus ($F(5,30) = 0.6760$; $p = 0.6449$) (**Figure 32C)**. Tuckey multiple comparisons revealed no significant between groups (with and without oxygen treatment), $p>0.05$. Lastly, a t-test was computed to compare each group with or without oxygen treatment. No significant difference was observed between the treated and untreated mice in each group, $p>0.05$. However, we observed a negative shift in the QSM of the cortex hippocampus and thalamus for all mice; treated and untreated except for CFA/PTX treated cortex and treated naïve thalamus (**Figure 32A and C**).

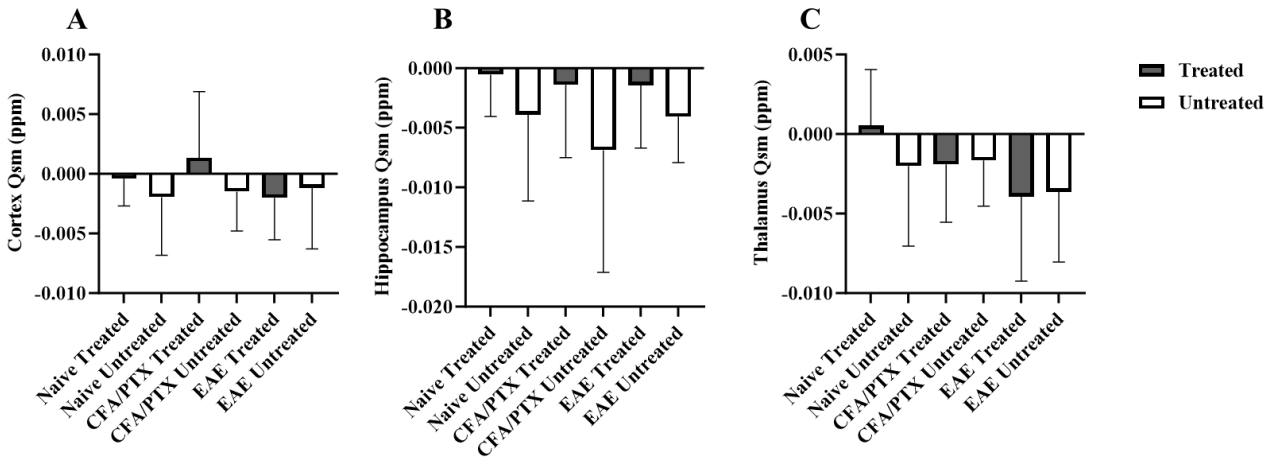

Figure 32: Mean QSM differences measured in the cortex (A), hippocampus (B), and thalamus (C) of all mice.

Mice were analyzed in the cortex, hippocampus, and thalamus at baseline. No significant differences were observed in each group and all investigated brain regions; p>0.05. Bars represented as the baseline mean±SD in the QSM cortex (EAE -0.00201 ± 0.0033 ppm; -0.0118 ppm ± 0.0048 ppm; CFA/PTX 0.001346 ± 0.0050 ppm; -0.00149 ± 0.0029 ppm; naïve -0.00041

± 0.0020 ppm; -0.00196 ± 0.0044 ppm), hippocampus (EAE -0.00147 ± 0.0049 ppm, -0.00407 ± 0.0036 ppm; CFA/PTX -0.0014 ± 0.0055 ppm, -0.0069 ± 0.0092 ppm, and naïve -0.00054 ± 0.0031 ppm, -0.00393 ± 0.0064 ppm), and the thalamus (EAE -0.00394 ± 0.0050 ppm, -0.00364 ± 0.0041 ppm; CFA/PTX -0.0019 ± 0.0033 ppm -0.00165 ± 0.0026 ppm; naïve 0.00054 ± 0.0031 ppm, -0.00201 ± 0.0045 ppm) treated and untreated mice respectively.

3.3.4 Reduction in Cortex CBF is Associated with an Increase in R_2* Values in the EAE Mice.

We examined the association between CBF and R_2*, a marker for hypoxia, using the Pearson correlation coefficient. Statistical analysis revealed a negative correlation between CBF and R_2*. Specifically, a significant negative correlation was observed in the cortex of treated mice (n = 9, r = -0.58; p = 0.01), whereas no significant difference was found in untreated EAE mice (n = 9, r = -0.45; p = 0.21) (**Figure 33**).

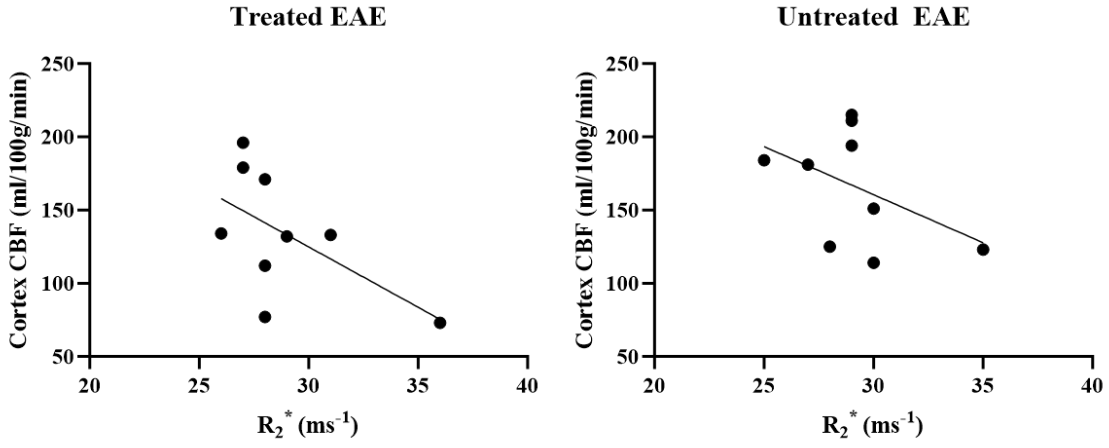

Figure 33: Correlation between EAE CBF vs. R_2* in the cortex after oxygen treatment.

Pearson's correlation performed between R_2 and CBF in the cortex of (n = 9, r = -0.58; p = 0.01 and n = 9, r = -0.45; p = 0.21) treated and untreated mice respectively.*

3.3.5 Reduction in Hippocampus CBF is Associated with an Increase in R_2* Values in the EAE Mice

In the hippocampus, a similar trend was observed. A weak negative correlation between CBF and R_2* in the hippocampus of untreated mice was observed but was not statistically significant (r = -0.27; p = 0.46) (**Figure 34**). However, a significant negative correlation was evident in the hippocampus of EAE-treated mice (r = -0.78; p = 0.01) (**Figure 34**). This suggests a close relationship between these two parameters.

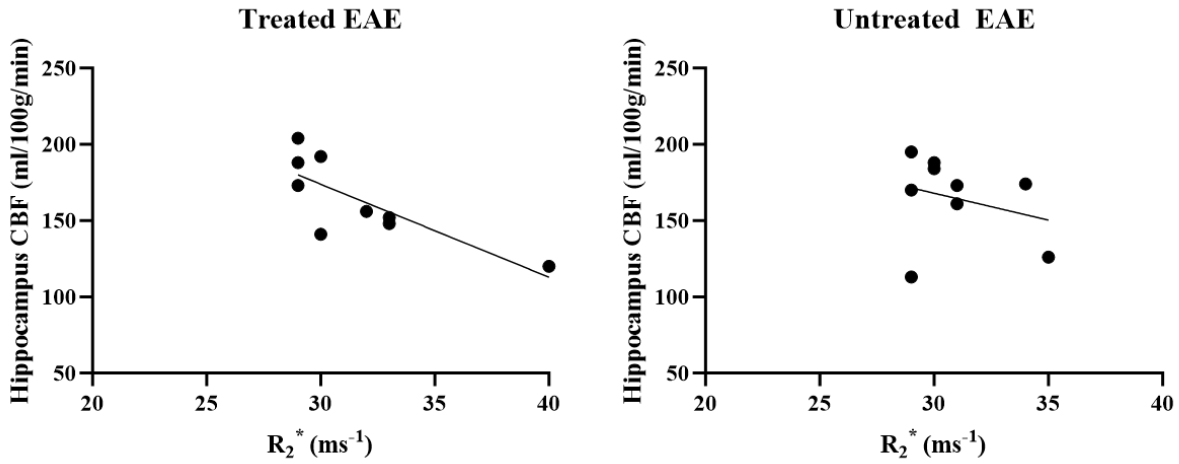

Figure 34: Correlation between EAE CBF vs. R_2* in the hippocampus after oxygen treatment.

Pearson's correlation performed between R_2 and CBF in the cortex of (n = 9, r = -0.27; p = 0.46 and n = 9, r = -0.78; p = 0.01) treated and untreated mice respectively.*

3.3.6 Reduction in CBF thalamus is Associated with R_2* increase in EAE mice.

Furthermore, we determined the linear relationship between the CBF and R_2* of treated and untreated thalamus (**Figure 35**). Using the Pearson correlation coefficient, we observed a statistically significant negative correlation in the thalamus of untreated EAE mice (r = -0.77; p = 0.01). In the treated thalamus, there was no significant negative correlation (r = -0.65; p = 0.05).

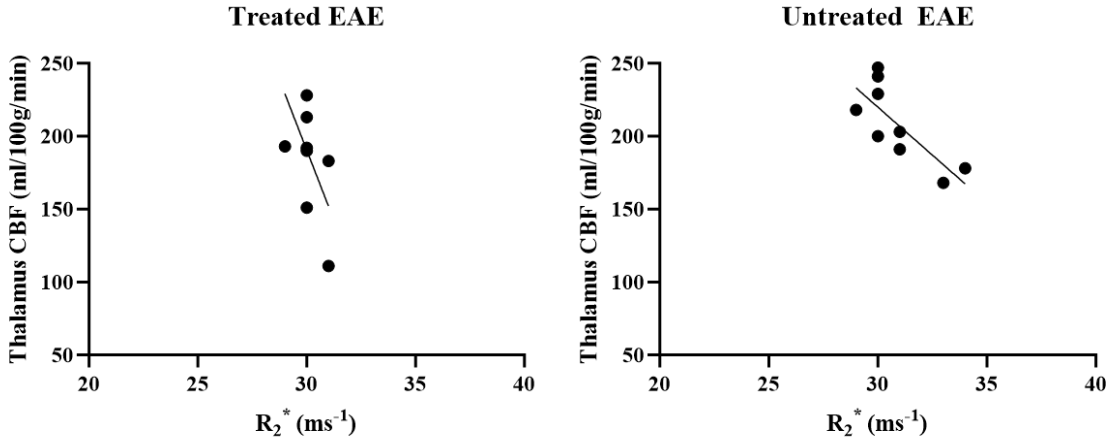

Figure 35: Correlation between EAE CBF vs. R_2*in the thalamus after oxygen treatment.

Pearson's correlation was performed between R_2 and CBF in the cortex of (n = 9, r = -0.65; p = 0.05 and n = 9, r = -0.77; p = 0.01) treated and untreated mice respectively.*

3.4 Discussion and Conclusion

This chapter investigated the impact of oxygen treatment on hypoxia using non-invasive MRI techniques. Hypoxia was assessed using R_2* and QSM. The hypothesis was that 6 hours of NBO treatment for 5 days would improve disease outcomes by reducing hypoxia in EAE mice. Student t-test was computed, and there was no significant difference between treated and

untreated EAE groups and in each group of the control mice. Systemic administration of CFA/PTX and MOG resulting in autoimmunity and inflammation could induce R_2* increased in untreated EAE compared to baseline in the cortex **(Figure 20A)** and thalamus.

R_2* increased in untreated EAE compared to baseline in the cortex **(Figure 20A)** and in the thalamus. There was also an increase in R_2* in the thalamus post-induction compared to naïve **(Figure 26A)**. For the change in parameter, in the cortex, QSM positive values decreased in both treated and untreated EAE while CFA treated increased **(Figure 32A)**. In the hippocampus, a negative shift was observed in all mice **(Figure 32B)**. The alterations in QSM that resulted in negative and positive shifts may be attributed to the QSM high and low sensitivity to deoxyhemoglobin. Additionally, these alterations could also be linked to high and low inflammatory areas, as evidenced in a recent clinical study (Gillen et al., 2021) Furthermore, in the thalamus, we found an increase in the negative QSM values for all mice except treated **(Figure 32C)**. A negative shift was found in treated and untreated EAE and CFA/PTX. These alterations could be due to low CBF discussed in **Chapter 2**. Our research findings were consistent with increased deoxyhemoglobin causing increased susceptibility in the EAE. This may be due to increased inflammation. More findings are needed to unveil potential pathological causes and explore treatment approaches for MS and other inflammatory diseases. In the correlation results, we observed a negative correlation between CBF and R_2*. Thus, an increase in R_2* is related to a decrease in CBF found in the gray matter domain. This makes sense, such that when blood flow is limited to tissue area, it indirectly tells us about the state of the tissue environment and oxygenation in that area, since tissue relies heavily on blood to get sufficient oxygen supply for proper function. Interestingly, NBO administration for 6 hours daily for 5 days probably did not increase oxygenation when oxygen was not being delivered. This would suggest that if the hypoxia were

caused by inflammation, the NBO did not decrease inflammation, more studies are needed to confirm this. It was interesting that the R_2* in the EAE cortex was increased in post-induction in the untreated group but not in the treated group. This indicates that oxygen therapy may have reduced hypoxia. A larger "n" would be required to be sure of the results.

CHAPTER FOUR:
ASSESSING THE EFFECT OF OXYGEN TREATMENT ON EAE DISEASE SEVERITY

4.1 Introduction

There has been an increasing interest in EAE clinical scores in various medical contexts, including neurological disorders, including MS. The study of disease clinical scores in the context of MS disease condition is critical for identifying potential treatment targets and developing effective interventions that can improve patient outcomes. EAE clinical score and OF test were utilized to assess the effect of treatment on disease progression. This thesis chapter explored the impact of 6 hours of normobaric oxygen treatment daily for 5 days on disease clinical score and OF after EAE immunization.

4.2 Methods

4.2.1. Ethics

All experiments followed the principles outlined in the current Guidelines of the Canadian Council of Animal Care. This study was approved by the Animal Care Committee, University of Calgary (AC19-0036). Mice used in this study had previously been employed in CBF and hypoxia experiments discussed in **Chapters 2 and 3**.

4.2.2. Animal

Female C57BL/6 mice aged (8-10 weeks) were purchased from Charles Rivers Laboratory. Female mice were used because of their high susceptibility to MOG injection. Five mice were housed per cage in the animal halfway house facility. Food and water were provided ad libitum.

All mice (EAE, n = 18, 9 treated, 9 untreated), CFA/PTX, n = 10 (5 treated, 5 untreated), and naïve, n =10 (5 treated, 5 untreated) were subjected to the same handling, clinical disease scoring and OF test. The Mice in this chapter were the same as in **Chapters 2** and **3**.

4.2.3. EAE Clinical Assessment

4.2.3.1 EAE Disease Clinical Score

Following induction as discussed in previous chapters, animals were monitored for symptoms at days 7 -14 post-induction. All clinical assessments and analysis were performed blindly. We assessed motor function and disease severity using a 15-point clinical grading scale looking at the tail and limb paralysis The 15-point clinical scoring was done daily after 7 days post-induction. Mice were scored as follows (**Table 3**). A total score of 15 represents a deceased mouse. However, no animal death was recorded throughout the course of the experiment.

Table 3: Table illustration of EAE clinical scoring.

Region	Score	Symptoms
Tail	0	No symptoms
	1	½ paralyzed tail
	2	Fully paralyzed tail
Hind limb (left and/or right)	0	No symptoms
	1	Partial paresis (weakness)
	2	Full paresis (limb drag but movement)
	3	Fully paralyzed (no limb movement)
Forelimb (left and/or right)	0	No symptoms
	1	Partial paresis
	2	Full paresis
	3	Fully paralyzed

4.2.4. Open-field (OF)Test

In 1934, Hall developed the OF test as a measure for evaluating emotional responses in rats (Mizuno et al., 2010). OF is a popular procedure applied in behavioral neuroscience (Prut & Belzung, 2003). Over the years, the open-field test has become the most common method used in animal studies to understand the neurobiological basis of anxiety-like behavior and locomotion (Kraeuter et al., 2019; Prut & Belzung, 2003). This examination utilizes a camera to quantify the locomotor activity of the experimental animal within the peripheral and central zones (Kraeuter et al., 2019). Over the years, the open-field test has become the most common method used in animal studies to understand the neurobiological basis of anxiety-like behavior and locomotion (Kraeuter et al., 2019; Prut & Belzung, 2003). Also, this test has been utilized for both the screening of potential anxiolytic drugs in novel research (Kraeuter et al., 2019), as well as in genetic studies and brain injury (Mizuno et al., 2010). In addition, the OF test has been utilized in EAE studies (Buddeberg et al., 2004; Takemiya & Takeuchi, 2013). One of these studies evaluated motor deficits by measuring the total distance travelled by animals (Takemiya & Takeuchi, 2013). Results from these studies reflect the extent of motor impairment following the onset of paralysis in EAE and underscores the significance of the OF test as a valuable tool for assessing motor deficits in the context of EAE and other related animal models.

For this study, motor assessment and exploratory behavior were determined with an open-field test (looking at movement for 10 minutes). OF was performed at 3 time points: pre-induction (baseline, day 0), pre-treatment (7-14 days post-induction), and post-treatment (20 days post-induction). The apparatus employed in the experiment was a transparent box measuring 12x9.5 inches, with walls standing at a height of 9 inches. OF behavioral test for motor ability was carried out at three different time points to assess progressive motor dysfunction and exploratory behavior.

Before that, animals were habituated for 10 minutes in the OF cage to get them acquainted (No video was recorded at this time). OF was performed by putting each mouse in a novel cage for 10 minutes (**Figure 36**), to assess and record motor function. We recorded with a tripod camera which was situated adjacent to the OF box and the camera lens pointed downwards to provide a clear aerial view of the box. To avoid distractions that could affect the result, OF was recorded with a noiseless background.

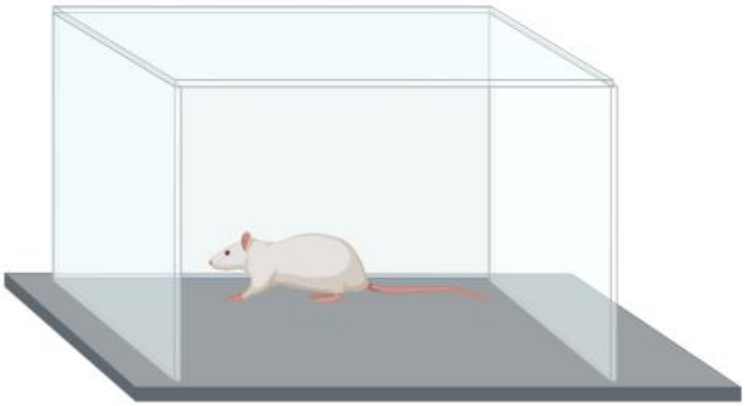

Figure 36: Open-field (OF)cage/box.

Open-Field Test (protocols.io)

4.2.5. Oxygen Administration

Oxygen administration for this chapter was the same for **Chapters 2 and 3** for all mice in the treatment groups.

4.2.6. Data Processing and Statistical Analysis

OF data were processed with ANY-maze software (version 7.0). Statistical analysis provided us with objective evidence to support the research hypotheses and draw meaningful conclusions from the data. In this section, we discussed the statistical methods used to analyze data and provided a summary of the results. Specifically, we used a one-way ANOVA test and Tukey multiple comparisons to determine the variability in locomotion (total distance travelled) and mean differences between treated and untreated groups of different experimental animals.

4.3 Results

4.3.1 EAE Disease Course

Clinical signs first appeared by tail paralysis, at 14 - 17 days after immunization. Paralysis then progressed to the hind limbs and subsequently extended to affect the forelimbs. This chronic paresis continued until the experimental endpoint. Clinical scores for treated and untreated EAE mice were assessed for each treatment day till the end of the experiment (**Figure 37**). We didn't record any deaths all through the experiment. However, for the EAE disease score, we employed the Wilcoxon non-parametric test to determine whether there was a difference between the clinical disease score in the treated and untreated EAE groups.

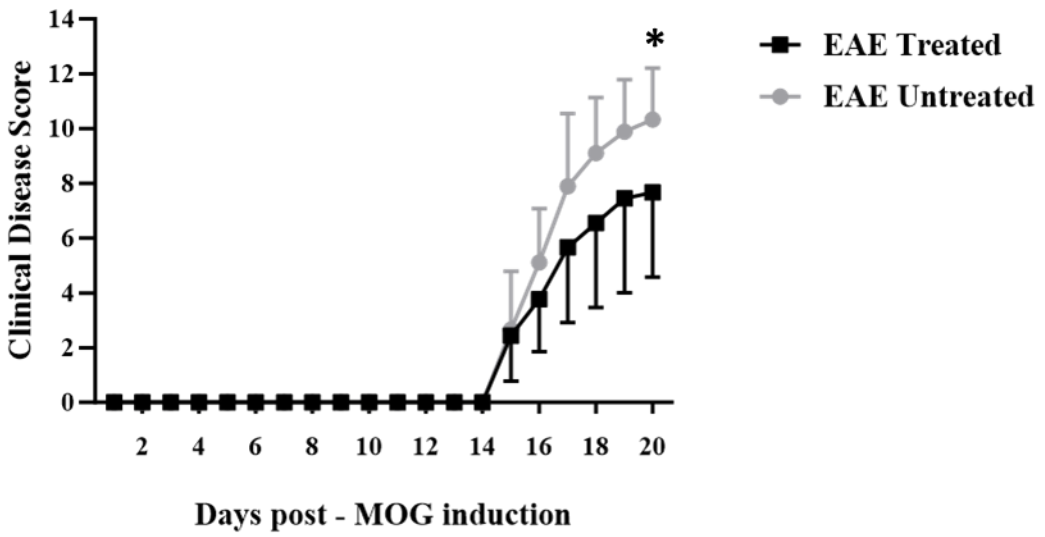

Figure 37: EAE Mean clinical score plot between treated and untreated EAE mice.

*The mean±SD values for each group were 6 ± 2.3, and 8 ± 1.5 in treated and untreated groups respectively. There was a significant difference between treated and untreated EAE; *p = 0.0313. Dark bars represented treated while light gray bars represented untreated groups. Bars represent the standard deviation on each day of the clinical score.*

Interestingly, after our analysis, we found that there was a significant difference in improvement between treated and untreated EAE, *p=0.0313 **(Figure 37)**. Mean EAE score values are shown in **Table 4**.

Table 4: Mean clinical score for treated and untreated EAE mice.

Days of oxygen treatment/MRI	**EAE mice**	**Mean ± STD**
Day 1	Treated Untreated	3 ± 2.1 2 ± 1.7
Day 2	Treated	5 ± 1.9

	Untreated	4 ± 2.0
Day 3	Treated	8 ± 2.6
	Untreated	6 ± 2.7
Day 4	Treated	9 ± 2.0
	Untreated	7 ± 3.0
Day 5	Treated	9 ± 1.9
	Untreated	7 ± 3.4
Day 6/ MRI	Treated	10 ±1.9
	Untreated	7 ± 3.0

4.3.2 Open-Field Test

In this section, we analyzed the open-field test performed prior to induction (baseline) with one-way ANOVA for all mice and found no significant difference at baseline. This was to rule out that group differences may be due to differences in mice before induction, EAE (treated 18 ± 4.3 m; untreated 17 ± 5.1 m) CFA/PTX (treated 18 ± 4.0 m; untreated 17 ±5.7 m), and naïve (treated 18 ± 5.9 m; untreated 20 ± 4.9 m); ($F(5,32) = 0.5002$, $p = 0.7738$) (**Figure 38**). Following induction, we asked if there were group differences after induction across groups, with one-way ANOVA, we found significant differences between the controls and EAE mice (treated 3.8 ± 3.4 m; untreated 3.3 ± 3.0 m, CFA/PTX treated 13.4 ± 2.1 m; untreated 12.6 ± 2.4 m, naïve treated 14.4 ± 8.1 m; untreated 18.6 ± 6.9 m); *$p<0.0201$,**$p<0.0090$,****$p<0.0001$ ($F(5,32) =12.15$, ***$p = 0.0001$) (**Figure 39A**). To determine the effect of treatment in treated mice, one-way ANOVA was computed. Following analysis, we found significant difference among treated groups; $p<0.05$ ($F(5,32) =13.68$, ***$p = 0.0001$, EAE (treated 3.8 ± 4.4 m; untreated 2.6 ± 2.0 m), CFA/PTX (treated 11.0 ± 3.9 m; untreated 11.6 ± 2.6 m), and naïve (treated 11.6 ± 2.4 m; untreated

15.0 ± 3.0 m) **(Figure 39B).** Furthermore, we asked if there were group differences without oxygen treatment after induction. Using a mixed-model ANOVA, a significant difference was observed between the EAE pre and post-induction OF vs. controls; CFA/PTX (12.6 ± 2.4 m), naïve (18.6 ± 6.9 m), and EAE (3.3 ± 3.0 m); ****$p<0.0001$, ***$p<0.001$, *$p<0.05$; ($F(2,32) = 0.5644$, **$p = 0.0080$) (**Figure 40**).

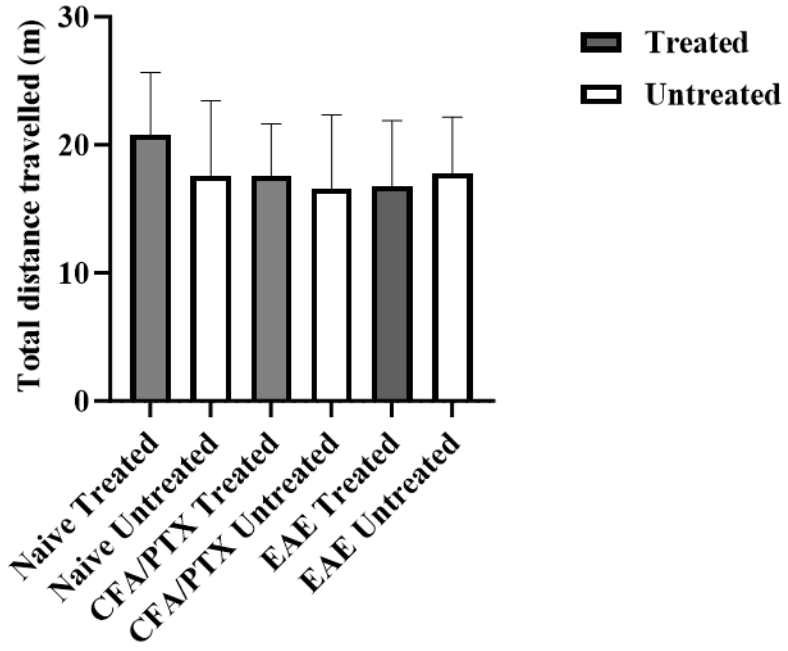

Figure 38: Baseline total distance travelled for all mice.

Animals analyzed in the OF test were EAE, CFA/PTX, for each group (treated/untreated). No significant difference was observed among groups; $p>0.05$. Bars are represented as mean±SD values of EAE (18 ± 4.3 m; untreated 17 ± 5.1 m) CFA (treated 18 ± 4.0 m; untreated 17 ±5.7 m), and naïve (treated 18 ± 5.9 m; untreated 20 ± 4.9 m) mice. Dark gray bars represent treated while white bars represent untreated mice. Bars represent standard deviation.

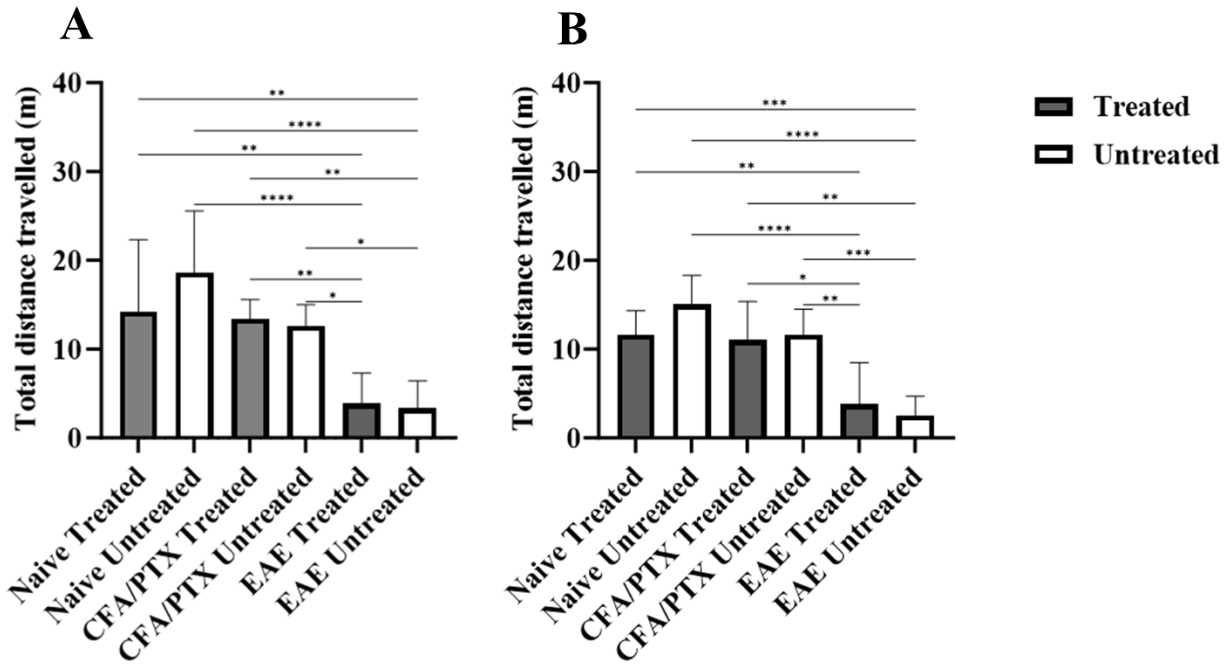

Figure 39: Post-induction/treatment total distance travelled for all mice.

*Animals analyzed in the OF test were EAE, CFA/PTX, and naive, for each group (treated/untreated), post-induction/treatment. Significant difference among group was found following induction; Figure A (day 14-17) and post-treatment; Figure B (day 18-20) ****p<0.0001, **p<0.01, ***p<0.001, *p<0.05. Bars are represented as mean±SD values of post-induction EAE (treated 3.8 ± 3.4 m; untreated 3.3 ± 3.0 m), CFA/PTX (treated 13.4 ± 2.1 m; untreated 12.6 ± 2.4 m), and naïve (treated 14.4 ± 8.1 m; untreated 18.6 ± 6.9 m) and post-treatment EAE (treated 3.8 ± 4.4 m; untreated 2.6 ± 2.0 m), CFA/PTX (treated 11.0 ± 3.9 m; untreated 11.6 ± 2.6 m), and naïve (treated 11.6 ± 2.4 m; untreated 15.0 ± 3.0 m) mice.*

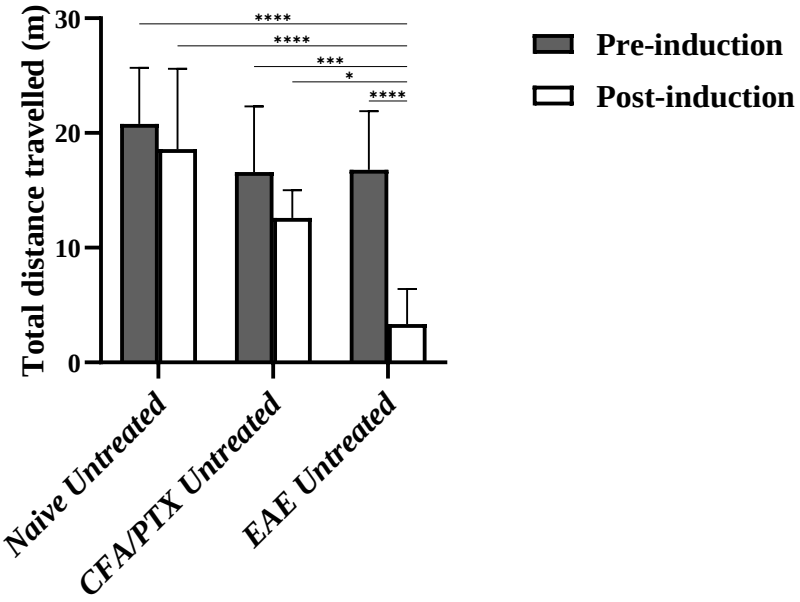

Figure 40: Pre and post-induction distance travelled in untreated mice.

*Animals analyzed in the OF test untreated group were, EAE, CFA/PTX, and naive, for each group (treated/untreated). Significant difference among the untreated group was found; ****p<0.0001, ***p<0.001, *p<0.05. Bars are represented as mean±SD values of pre-induction (Figure 40) and post-induction (Figure 41) distance travelled.*

In the oxygen-treated group, before treatment (14-17 days post-induction), we used a mixed-model ANOVA to compare differences among groups before treatment. We found significant difference between groups, EAE (3.8 ± 3.4 m); CFA/PTX (13.4 ± 2.1 m) and, naïve (14.4 ± 8.1 m), ****p<0.0001, ***p <0.0002, **p<0.0062, *p=0.0146; (F(2,32) =5.281, *p = 0.0104) (**Figure 42**).

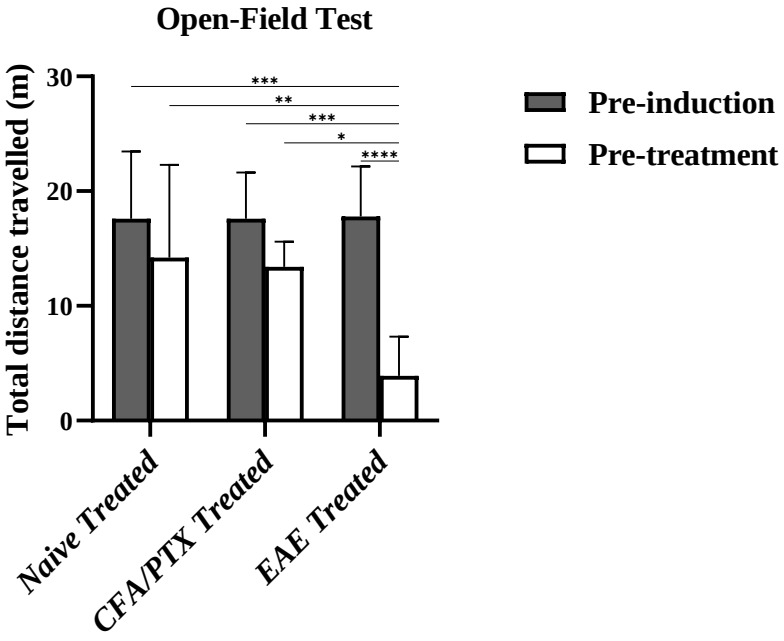

Figure 41: Pre-induction and pre-treatment distance travelled in treated mice.

*Animals analyzed in the OF test treated group were EAE, CFA/PTX, and naive, for each group (treated/untreated). Significant difference was found in the treated group; ****p<0.0001, ***p<0.001, **p<0.01, *p<0.05. Bars are represented as mean±SD values of pre-induction (Figure 40) and post-induction (Figure 41) distance travelled.*

Finally, after oxygen treatment, we carried out the last OF for all mice (EAE mice treated 3.6 ± 4.5m; untreated 2.5 ± 2.1 m); CFA/PTX treated 11.0 ± 4.3; untreated 11.6 ±2.8 m, and naïve treated 11.6 ± 2.7m; untreated 15.0 ± 3.3 m). Then, we compared the effect of treatment by employing two different comparisons. First, we calculated the change in the OF parameter for all mice before and after treatment. We subtracted OF post-induction/pre-treatment values from baseline (Figure **42A**), and then did the same for post-induction/pre-treatment OF values and post-treatment **(Figure 42B)**. Thereafter, we analyzed it with one-way ANOVA.

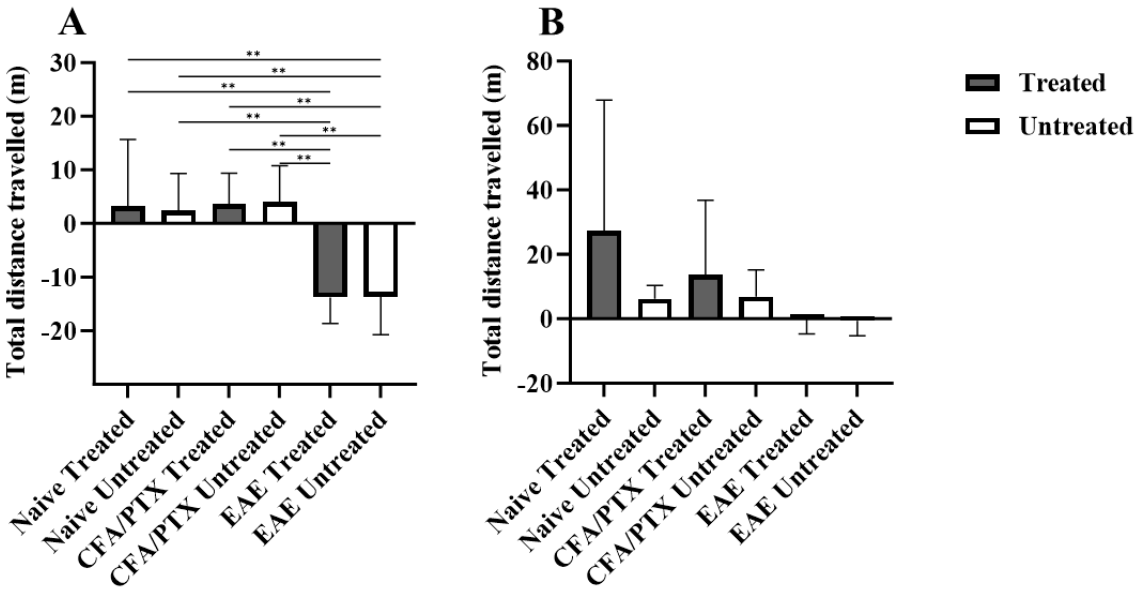

Figure 42: Differences in open-field (OF) for all mice.

*Differences were analyzed in the pre-and post-induction (A) OF and B: pre-treatment and post-treatment (B) OF. Animals analyzed were EAE, CFA/PTX, and naive, for each group (treated/untreated). A significant difference was observed in the treated group; **p<0.01. Bars are represented as mean±SD values of the EAE (-13.7 ± 4.6, -13.6 ± 6.6), CFA/PTX (3.6 ± 5.2, 4 ± 6.1) and naive (3.2± 11.2, 2.4± 6.2) (Figure A) and EAE (-0.2 ± 4.2, -0.6 ± 4.3), CFA/PTX (13.6 ± 20.7, 8± 7.9) and naive (27.2 ± 36.4, 6.2± 3.8 (Figure B).*

In pre-induction/treatment vs. baseline, distance travelled (OF), Tukey multiple comparisons result showed a significant difference in the total distance travelled between the controls (naïve and CFA/PTX) and the EAE mice, **p<0.0031; F(5,32) =10.26, ****p = 0.0001 **(Figure 42A)**. In the post-induction/pre-treatment vs. post-treatment OF comparison, no significant differences were found among groups, p>0.05; however, we found no significant ANOVA interaction F(5,32) =2.207, p = 0.0780 **(Figure 42B)**. Lastly, using a paired t-test, we compared each group with or

without treatment and found no significant difference between treated and untreated mice for each group, $p>0.05$.

4.3.3 Changes in Locomotion are Associated with an Increase in the EAE Clinical Score.

We conducted a correlation analysis between locomotion and clinical disease scores in treated and untreated EAE mice **(Figure 43).** A Pearson correlation coefficient was computed to assess the linear relationship between the total distance travelled and disease score after oxygen treatment There was a significant negative correlation between the two variables (treated n = 9, r = -0.88; p = 0.001; untreated n = 9, r = -0.86; p = 0.002). This showed that an increase in clinical disease score was seen on the 15-point scale and was associated with a decline in motor function after MOG induction and oxygen treatment.

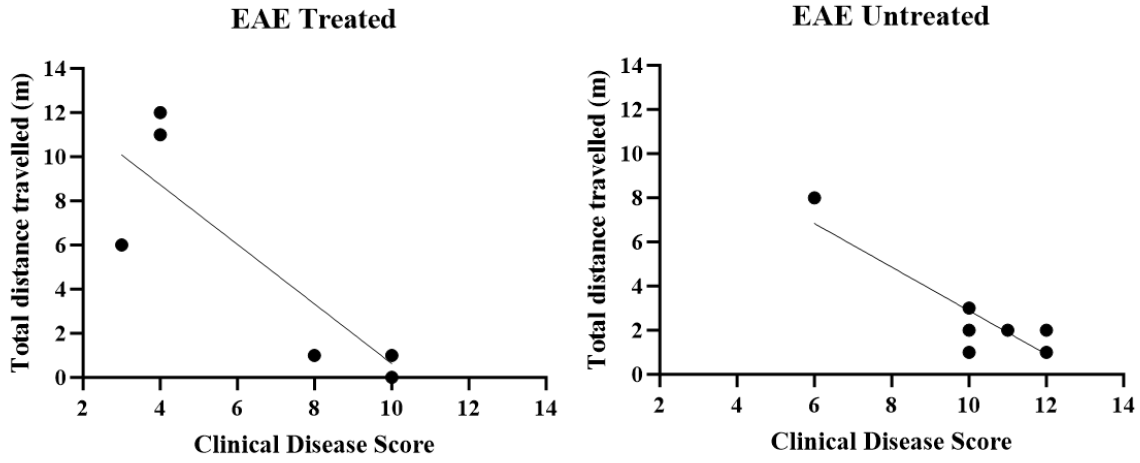

Figure 43: Correlation between EAE locomotion vs. clinical score after oxygen treatment.

Pearson's correlation performed between locomotion represented as the total distance travelled and disease clinical score (n = 9, r = -0.88; p = 0.001 and n = 9, r = -0.86; p = 0.002) treated and untreated mice respectively.

4.3.4 Correlation Study Between the EAE Clinical Score and MRI Parameters (CBF and R_2*)

For the correlation study, we took MRI data from **Chapters 2**, **3,** and **4** and conducted a series of Pearson correlations between various parameters using GraphPad Prism Version 10.0.1. The parameters listed below were compared:

- Total distance travelled vs. clinical score (EAE treated and untreated cortex, hippocampus, and thalamus).
- Total distance travelled vs. CBF in each ROI analyzed (EAE treated and untreated cortex, hippocampus, and thalamus).
- Clinical scores vs. CBF in each ROI analyzed (EAE treated and untreated cortex, hippocampus, and thalamus).
- Total distance travelled on vs. R_2*in each RO1 analyzed (EAE treated and untreated cortex, hippocampus, and thalamus).
- Clinical scores vs. R_2* in each ROI analyzed (EAE treated and untreated cortex, hippocampus, and thalamus).

We performed all correlations using OF and disease clinical score data from day 20, which was the last imaging day. This reflected the cumulative effect of oxygen exposure in the EAE mice. It is also the cumulative effect of oxygen treatment on clinical score data that most aligns with MRI parameters.

4.3.4.1 Changes in MRI Parameters are Associated with a Decline in the EAE Clinical Score and Open-field Test.

Further investigation of the relationship between MRI parameters (CBF and R_2*) vs. disease score and locomotion (total distance travelled) in the OF test were conducted following induction/oxygen treatment in the different RIs. Using the Pearson correlation coefficient test for statistical significance, the correlation analysis revealed a positive correlation between R_2* and clinical score, and a negative correlation between R_2* and OF test for locomotion (Figure 50 – 53). CBF was found to be negatively correlated with clinical disease score and positively correlated with OF test for locomotion (Figure 44 – 46). This was discussed in the following paragraphs section.

4.3.4.2 Changes in CBF Measures are Associated with Poor Clinical Outcomes in the EAE Mice After Oxygen Treatment.

Following oxygen treatment, the reduced CBF found in different ROIs in the EAE mice, shown previously in **Chapter 2** was correlated with disease clinical scores. In line with this, we determined the linear relationship between CBF and clinical score (EAE treated and untreated) measurements to reveal their strength of connection in different ROIs between the two measures after oxygen treatment.

Using a Pearson correlation coefficient, we observed a negative correlation in the CBF cortex (treated n = 9, r = -0.05; p = .88; untreated n = 9, r = - 0.48; p = .18) of treated and untreated EAE vs clinical score **(Figure 44)**. We observed a similar trend also in the hippocampus CBF vs. clinical score (treated r = -.34; p = .35, untreated n = 9, r = -.32; p =.40), and thalamus CBF vs. clinical score **(Figure 45)**, and thalamus (EAE treated, r = -.33; p = .37, untreated, r = -.42; p = .25) **(Figure 46).** There was no significant correlation observed.

However, a linear trend was observed between a CBF decline in the ROIs and increased clinical scores in both treated and untreated EAE mice. Correlation was found to be insignificant with a corresponding p-value greater than 0.05.

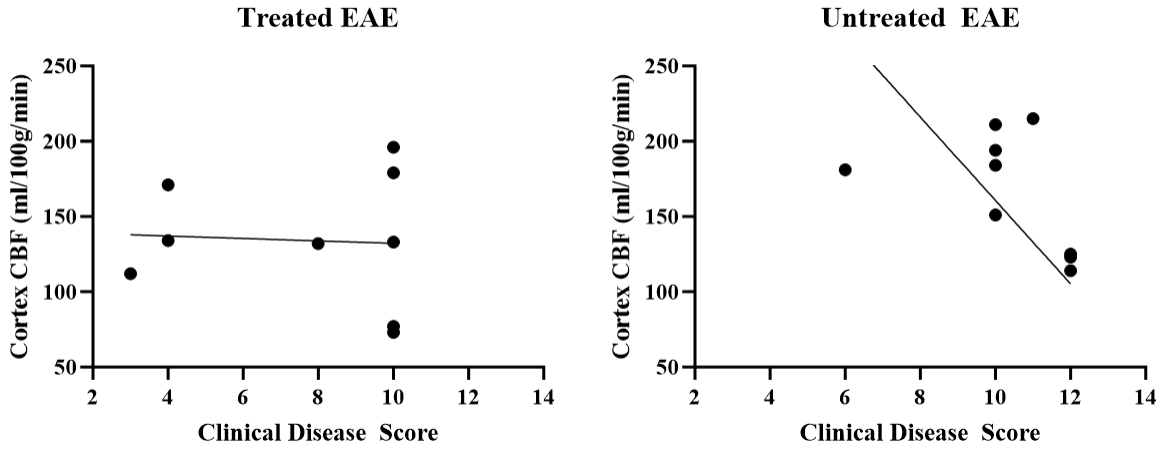

Figure 44: Correlation between EAE disease clinical score vs. CBF in the cortex after oxygen treatment.

Pearson's correlation was performed between disease score and CBF in the cortex (EAE, r = -0.05; p = .88; r = - 0.48; p = .18) of treated and untreated mice respectively.

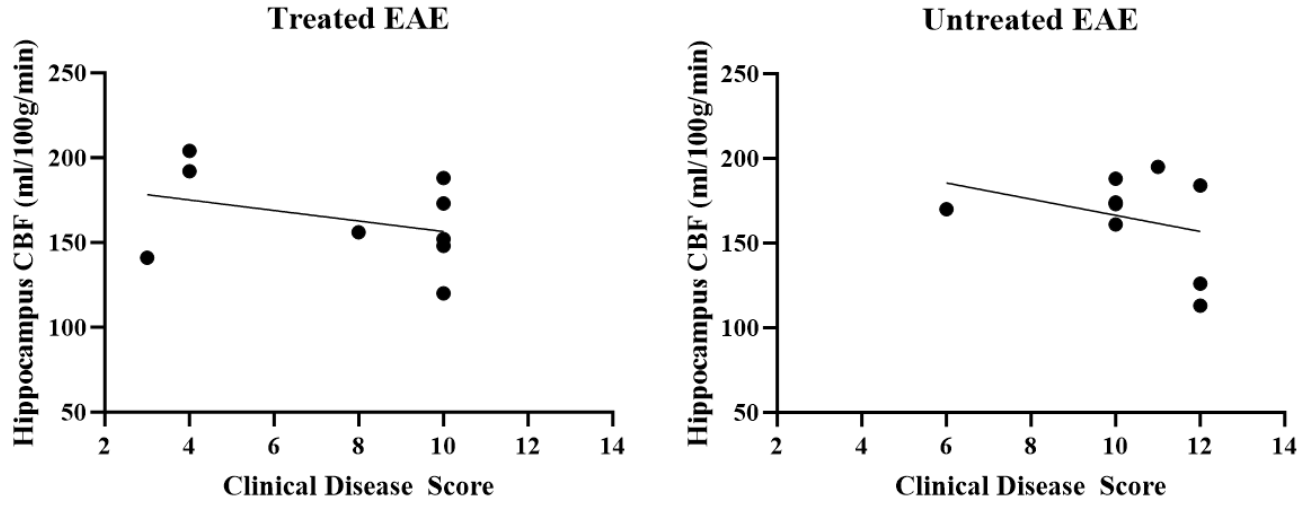

Figure 45: Correlation between EAE disease clinical score vs. CBF in the hippocampus after oxygen treatment.

Pearson's correlation was performed between disease score and CBF in the hippocampus (EAE treated r = -.34; p = .35, untreated, r = -.32; p =.40).

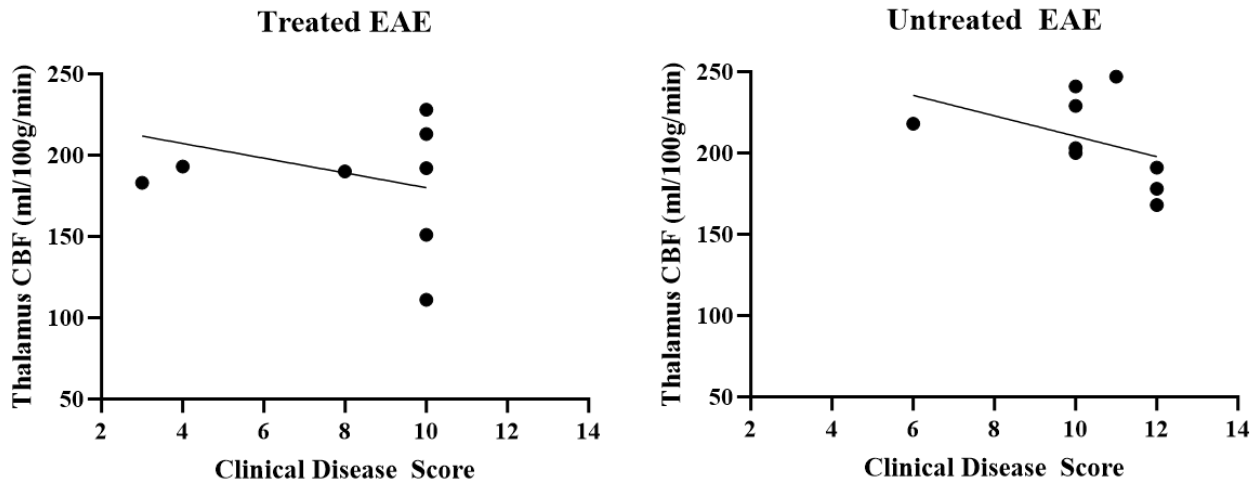

Figure 46: Correlation between EAE clinical score vs. CBF in the thalamus after oxygen treatment.

Pearson's correlation performed in the thalamus CBF vs disease score (EAE treated, r = -.33; p = .37, untreated, r = -.42; p = .25).

4.3.4.3 Changes in CBF are associated with a decline in the open-field of the EAE mice after oxygen treatment.

First, we examined the connection between locomotion in the OF test, measured as total distance travelled vs. CBF in ROIs under study investigation. We evaluated the cortex **(Figure 47),** a Pearson correlation coefficient of r = .18 was found between the CBF and OF test for locomotion with a corresponding p -p-value of .63 for treated EAE, and untreated, r = .25 with a complementary p-value of 0.50.

In the same vein, Pearson correlation coefficient of r = .60; p = .08, and r = .08; p =.83 was found between hippocampus CBF vs. total distance travelled in the treated and untreated EAE mice respectively (**Figure 48)**, and as well as the thalamus, (treated, r = .43; p = .23, EAE untreated, r = .15; p = .69), **Figure 49**. These two measures are positively correlated, for example, a decrease in CBF was caused by a decline in motor function in both treated and untreated EAE mice irrespective of oxygen treatment. Nonetheless, we found no significant positive correlation between CBF vs total distance travelled in the hippocampus and thalamus p>0.05.

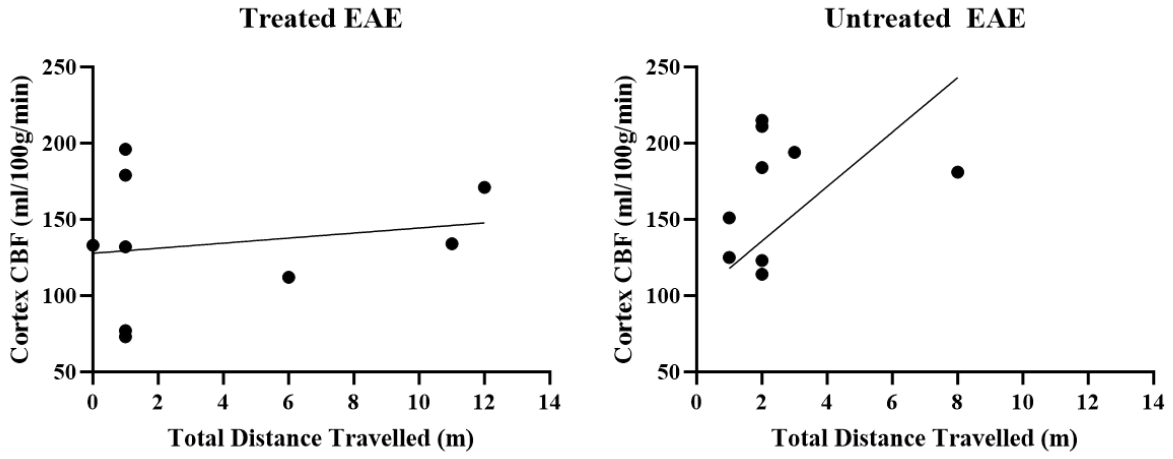

Figure 47: Correlation between EAE locomotion vs. CBF in the cortex after oxygen treatment. *Pearson's correlation was performed between locomotion and CBF in the cortex; r = .18 with a corresponding p-value of .63 for treated EAE, and untreated, r = .25 with a complementary p-value of .50.*

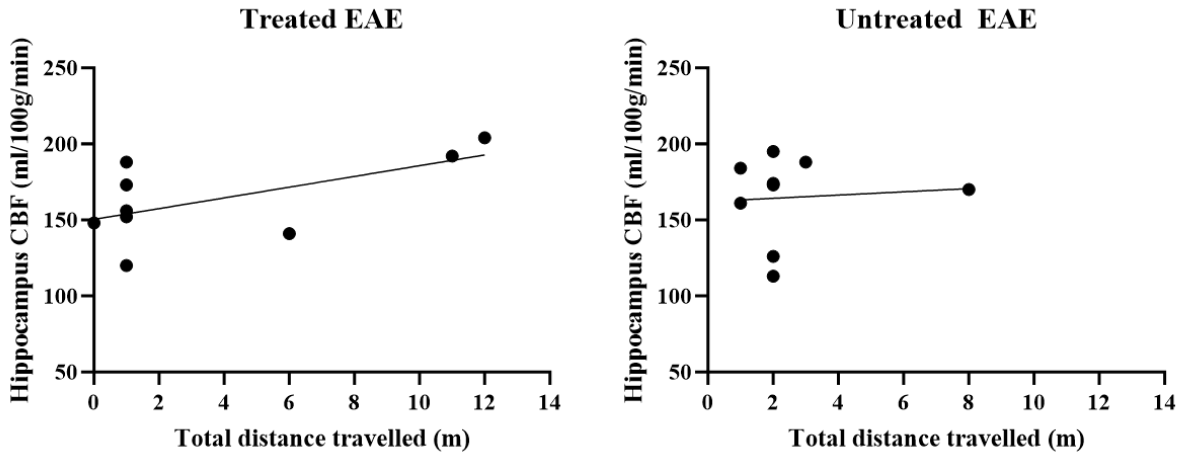

Figure 48: Correlation between EAE locomotion vs. CBF in the hippocampus after oxygen treatment.

Pearson's correlation performed between R_2 and CBF in the cortex (, r = .60; p = .08, and r = .08; p =.83) of treated and untreated mice respectively.*

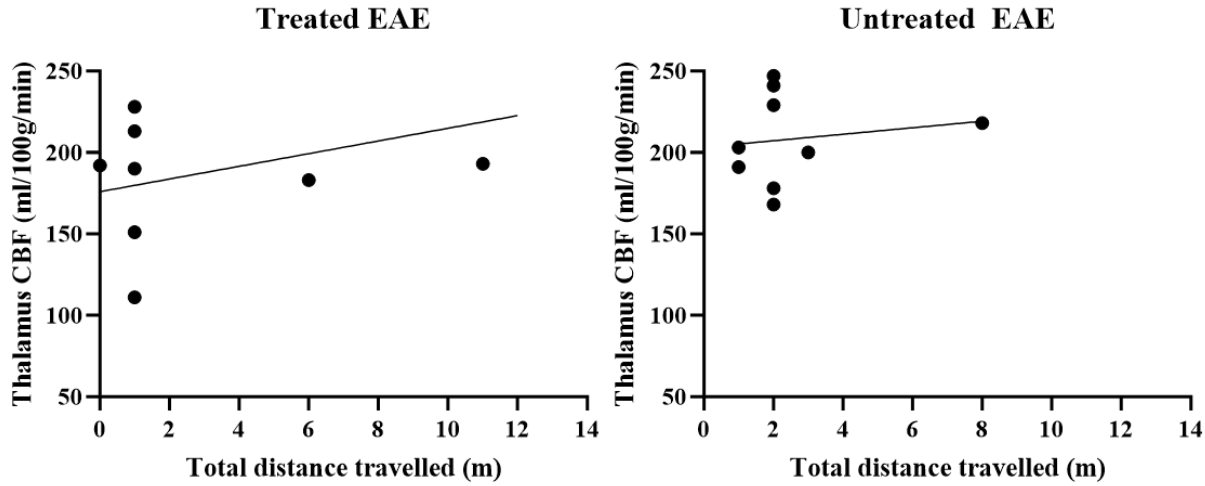

Figure 49: Correlation between EAE locomotion vs. CBF in the EAE thalamus after oxygen treatment.

Pearson's correlation performed between R_2 and CBF in the cortex; EAE treated, r = .43; p = .23, EAE untreated, r = .15; p = .69.*

4.3.4.5 Changes in R_2* measures are associated with poor locomotory activity in the EAE mice after oxygen treatment.

Similarly, the Pearson correlation coefficient was computed between R_2* MRI and the total distance travelled in the cortex, hippocampus, and thalamus of the EAE treated and untreated following oxygen treatment. Correlation analysis revealed an insignificant negative correlation between the two parameters in the cortex (r = -.39; p = .28; r = -27; p = .47) **(Figure 50)**, hippocampus (r = -.41; p = .26; r = -30; p = .42) **(Figure 51)**, and the thalamus (r = -.60; p = .08; r = -45; p = .22) **(Figure 52)**, treated and untreated respectively.

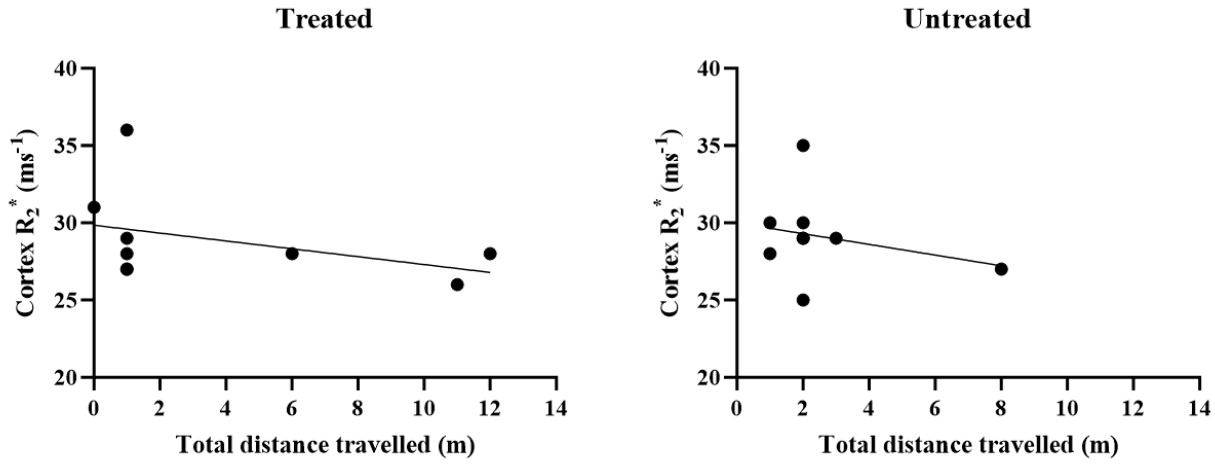

Figure 50: Correlation between EAE locomotion vs. R_2* in the cortex after oxygen treatment.

Pearson's correlation performed between locomotion and R_2 in the cortex (n = 9, r = -.39; p = .28; n = 9 r = -27; p = .47) of treated and untreated mice respectively.*

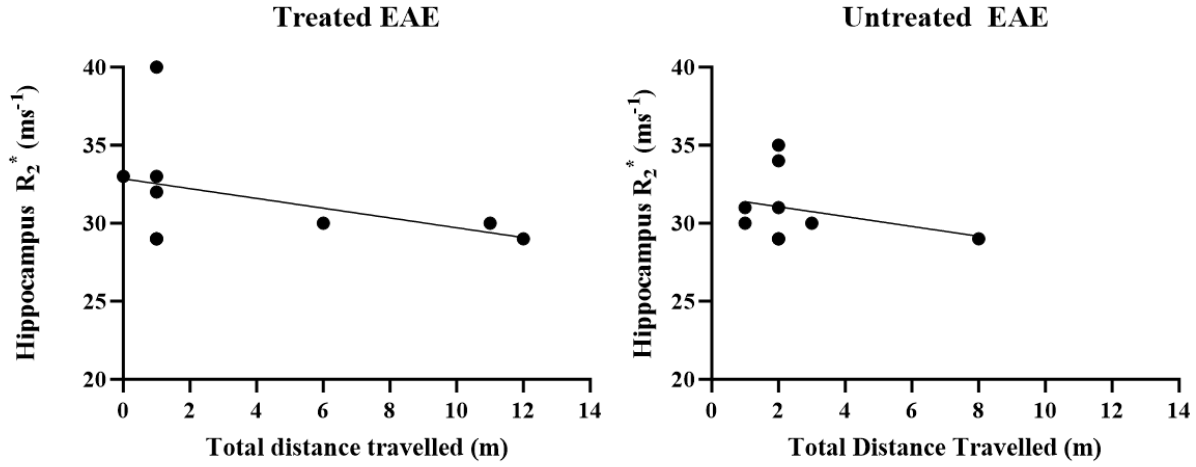

Figure 51: Correlation between EAE locomotion vs. R_2* in the hippocampus after oxygen treatment.

Pearson's correlation performed between locomotion and R_2 in the hippocampus (r = -.41; p = .26; nr = -30; p = .42) of treated and untreated mice respectively.*

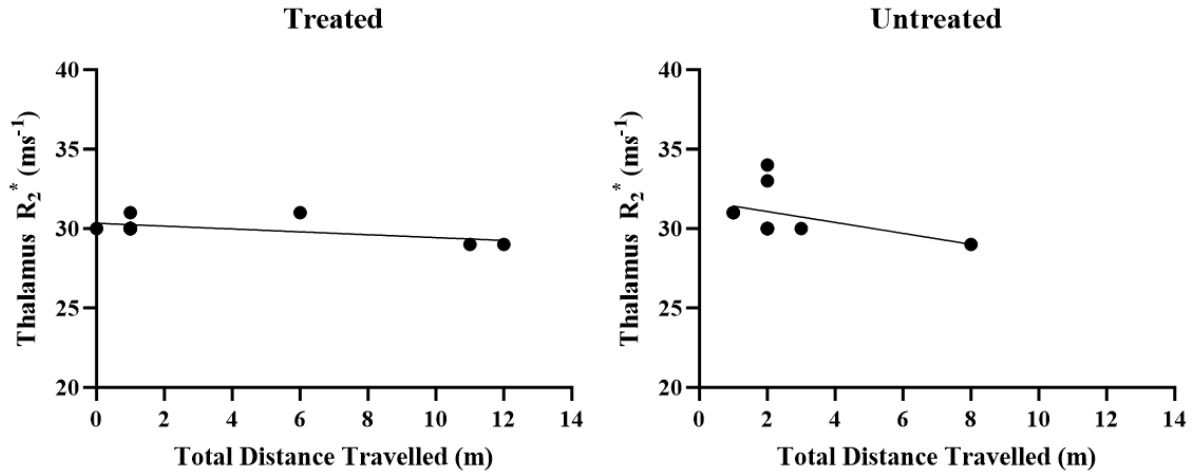

Figure 52: Correlation between EAE locomotion vs. R_2*in the thalamus after oxygen treatment.

Pearson's correlation was performed between locomotion and R_2 in the thalamus (r = -.60; p = .08; r = -45; p = .22) of treated and untreated mice respectively.*

4.3.4.5 Changes in R_2* measures are associated with an increase in clinical disease score in the EAE mice after oxygen treatment.

MRI R_2* was correlated with disease scores in ROIs after oxygen treatment. Conversely to the negative correlation found between R_2* and OF locomotion in the previous section above. Pearson correlation coefficient was computed in the cortex (treated, r = .38; p = .30, untreated r = .48; p = .18) (**Figure 53**), hippocampus (treated, r = 42; p = .25, r = .25; p = .51) (**Figure 54**) and thalamus (treated, r = .28; p = .45, untreated r = .71; p = .02) (**Figure 55**) between R_2* and clinical score. Notably, there was a significant positive correlation only in the EAE untreated thalamus in the sense that an increase in MRI R_2* was associated with an increase in EAE clinical score.

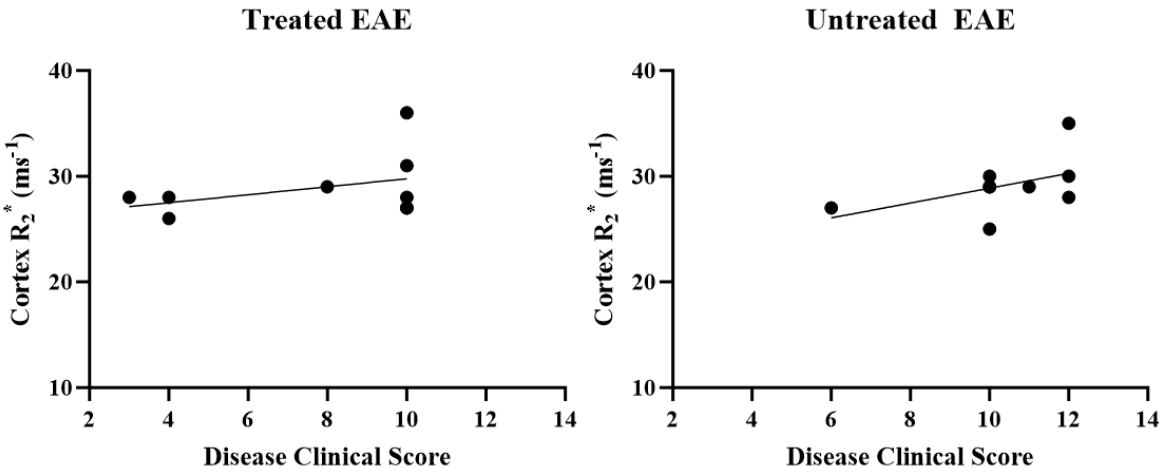

Figure 53: Correlation between EAE R_2* vs. clinical score in the cortex after oxygen treatment.

Pearson's correlation was performed between R_2 and clinical score in the cortex (, r = .38; p = .30, r = .48; p = .18) of treated and untreated mice respectively.*

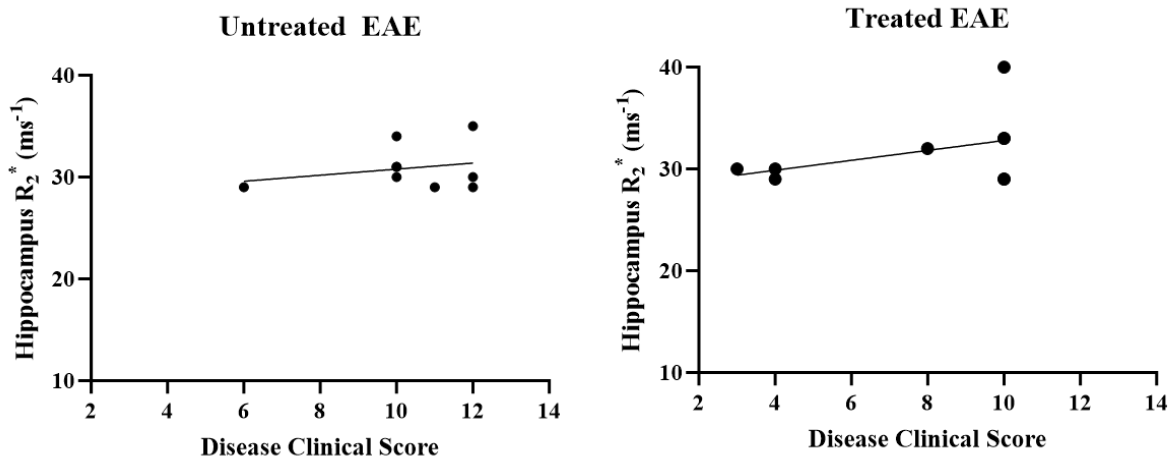

Figure 54: Correlation between EAE R_2* vs. clinical score in the hippocampus after oxygen treatment.

Pearson's correlation was performed between R_2 and clinical score in the hippocampus (r = 42; p = .25; r = .25; p = .51) of treated and untreated mice respectively.*

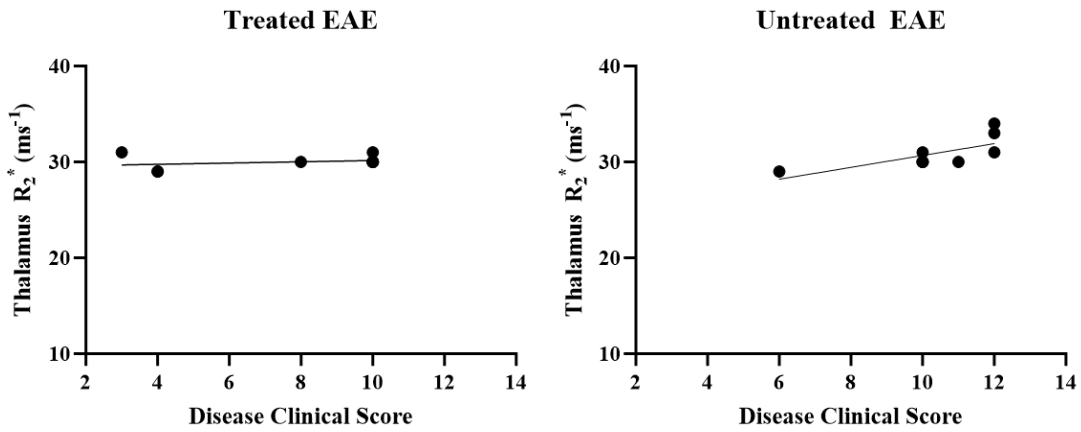

Figure 55: Correlation between EAE R_2* vs. clinical score in the thalamus after oxygen treatment.

Pearson's correlation was performed between R_2 and disease score in the thalamus (r = .28; p = .45, r = .71; p = .02) of treated and untreated mice respectively.*

4.1 Discussion and Conclusion

This chapter investigated the effect of NBOT oxygen treatment on disease clinical scores. We reported that MOG and CFA/PTX caused a reduction in CBF as discussed in **Chapter 2** and R_2* alterations in **Chapter 3.** Reduction in CBF and increased R_2* are consistent with the presence of hypoxia. The alteration in these two MRI parameters may have contributed to EAE clinical outcomes. Remarkably, after oxygen treatment, we found a significant difference between the disease clinical score of treated and untreated EAE which was promising. These results showed that the inflammation-hypoxia cycle contributed to the decreased motor function seen in the EAE mice, and a longer duration of oxygen treatment may be promising in the EAE disease condition observed and as proposed (Amatruda et al., 2023).

In contrast to the clinical disease score, there was no significant difference in the OF test for locomotion between each experimental group (treated and untreated) $p>0.05$. We found a remarkable decrease in locomotion in both the EAE groups (treated and untreated), compared to baseline locomotion.

In the correlation analysis, some observations were made about oxygen treatment. Most of the comparisons between treated and untreated EAE mice showed no significant correlation in the evaluated parameters. This suggests that the observed effects of oxygen treatment on EAE clinical disease score may not be strongly reflected in the compared parameters.

CHAPTER FIVE:
GENERAL DISCUSSION AND FUTURE DIRECTION

5.1 Summary

EAE has been described as an autoimmune disease with inflammation/hypoxia components (Yang & Dunn, 2019). However, the use of NBO treatment in this model is poorly understood. There has been limited work done using oxygen in EAE (Wilson & Fuchs, 2022). Few studies have raised a contradictory report regarding the use of oxygen administration in preclinical and clinical MS research, due to its plausible and non-plausible benefits (Fischer et al., 1983). Recently, a study found that HBO attenuated EAE, by modulation of T cell response (Chiou et al., 2021). It is unclear whether this benefit resulted from pressurized oxygen administration of HBO or just the oxygen effect irrespective of pressure. Contrarily, a clinical study revealed the non-beneficial effect of HBO (Bennett & Heard, 2010). However, a recent study in the spinal cord of EAE rats, revealed a beneficial effect of NBO in reducing neurological deficits (Amatruda et al., 2023).

The main objective of this thesis was to demonstrate the beneficial effect of 6 hours of NBO administration for 5 days duration in the EAE mouse model of MS. From the results, several observations were made on the effect of oxygen on CBF, R_2*, and EAE clinical disease score. Firstly, CBF in the EAE mice was lower than naïve mice. Post-induction EAE R_2* was higher in the untreated compared to pre-induction. The elevated MRI R_2* values in the EAE groups indicated an alteration in tissue oxygenation or other factors that may influence the magnetic susceptibility of the tissue being investigated. However, a significant difference was observed between the controls and the EAE.

Alteration in CBF has been proposed to relate to impaired cognition in people with MS (pwMS) (Berard et al., 2020; De Keyser et al., 2008). Reactive astrocytes have been reported to

play a role in cerebral hypoperfusion in MS (D'Haeseleer et al., 2013), and need more investigation. Our study revealed that hypoperfusion occurs in the EAE. Hypoperfusion could relate to hypoxia caused by neuroinflammation which needs to be determined. Hypoperfusion has been theorized to be one of the causes of MS lesions (Juurlink, 2013). This result is supported by hypoperfusion resulting from brain injury (Sankar et al., 2019). Studies have provided evidence of hypoxia lesions in MS (Lassmann, 2003; Lucchinetti et al., 2000).

Our study found little impact of NBO in improving blood flow and reducing hypoxia in EAE. CBF was reduced more in the EAE-treated group compared to the untreated group; however, this difference did not reach statistical significance. Further investigations are required to understand the underlying reasons for this outcome. A study provided insights into how mild hypoxic preconditioning, initiated before the onset of EAE, can reduce vascular breakdown and leukocyte infiltration, potentially influencing CBF. This approach could be relevant in improving CBF (in preclinical) EAE and (clinical settings) MS disease.

We explored the outcome of NBO on EAE disease score in **Chapter 4**. Previous studies found inflammation to be one of the leading causes of EAE sickness behavior (Pollak et al., 2003). Also, therapeutic benefits of NBO in EAE score have been proposed. The study reported reduced neurological deficit and HIF1 α expression in the spinal cord of EAE after oxygen treatment (Amatruda et al., 2023). In line with this, we found NBO beneficial on disease clinical score in the treated EAE mice compared to untreated (**Figure 38**) with a significant p-value of 0.04. However, both treated and untreated (room air) showed a remarkable decrease in locomotor activity in the OF in comparison with controls (CFA/PTX and naive) after induction and oxygen treatment; $p<0.05$.

Taken together, EAE and CFA/PTX-induced inflammation cause alteration in CBF and brain oxygenation. Hypoperfusion and poor brain oxygenation observed in both the treated and untreated EAE groups are associated with an increase in the EAE clinical score and significantly reduced locomotion in the EAE after MOG immunization as demonstrated in the correlation graphs (**Chapter 4**). Additional evidence was provided on the capabilities of MRI in monitoring treatment. Notably, low CBF and hypoxia could contribute significantly to various key aspects of MS, including neurological impairments, lesions, demyelination, and oligodendrocyte loss.

The NBO improved clinical score in the EAE. However, the OF test did not show an improvement. This is promising in that there was some improvement. It may be that NBO does not have a large impact on motor function, which these tests are more sensitive to. Interestingly, the most effective result on oxygen treatment with different concentrations in the EAE were done in the spinal cord (Amatruda et al., 2023; Esen et al., 2016; Tokarska et al., 2023). There could be reasons why treatment was not effective in the brain EAE. One possible reason is that EAE is ascending and most of the pathology is seen first in the spinal cord.

During inflammation, the BBB can become compromised, allowing immune cells and other substances to enter the brain and cause damage. This could affect the effectiveness of oxygen treatment in the brain, and restoration of the BBB has also been suggested as a promising approach for treating brain disorders (Sun et al., 2021).

A recent study from Dunn's laboratory, used an oxygen probe to investigate the effects of inflammation on the brain in a lipopolysaccharide inflammatory model. We found that there was an increased hypoxia and hyperoxia in the brain during inflammation (Shafqat et al., 2023). The hypoxia and hyperoxia switch have been confirmed in the EAE as well (Johnson et al., 2016). Administering oxygen without prior control of this change in vascular regulation could reduce the

statistical power if only a subset of the population (the hypoxic subset) would respond. Additionally, hypoxia and hyperoxia can have different effects on different tissues, and the optimal concentration and duration of oxygen treatment may vary depending on the specific condition being treated. Therefore, we suggest close monitoring of tissue oxygen levels and prophylactic administration of oxygen treatment after MOG immunization. We also recommend reducing the percentage of oxygen exposure as reported (Tokarska et al., 2023), and extending the duration of treatment to more hours or days. to

In summary, we found that administering oxygen without prior quantification of which animals were hypoxic showed small improvements.

5.2 Limitations

5.2.1 MRI

Despite the numerous applications of MRI in MS diagnosis, it is important to note its limitations. It is expensive and often requires complex processing. MRI is not a direct marker for tissue hypoxia (R_2*). However, it provides information based on the susceptibility of the tissue environment being imaged. Magnetic resonance imaging does not image the iron directly but instead images water protons as they diffuse near iron deposits in the tissue of interest (Wood et al., 2004; Wood & Ghugre, 2008). For example, MRI is sensitive to tissue iron and doesn't directly quantify the amount of oxygen in the cellular environment. However, we don't know the level of R_2* susceptibility and deoxyhemoglobin in the ROI investigated. It is unclear whether hypoxia is mild or severe, which calls for further investigation. On the other hand, QSM is sensitive to not just iron but myelin (Zhang et al., 2016). However, we were not able to disentangle these two elements (myelin and iron) from our data to know which is more susceptible to both MRI

measures. The sensitivity of QSM to magnetic field distortions of air-tissue (artifact) interfaces like the sinuses can impact the accuracy and reliability of measurements. Susceptibility differences in tissue inhomogeneities in the magnetic field can influence the accuracy of the result. Background noise in MRI can reduce the quality of susceptibility maps.

Furthermore, anesthesia could influence our MRI results, as that is a common way to get mice to remain in the coil before/during imaging. Even though we minimized this by imaging twice, at baseline and after treatment. No imaging was done before we administered oxygen to determine if mice experienced mild or severe changes in R_2* and QSM MRI measurements of hypoxia. However, we didn't determine the effect of anesthesia in mice, this needs more investigation on how this can influence MRI data.

5.2.3 Oxygen Treatment and EAE

We didn't confirm hypoxia/hyperoxia in mice either by other oxygen markers such as oxygen probe sensors or other techniques that could directly quantify blood oxygen saturation in the brain. We only regulated the amount of oxygen that goes into the chamber with an oxygen flow meter. However, we didn't measure the amount of oxygen in the chamber. One major limitation is that we don't know if this inhaled oxygen increased blood oxygen saturation. Poor treatment outcomes may be due to reduced arterial supply from an unknown mechanism obstructing blood flow to the brain restricted venous return, or a combination of both (Juurlink, 2013). EAE has found numerous applications in studying and uncovering MS pathogenesis. However, it doesn't model all aspects of human MS. Hence, it is important to choose this model having in mind specific research questions to explore. EAE models are of inflammatory origin while other models, model

demyelination in the brain and spinal cord (Mannie et al., 2009a). Therefore, EAE models are suited for immunological and neuroscience studies (Weissert, 2012).

However, the results of our study were no less interesting as they further contributed to a better understanding of the effect of oxygen treatment on MS pathophysiology. More findings are needed to explore the CBF and R_2* alteration in EAE and medications that can improve blood flow, which include drugs that dilate blood vessels (vasodilators) along with oxygen treatment in MS.

References

Adingupu, D. D., Soroush, A., Hansen, A., Twomey, R., & Dunn, J. F. (2023). Brain hypoxia, neurocognitive impairment, and quality of life in people post-COVID-19. *J Neurol*, 1-12. https://doi.org/10.1007/s00415-023-11767-2

Alenazy, M., Daneshgar Asl, S., Petrigna, L., Feka, K., Alvarez, E., Almuklass, A. M., & Enoka, R. M. (2021). Treatment with electrical stimulation of sensory nerves improves motor function and disability status in persons with multiple sclerosis: A pilot study. *J Electromyogr Kinesiol*, *61*, 102607. https://doi.org/10.1016/j.jelekin.2021.102607

Almuklass, A. M., Capobianco, R. A., Feeney, D. F., Alvarez, E., & Enoka, R. M. (2020). Sensory nerve stimulation causes an immediate improvement in motor function of persons with multiple sclerosis: A pilot study. *Mult Scler Relat Disord*, *38*, 101508. https://doi.org/10.1016/j.msard.2019.101508

Amann, M., Achtnichts, L., Hirsch, J. G., Naegelin, Y., Gregori, J., Weier, K., Thöni, A., Mueller-Lenke, N., Radue, E. W., Günther, M., Kappos, L., & Gass, A. (2012). 3D GRASE arterial spin labelling reveals an inverse correlation of cortical perfusion with the white matter lesion volume in MS. *Mult Scler*, *18*(11), 1570-1576. https://doi.org/10.1177/1352458512441984

Amatruda, M., Harris, K., Matis, A., Davies, A. L., McElroy, D., Clark, M., Linington, C., Desai, R., & Smith, K. J. (2023). Oxygen treatment reduces neurological deficits and demyelination in two animal models of multiple sclerosis. *Neuropathol Appl Neurobiol*, *49*(1), e12868. https://doi.org/10.1111/nan.12868

Angleys, H., Ostergaard, L., & Jespersen, S. N. (2015). The effects of capillary transit time heterogeneity (CTH) on brain oxygenation. *J Cereb Blood Flow Metab*, *35*(5), 806-817. https://doi.org/10.1038/jcbfm.2014.254

Bagnato, F., Hametner, S., Boyd, E., Endmayr, V., Shi, Y., Ikonomidou, V., Chen, G., Pawate, S., Lassmann, H., Smith, S., & Welch, E. B. (2018). Untangling the R2* contrast in multiple sclerosis: A combined MRI-histology study at 7.0 Tesla. *PLoS One*, *13*(3), e0193839. https://doi.org/10.1371/journal.pone.0193839

Bahrani, A. A., Powell, D. K., Yu, G., Johnson, E. S., Jicha, G. A., & Smith, C. D. (2017). White Matter Hyperintensity Associations with Cerebral Blood Flow in Elderly Subjects Stratified by Cerebrovascular Risk. *J Stroke Cerebrovasc Dis*, *26*(4), 779-786. https://doi.org/10.1016/j.jstrokecerebrovasdis.2016.10.017

Barboza, A. G., Carnero Contentti, E., Curbelo, M. C., Halfon, M. J., Rojas, J. I., Silva, B. A., Sinay, V., Tizio, S., Ysrraelit, M. C., & Alonso, R. (2021). Radiologically isolated syndrome: from biological bases to practical management. *Neurol Sci*, *42*(4), 1335-1344. https://doi.org/10.1007/s10072-021-05069-6

Barnes, M. P., Bates, D., Cartlidge, N. E., French, J. M., & Shaw, D. A. (1987). Hyperbaric oxygen and multiple sclerosis: final results of a placebo-controlled, double-blind trial. *J Neurol Neurosurg Psychiatry*, *50*(11), 1402-1406. https://doi.org/10.1136/jnnp.50.11.1402

Bennett, M., & Heard, R. (2004). Hyperbaric oxygen therapy for multiple sclerosis. *Cochrane Database Syst Rev*, *2004*(1), CD003057. https://doi.org/10.1002/14651858.CD003057.pub2

Bennett, M., & Heard, R. (2010). Hyperbaric oxygen therapy for multiple sclerosis. *CNS Neurosci Ther*, *16*(2), 115-124. https://doi.org/10.1111/j.1755-5949.2009.00129.x

Berard, J. A., Fang, Z., Walker, L. A. S., Lindsay-Brown, A., Osman, L., Cameron, I., Cruce, R., Cron, G. O., Freedman, M. S., & Smith, A. M. (2020). Imaging cognitive fatigability in multiple sclerosis: objective quantification of cerebral blood flow during a task of sustained attention using ASL perfusion fMRI. *Brain Imaging Behav*, *14*(6), 2417-2428. https://doi.org/10.1007/s11682-019-00192-7

Binnewijzend, M. A., Benedictus, M. R., Kuijer, J. P., van der Flier, W. M., Teunissen, C. E., Prins, N. D., Wattjes, M. P., van Berckel, B. N., Scheltens, P., & Barkhof, F. (2016). Cerebral perfusion in the predementia stages of Alzheimer's disease. *Eur Radiol*, *26*(2), 506-514. https://doi.org/10.1007/s00330-015-3834-9

Blaimer, M., Breuer, F., Mueller, M., Heidemann, R. M., Griswold, M. A., & Jakob, P. M. (2004). SMASH, SENSE, PILS, GRAPPA: how to choose the optimal method. *Top Magn Reson Imaging*, *15*(4), 223-236. https://doi.org/10.1097/01.rmr.0000136558.09801.dd

Blockley, N. P., & Stone, A. J. (2016). Improving the specificity of R2' to the deoxyhaemoglobin content of brain tissue: Prospective correction of macroscopic magnetic field gradients. *Neuroimage*, *135*, 253-260. https://doi.org/10.1016/j.neuroimage.2016.04.013

Bokkers, R. P., Hernandez, D. A., Merino, J. G., Mirasol, R. V., van Osch, M. J., Hendrikse, J., Warach, S., Latour, L. L., & National Institutes of Health Stroke Natural History, I. (2012). Whole-brain arterial spin labeling perfusion MRI in patients with acute stroke. *Stroke*, *43*(5), 1290-1294. https://doi.org/10.1161/STROKEAHA.110.589234

Candelario-Jalil, E., Dijkhuizen, R. M., & Magnus, T. (2022). Neuroinflammation, Stroke, Blood-Brain Barrier Dysfunction, and Imaging Modalities. *Stroke*, *53*(5), 1473-1486. https://doi.org/10.1161/STROKEAHA.122.036946

Chen, L., Cai, C., Yang, T., Lin, J., Cai, S., Zhang, J., & Chen, Z. (2017). Changes in brain iron concentration after exposure to high-altitude hypoxia measured by quantitative susceptibility mapping. *Neuroimage*, *147*, 488-499. https://doi.org/10.1016/j.neuroimage.2016.12.033

Chen, L., Deng, H., Cui, H., Fang, J., Zuo, Z., Deng, J., Li, Y., Wang, X., & Zhao, L. (2018). Inflammatory responses and inflammation-associated diseases in organs. *Oncotarget*, *9*(6), 7204-7218. https://doi.org/10.18632/oncotarget.23208

Chiou, H. C., Huang, S. H., Hung, C. H., Tsai, S. M., Kuo, H. R., Huang, Y. R., Wang, J. W., Chen, S. C., Kuo, C. H., Wu, D. C., Huang, S. K., Hsu, S. H., & Lin, M. H. (2021). Hyperbaric Oxygen Therapy Alleviates the Autoimmune Encephalomyelitis via the Reduction of IL-17a and GM-Csf Production of Autoreactive T Cells as Well as Boosting the Immunosuppressive IL-10 in the Central Nervous System Tissue Lesions. *Biomedicines*, *9*(8). https://doi.org/10.3390/biomedicines9080943

Choi, H. Y., Ko, E. S., Han, B. K., Kim, E. J., Kim, S. M., Lim, Y., & Kim, R. B. (2016). Prognostic Significance of Transverse Relaxation Rate (R2*) in Blood Oxygenation Level-Dependent Magnetic Resonance Imaging in Patients with Invasive Breast Cancer. *PLoS One*, *11*(7), e0158500. https://doi.org/10.1371/journal.pone.0158500

Chou, I. J., Kuo, C. F., Tanasescu, R., Tench, C. R., Tiley, C. G., Constantinescu, C. S., & Whitehouse, W. P. (2020). Comorbidity in multiple sclerosis: its temporal relationships with disease onset and dose effect on mortality. *Eur J Neurol*, *27*(1), 105-112. https://doi.org/10.1111/ene.14040

Collij, L. E., Heeman, F., Kuijer, J. P., Ossenkoppele, R., Benedictus, M. R., Moller, C., Verfaillie, S. C., Sanz-Arigita, E. J., van Berckel, B. N., van der Flier, W. M., Scheltens, P., Barkhof, F., & Wink, A. M. (2016). Application of Machine Learning to Arterial Spin Labeling in Mild Cognitive Impairment and Alzheimer Disease. *Radiology*, *281*(3), 865-875. https://doi.org/10.1148/radiol.2016152703

Constantinescu, C. S., Farooqi, N., O'Brien, K., & Gran, B. (2011). Experimental autoimmune encephalomyelitis (EAE) as a model for multiple sclerosis (MS). *British Journal of Pharmacology*, *164*(4), 1079-1106. https://doi.org/10.1111/j.1476-5381.2011.01302.x

Constantinescu, C. S., Farooqi, N., O'Brien, K., & Gran, B. (2011). Experimental autoimmune encephalomyelitis (EAE) as a model for multiple sclerosis (MS). *Br J Pharmacol*, *164*(4), 1079-1106. https://doi.org/10.1111/j.1476-5381.2011.01302.x

Criste, G., Trapp, B., & Dutta, R. (2014). Axonal loss in multiple sclerosis: causes and mechanisms. *Handb Clin Neurol*, *122*, 101-113. https://doi.org/10.1016/B978-0-444-52001-2.00005-4

Crystal, G. J., & Pagel, P. S. (2020). The Physiology of Oxygen Transport by the Cardiovascular System: Evolution of Knowledge. *J Cardiothorac Vasc Anesth*, *34*(5), 1142-1151. https://doi.org/10.1053/j.jvca.2019.12.029

D'Haeseleer, M., Beelen, R., Fierens, Y., Cambron, M., Vanbinst, A. M., Verborgh, C., Demey, J., & De Keyser, J. (2013). Cerebral hypoperfusion in multiple sclerosis is reversible and mediated by endothelin-1. *Proc Natl Acad Sci U S A*, *110*(14), 5654-5658. https://doi.org/10.1073/pnas.1222560110

De Keyser, J., Steen, C., Mostert, J. P., & Koch, M. W. (2008). Hypoperfusion of the cerebral white matter in multiple sclerosis: possible mechanisms and pathophysiological significance. *J Cereb Blood Flow Metab*, *28*(10), 1645-1651. https://doi.org/10.1038/jcbfm.2008.72

de la Pena, M. J., Pena, I. C., Garcia, P. G., Gavilan, M. L., Malpica, N., Rubio, M., Gonzalez, R. A., & de Vega, V. M. (2019). Early perfusion changes in multiple sclerosis patients as assessed by MRI using arterial spin labeling. *Acta Radiol Open*, *8*(12), 2058460119894214. https://doi.org/10.1177/2058460119894214

Deistung, A., Schweser, F., & Reichenbach, J. R. (2017). Overview of quantitative susceptibility mapping. *NMR Biomed*, *30*(4). https://doi.org/10.1002/nbm.3569

Desai, R. A., Davies, A. L., Del Rossi, N., Tachrount, M., Dyson, A., Gustavson, B., Kaynezhad, P., Mackenzie, L., van der Putten, M. A., McElroy, D., Schiza, D., Linington, C., Singer, M., Harvey, A. R., Tachtsidis, I., Golay, X., & Smith, K. J. (2020). Nimodipine Reduces Dysfunction and Demyelination in Models of Multiple Sclerosis. *Ann Neurol*, *88*(1), 123-136. https://doi.org/10.1002/ana.25749

Desai, R. A., & Smith, K. J. (2017). Experimental autoimmune encephalomyelitis from a tissue energy perspective. *F1000Res*, *6*, 1973. https://doi.org/10.12688/f1000research.11839.1

Ding, J., Zhou, D., Liu, C., Pan, L., Ya, J., Ding, Y., Ji, X., & Meng, R. (2019). Normobaric oxygen: a novel approach for treating chronic cerebral circulation insufficiency. *Clin Interv Aging*, *14*, 565-570. https://doi.org/10.2147/CIA.S190984

Dixon, S. J., Lemberg, K. M., Lamprecht, M. R., Skouta, R., Zaitsev, E. M., Gleason, C. E., Patel, D. N., Bauer, A. J., Cantley, A. M., Yang, W. S., Morrison, B., 3rd, & Stockwell, B. R. (2012). Ferroptosis: an iron-dependent form of nonapoptotic cell death. *Cell*, *149*(5), 1060-1072. https://doi.org/10.1016/j.cell.2012.03.042

Dore-Duffy, P., Wencel, M., Katyshev, V., & Cleary, K. (2011). Chronic mild hypoxia ameliorates chronic inflammatory activity in myelin oligodendrocyte glycoprotein (MOG) peptide induced experimental autoimmune encephalomyelitis (EAE). *Adv Exp Med Biol*, *701*, 165-173. https://doi.org/10.1007/978-1-4419-7756-4_23

Doshi, A., & Chataway, J. (2016). Multiple sclerosis, a treatable disease. *Clin Med (Lond)*, *16*(Suppl 6), s53-s59. https://doi.org/10.7861/clinmedicine.16-6-s53

Dunn, J. O., Mythen, M., & Grocott, M. (2016). Physiology of oxygen transport. *BJA Education*, *16*(10), 341-348. https://doi.org/10.1093/bjaed/mkw012

Duong, T. Q. (2011). MRI in experimental stroke. *Methods Mol Biol*, *711*, 473-485. https://doi.org/10.1007/978-1-61737-992-5_24

Esen, N., Katyshev, V., Serkin, Z., Katysheva, S., & Dore-Duffy, P. (2016). Endogenous adaptation to low oxygen modulates T-cell regulatory pathways in EAE. *J Neuroinflammation*, *13*, 13. https://doi.org/10.1186/s12974-015-0407-4

Fan, J. L., Brassard, P., Rickards, C. A., Nogueira, R. C., Nasr, N., McBryde, F. D., Fisher, J. P., & Tzeng, Y. C. (2022). Integrative cerebral blood flow regulation in ischemic stroke. *J Cereb Blood Flow Metab*, *42*(3), 387-403. https://doi.org/10.1177/0271678X211032029

Filippi, M., Bar-Or, A., Piehl, F., Preziosa, P., Solari, A., Vukusic, S., & Rocca, M. A. (2018). Multiple sclerosis. *Nature Reviews Disease Primers*, *4*(1). https://doi.org/10.1038/s41572-018-0041-4

Fischer, B. H., Marks, M., & Reich, T. (1983). Hyperbaric-oxygen treatment of multiple sclerosis. A randomized, placebo-controlled, double-blind study. *N Engl J Med*, *308*(4), 181-186. https://doi.org/10.1056/NEJM198301273080402

Fujita, N., Shinohara, M., Tanaka, H., Yutani, K., Nakamura, H., & Murase, K. (2003). Quantitative mapping of cerebral deoxyhemoglobin content using MR imaging. *Neuroimage*, *20*(4), 2071-2083. https://doi.org/10.1016/j.neuroimage.2003.06.002

Garcia, D. M., Duhamel, G., & Alsop, D. C. (2005). Efficiency of inversion pulses for background suppressed arterial spin labeling. *Magn Reson Med*, *54*(2), 366-372. https://doi.org/10.1002/mrm.20556

Ghadery, C., Pirpamer, L., Hofer, E., Langkammer, C., Petrovic, K., Loitfelder, M., Schwingenschuh, P., Seiler, S., Duering, M., Jouvent, E., Schmidt, H., Fazekas, F., Mangin, J. F., Chabriat, H., Dichgans, M., Ropele, S., & Schmidt, R. (2015). R2* mapping for brain iron: associations with cognition in normal aging. *Neurobiol Aging*, *36*(2), 925-932. https://doi.org/10.1016/j.neurobiolaging.2014.09.013

Gillen, K. M., Mubarak, M., Park, C., Ponath, G., Zhang, S., Dimov, A., Levine-Ritterman, M., Toro, S., Huang, W., Amici, S., Kaunzner, U. W., Gauthier, S. A., Guerau-de-Arellano, M., Wang, Y., Nguyen, T. D., & Pitt, D. (2021). QSM is an imaging biomarker for chronic glial

activation in multiple sclerosis lesions. *Ann Clin Transl Neurol*, *8*(4), 877-886. https://doi.org/10.1002/acn3.51338
Gilmour, H., Ramage-Morin, P. L., & Wong, S. L. (2018). Multiple sclerosis: Prevalence and impact. *Health Rep*, *29*(1), 3-8.
Godoy, D. A., Rubiano, A. M., Paranhos, J., Robba, C., & Lazaridis, C. (2023). Avoiding brain hypoxia in severe traumatic brain injury in settings with limited resources - A pathophysiological guide. *J Crit Care*, *75*, 154260. https://doi.org/10.1016/j.jcrc.2023.154260
Haacke, E. M., Bernitsas, E., Subramanian, K., Utriainen, D., Palutla, V. K., Yerramsetty, K., Kumar, P., Sethi, S. K., Chen, Y., Latif, Z., Jella, P., Gharabaghi, S., Wang, Y., Zhang, X., Comley, R. A., Beaver, J., & Luo, Y. (2021). A Comparison of Magnetic Resonance Imaging Methods to Assess Multiple Sclerosis Lesions: Implications for Patient Characterization and Clinical Trial Design. *Diagnostics (Basel)*, *12*(1). https://doi.org/10.3390/diagnostics12010077
Habler, O. P., & Messmer, K. F. (1997). The physiology of oxygen transport. *Transfus Sci*, *18*(3), 425-435. https://doi.org/10.1016/S0955-3886(97)00041-6
Hadanny, A., & Efrati, S. (2015). Oxygen--a limiting factor for brain recovery. *Crit Care*, *19*(1), 307. https://doi.org/10.1186/s13054-015-1034-2
Hashem, M., Shafqat, Q., Wu, Y., Rho, J. M., & Dunn, J. F. (2022). Abnormal oxidative metabolism in the cuprizone mouse model of demyelination: An in vivo NIRS-MRI study. *Neuroimage*, *250*, 118935. https://doi.org/10.1016/j.neuroimage.2022.118935
Hashem, M., Zhang, Q., Wu, Y., Johnson, T. W., & Dunn, J. F. (2020). Using a multimodal near-infrared spectroscopy and MRI to quantify gray matter metabolic rate for oxygen: A hypothermia validation study. *Neuroimage*, *206*, 116315. https://doi.org/10.1016/j.neuroimage.2019.116315
Hernandez-Garcia, L., Lahiri, A., & Schollenberger, J. (2019). Recent progress in ASL. *Neuroimage*, *187*, 3-16. https://doi.org/10.1016/j.neuroimage.2017.12.095
Hohlfeld, R., & Wekerle, H. (2001). Immunological update on multiple sclerosis. *Curr Opin Neurol*, *14*(3), 299-304. https://doi.org/10.1097/00019052-200106000-00006
Hostenbach, S., Raeymaekers, H., Van Schuerbeek, P., Vanbinst, A. M., Cools, W., De Keyser, J., & D'Haeseleer, M. (2020). The Role of Cerebral Hypoperfusion in Multiple Sclerosis (ROCHIMS) Trial in Multiple Sclerosis: Insights From Negative Results. *Front Neurol*, *11*, 674. https://doi.org/10.3389/fneur.2020.00674
Huang, C. J., Zhou, X., Yuan, X., Zhang, W., Li, M. X., You, M. Z., Zhu, X. Q., & Sun, Z. W. (2021). Contribution of Inflammation and Hypoperfusion to White Matter Hyperintensities-Related Cognitive Impairment. *Front Neurol*, *12*, 786840. https://doi.org/10.3389/fneur.2021.786840
Jacoby, I. J. (2001). Hyperbaric oxygen therapy, multiple sclerosis, and unapproved indications: taking a stand. *Undersea Hyperb Med*, *28*(3), 113-115. https://www.ncbi.nlm.nih.gov/pubmed/12067145
Jakimovski, D., Bergsland, N., Dwyer, M. G., Choedun, K., Marr, K., Weinstock-Guttman, B., & Zivadinov, R. (2022). Cerebral blood flow dependency on systemic arterial circulation in progressive multiple sclerosis. *European Radiology*, *32*(9), 6468-6479. https://doi.org/10.1007/s00330-022-08731-5

Jakimovski, D., Bergsland, N., Dwyer, M. G., Traversone, J., Hagemeier, J., Fuchs, T. A., Ramasamy, D. P., Weinstock-Guttman, B., Benedict, R. H. B., & Zivadinov, R. (2020). Cortical and Deep Gray Matter Perfusion Associations With Physical and Cognitive Performance in Multiple Sclerosis Patients. *Front Neurol*, *11*, 700. https://doi.org/10.3389/fneur.2020.00700

Jespersen, S. N., & Ostergaard, L. (2012). The roles of cerebral blood flow, capillary transit time heterogeneity, and oxygen tension in brain oxygenation and metabolism. *J Cereb Blood Flow Metab*, *32*(2), 264-277. https://doi.org/10.1038/jcbfm.2011.153

Johnson, T. W., Wu, Y., Nathoo, N., Rogers, J. A., Wee Yong, V., & Dunn, J. F. (2016). Gray Matter Hypoxia in the Brain of the Experimental Autoimmune Encephalomyelitis Model of Multiple Sclerosis. *PLoS One*, *11*(12), e0167196. https://doi.org/10.1371/journal.pone.0167196

Juurlink, B. H. (2013). The evidence for hypoperfusion as a factor in multiple sclerosis lesion development. *Mult Scler Int*, *2013*, 598093. https://doi.org/10.1155/2013/598093

Kauppinen, T. M., Suh, S. W., Genain, C. P., & Swanson, R. A. (2005). Poly(ADP-ribose) polymerase-1 activation in a primate model of multiple sclerosis. *J Neurosci Res*, *81*(2), 190-198. https://doi.org/10.1002/jnr.20525

Klineova, S., & Lublin, F. D. (2018). Clinical Course of Multiple Sclerosis. *Cold Spring Harb Perspect Med*, *8*(9). https://doi.org/10.1101/cshperspect.a028928

Kossorotoff, M. (2012). Cognitive decline in moyamoya: influence of chronic cerebral hypoxia, history of stroke, or comorbid conditions? *Dev Med Child Neurol*, *54*(1), 5-6. https://doi.org/10.1111/j.1469-8749.2011.04159.x

Kraeuter, A. K., Guest, P. C., & Sarnyai, Z. (2019). The Open Field Test for Measuring Locomotor Activity and Anxiety-Like Behavior. *Methods Mol Biol*, *1916*, 99-103. https://doi.org/10.1007/978-1-4939-8994-2_9

Kramer, J., Bruck, W., Zipp, F., Cerina, M., Groppa, S., & Meuth, S. G. (2019). Imaging in mice and men: Pathophysiological insights into multiple sclerosis from conventional and advanced MRI techniques. *Prog Neurobiol*, *182*, 101663. https://doi.org/10.1016/j.pneurobio.2019.101663

Lambrou, G. N., Kopferschmitt, J., Jaeger, A., & Brini, A. (1987). [Slowly reversible central scotoma: iatrogenic effect of hyperbaric oxygenation in the treatment of multiple sclerosis]. *J Fr Ophtalmol*, *10*(1), 51-59. https://www.ncbi.nlm.nih.gov/pubmed/3598057 (Le scotome central lentement reversible: un effet iatrogene de l'oxygenotherapie hyperbare dans le traitement de la sclerose en plaques.)

Langkammer, C., Schweser, F., Krebs, N., Deistung, A., Goessler, W., Scheurer, E., Sommer, K., Reishofer, G., Yen, K., Fazekas, F., Ropele, S., & Reichenbach, J. R. (2012). Quantitative susceptibility mapping (QSM) as a means to measure brain iron? A post mortem validation study. *Neuroimage*, *62*(3), 1593-1599. https://doi.org/10.1016/j.neuroimage.2012.05.049

Larsen, E. H., Hellsten, Y., & Wojtaszewski, J. (2011). Homage to August Krogh celebrating the 90th anniversary of his Nobel prize in Physiology or Medicine. *Acta Physiol (Oxf)*, *202*(3), 211-212. https://doi.org/10.1111/j.1748-1716.2011.02325.x

Lassmann, H. (2003). Hypoxia-like tissue injury as a component of multiple sclerosis lesions. *Journal of the Neurological Sciences*, *206*(2), 187-191. https://doi.org/10.1016/s0022-510x(02)00421-5

Lassmann, H. (2013). Pathology and disease mechanisms in different stages of multiple sclerosis. *J Neurol Sci*, *333*(1-2), 1-4. https://doi.org/10.1016/j.jns.2013.05.010

Liu, C., Wang, C., Zhang, H., Gao, X., Xiao, P., Yu, M., Wang, X., Wang, X., & Wang, X. (2023). Hypoxia ischemia results in blood brain barrier damage via AKT/GSK-3beta/CREB pathway in neonatal rats. *Brain Res*, *1822*, 148640. https://doi.org/10.1016/j.brainres.2023.148640

Liu, W., Yeh, P. H., Nathan, D. E., Song, C., Wu, H., Bonavia, G. H., Ollinger, J., & Riedy, G. (2019). Assessment of Brain Venous Structure in Military Traumatic Brain Injury Patients using Susceptibility Weighted Imaging and Quantitative Susceptibility Mapping. *J Neurotrauma*, *36*(14), 2213-2221. https://doi.org/10.1089/neu.2018.5970

Lublin, F. D. (2014). New multiple sclerosis phenotypic classification. *Eur Neurol*, *72 Suppl 1*, 1-5. https://doi.org/10.1159/000367614

Lublin, F. D., Baier, M., & Cutter, G. (2003). Effect of relapses on development of residual deficit in multiple sclerosis. *Neurology*, *61*(11), 1528-1532. https://doi.org/10.1212/01.wnl.0000096175.39831.21

Lucchinetti, C., Bruck, W., Parisi, J., Scheithauer, B., Rodriguez, M., & Lassmann, H. (2000). Heterogeneity of multiple sclerosis lesions: implications for the pathogenesis of demyelination. *Ann Neurol*, *47*(6), 707-717. https://doi.org/10.1002/1531-8249(200006)47:6<707::aid-ana3>3.0.co;2-q

Maillard, P., Clanet, M., Bourdiol, A. M., & Arne, J. L. (1987). [Effects of hyperbaric oxygen therapy on the visual evoked potentials of patients with multiple sclerosis]. *Bull Soc Ophtalmol Fr*, *87*(1), 43-45. https://www.ncbi.nlm.nih.gov/pubmed/3301038 (Effets de l'oxygenotherapie hyperbarre sur les P.E.V. de malades porteurs de sclerose en plaque.)

Mannara, F., Valente, T., Saura, J., Graus, F., Saiz, A., & Moreno, B. (2012). Passive experimental autoimmune encephalomyelitis in C57BL/6 with MOG: evidence of involvement of B cells. *PLoS One*, *7*(12), e52361. https://doi.org/10.1371/journal.pone.0052361

Mannie, M., Swanborg, R. H., & Stepaniak, J. A. (2009a). Experimental autoimmune encephalomyelitis in the rat. *Curr Protoc Immunol*, *Chapter 15*, 15 12 11-15 12 15. https://doi.org/10.1002/0471142735.im1502s85

Mannie, M., Swanborg, R. H., & Stepaniak, J. A. (2009b). Experimental autoimmune encephalomyelitis in the rat. *Curr Protoc Immunol*, *Chapter 15*, Unit 15.12. https://doi.org/10.1002/0471142735.im1502s85

Manole, M. D., Kochanek, P. M., Bayir, H., Alexander, H., Dezfulian, C., Fink, E. L., Bell, M. J., & Clark, R. S. (2014). Brain tissue oxygen monitoring identifies cortical hypoxia and thalamic hyperoxia after experimental cardiac arrest in rats. *Pediatr Res*, *75*(2), 295-301. https://doi.org/10.1038/pr.2013.220

Mansilla, M. J., Presas-Rodriguez, S., Teniente-Serra, A., Gonzalez-Larreategui, I., Quirant-Sanchez, B., Fondelli, F., Djedovic, N., Iwaszkiewicz-Grzes, D., Chwojnicki, K., Miljkovic, D., Trzonkowski, P., Ramo-Tello, C., & Martinez-Caceres, E. M. (2021). Paving the way towards an effective treatment for multiple sclerosis: advances in cell therapy. *Cell Mol Immunol*, *18*(6), 1353-1374. https://doi.org/10.1038/s41423-020-00618-z

Marrie, R. A., Elliott, L., Marriott, J., Cossoy, M., Blanchard, J., Leung, S., & Yu, N. (2015). Effect of comorbidity on mortality in multiple sclerosis. *Neurology*, *85*(3), 240-247. https://doi.org/10.1212/WNL.0000000000001718

Masaldan, S., Bush, A. I., Devos, D., Rolland, A. S., & Moreau, C. (2019). Striking while the iron is hot: Iron metabolism and ferroptosis in neurodegeneration. *Free Radic Biol Med*, *133*, 221-233. https://doi.org/10.1016/j.freeradbiomed.2018.09.033

McFarland, H. F., & Martin, R. (2007). Multiple sclerosis: a complicated picture of autoimmunity. *Nat Immunol*, *8*(9), 913-919. https://doi.org/10.1038/ni1507

McGinley, M. P., Goldschmidt, C. H., & Rae-Grant, A. D. (2021). Diagnosis and Treatment of Multiple Sclerosis. *JAMA*, *325*(8), 765. https://doi.org/10.1001/jama.2020.26858

Miller, D. H., Grossman, R. I., Reingold, S. C., & McFarland, H. F. (1998). The role of magnetic resonance techniques in understanding and managing multiple sclerosis. *Brain*, *121 (Pt 1)*, 3-24. https://doi.org/10.1093/brain/121.1.3

Mizuno, T. M., Padhi, A., Fineberg, N., Fineberg, N. A., Padhi, A., Bloch, M. H., Leckman, J. F., Padhi, A., Fineberg, N. A., Bevins, R. A., Palmatier, M. I., Viollet, C., Epelbaum, J., Hoyer, D., Bitter, I., Wadenberg, M.-L. G., Bari, A., Belzung, C., Odlaug, B. L., . . . Thompson, M. R. (2010). Open-Field Test. In (pp. 923-926). Springer Berlin Heidelberg. https://doi.org/10.1007/978-3-540-68706-1_158

Moore, L., Eggleton, P., Smerdon, G., Newcombe, J., Holley, J. E., Gutowski, N. J., & Smallwood, M. (2020). Engagement of people with multiple sclerosis to enhance research into the physiological effect of hyperbaric oxygen therapy. *Mult Scler Relat Disord*, *43*, 102084. https://doi.org/10.1016/j.msard.2020.102084

Mowry, E. M., Pesic, M., Grimes, B., Deen, S. R., Bacchetti, P., & Waubant, E. (2009). Clinical predictors of early second event in patients with clinically isolated syndrome. *J Neurol*, *256*(7), 1061-1066. https://doi.org/10.1007/s00415-009-5063-0

Muthuraju, S., Pati, S., Rafiqul, M., Abdullah, J. M., & Jaafar, H. (2013). Effect of normabaric hyperoxia treatment on neuronal damage following fluid percussion injury in the striatum of mice: a morphological approach. *J Biosci*, *38*(1), 93-103. https://doi.org/10.1007/s12038-012-9290-7

Naito, S., Namerow, N., Mickey, M. R., & Terasaki, P. I. (1972). Multiple sclerosis: association with HL-A3. *Tissue Antigens*, *2*(1), 1-4. https://doi.org/10.1111/j.1399-0039.1972.tb00111.x

Nathoo, N., Agrawal, S., Wu, Y., Haylock-Jacobs, S., Yong, V. W., Foniok, T., Barnes, S., Obenaus, A., & Dunn, J. F. (2013). Susceptibility-weighted imaging in the experimental autoimmune encephalomyelitis model of multiple sclerosis indicates elevated deoxyhemoglobin, iron deposition and demyelination. *Mult Scler*, *19*(6), 721-731. https://doi.org/10.1177/1352458512460602

Nathoo, N., Rogers, J. A., Yong, V. W., & Dunn, J. F. (2015). Detecting deoxyhemoglobin in spinal cord vasculature of the experimental autoimmune encephalomyelitis mouse model of multiple sclerosis using susceptibility MRI and hyperoxygenation. *PLoS One*, *10*(5), e0127033. https://doi.org/10.1371/journal.pone.0127033

Nathoo, N., Yong, V. W., & Dunn, J. F. (2014). Using magnetic resonance imaging in animal models to guide drug development in multiple sclerosis. *Mult Scler*, *20*(1), 3-11. https://doi.org/10.1177/1352458513512709

Nessler, S., Boretius, S., Stadelmann, C., Bittner, A., Merkler, D., Hartung, H. P., Michaelis, T., Bruck, W., Frahm, J., Sommer, N., & Hemmer, B. (2007). Early MRI changes in a mouse model of multiple sclerosis are predictive of severe inflammatory tissue damage. *Brain*, *130*(Pt 8), 2186-2198. https://doi.org/10.1093/brain/awm105

Noseworthy, J. H., Lucchinetti, C., Rodriguez, M., & Weinshenker, B. G. (2000). Multiple sclerosis. *N Engl J Med*, *343*(13), 938-952. https://doi.org/10.1056/NEJM200009283431307

O'Riordan, J. I., Thompson, A. J., Kingsley, D. P., MacManus, D. G., Kendall, B. E., Rudge, P., McDonald, W. I., & Miller, D. H. (1998). The prognostic value of brain MRI in clinically isolated syndromes of the CNS. A 10-year follow-up. *Brain*, *121 (Pt 3)*, 495-503. https://doi.org/10.1093/brain/121.3.495

Olsson, T., Barcellos, L. F., & Alfredsson, L. (2017). Interactions between genetic, lifestyle and environmental risk factors for multiple sclerosis. *Nat Rev Neurol*, *13*(1), 25-36. https://doi.org/10.1038/nrneurol.2016.187

Ortega, M. A., Fraile-Martinez, O., García-Montero, C., Callejón-Peláez, E., Sáez, M. A., Álvarez-Mon, M. A., García-Honduvilla, N., Monserrat, J., Álvarez-Mon, M., Bujan, J., & Canals, M. L. (2021). A General Overview on the Hyperbaric Oxygen Therapy: Applications, Mechanisms and Translational Opportunities. *Medicina*, *57*(9), 864. https://doi.org/10.3390/medicina57090864

Ostergaard, L. (2020). Blood flow, capillary transit times, and tissue oxygenation: the centennial of capillary recruitment. *J Appl Physiol (1985)*, *129*(6), 1413-1421. https://doi.org/10.1152/japplphysiol.00537.2020

Ota, M., Sato, N., Nakata, Y., Ito, K., Kamiya, K., Maikusa, N., Ogawa, M., Okamoto, T., Obu, S., Noda, T., Araki, M., Yamamura, T., & Kunugi, H. (2013). Abnormalities of cerebral blood flow in multiple sclerosis: a pseudocontinuous arterial spin labeling MRI study. *Magn Reson Imaging*, *31*(6), 990-995. https://doi.org/10.1016/j.mri.2013.03.016

Perrins, D. J., & James, P. B. (2002). Hyperbaric oxygen therapy and multiple sclerosis. *Undersea Hyperb Med*, *29*(4), 236-238; discussion 238-241. https://www.ncbi.nlm.nih.gov/pubmed/12797664

Pike, S. C., Welsh, N., Linzey, M., & Gilli, F. (2022). Theiler's virus-induced demyelinating disease as an infectious model of progressive multiple sclerosis. *Front Mol Neurosci*, *15*, 1019799. https://doi.org/10.3389/fnmol.2022.1019799

Pollak, Y., Ovadia, H., Orion, E., Weidenfeld, J., & Yirmiya, R. (2003). The EAE-associated behavioral syndrome: I. Temporal correlation with inflammatory mediators. *J Neuroimmunol*, *137*(1-2), 94-99. https://doi.org/10.1016/s0165-5728(03)00075-4

Prinz, C., Starke, L., Millward, J. M., Fillmer, A., Delgado, P. R., Waiczies, H., Pohlmann, A., Rothe, M., Nazare, M., Paul, F., Niendorf, T., & Waiczies, S. (2021). In vivo detection of teriflunomide-derived fluorine signal during neuroinflammation using fluorine MR spectroscopy. *Theranostics*, *11*(6), 2490-2504. https://doi.org/10.7150/thno.47130

Prut, L., & Belzung, C. (2003). The open field as a paradigm to measure the effects of drugs on anxiety-like behaviors: a review. *Eur J Pharmacol*, *463*(1-3), 3-33. https://doi.org/10.1016/s0014-2999(03)01272-x

Rae-Grant, A. D., Eckert, N. J., Bartz, S., & Reed, J. F. (1999). Sensory symptoms of multiple sclerosis: a hidden reservoir of morbidity. *Mult Scler*, *5*(3), 179-183. https://doi.org/10.1177/135245859900500307

Rahmanzadeh, R., Weigel, M., Lu, P. J., Melie-Garcia, L., Nguyen, T. D., Cagol, A., La Rosa, F., Barakovic, M., Lutti, A., Wang, Y., Bach Cuadra, M., Radue, E. W., Gaetano, L., Kappos, L., Kuhle, J., Magon, S., & Granziera, C. (2022). A comparative assessment of myelin-sensitive measures in multiple sclerosis patients and healthy subjects. *Neuroimage Clin*, *36*, 103177. https://doi.org/10.1016/j.nicl.2022.103177

Ramagopalan, S. V., Dyment, D. A., Guimond, C., Yee, I. M., Ebers, G. C., & Sadovnick, A. D. (2010). No effect of parental age on risk of multiple sclerosis: a population-based study. *Neuroepidemiology*, *34*(2), 106-109. https://doi.org/10.1159/000268822

Ravanfar, P., Loi, S. M., Syeda, W. T., Van Rheenen, T. E., Bush, A. I., Desmond, P., Cropley, V. L., Lane, D. J. R., Opazo, C. M., Moffat, B. A., Velakoulis, D., & Pantelis, C. (2021). Systematic Review: Quantitative Susceptibility Mapping (QSM) of Brain Iron Profile in Neurodegenerative Diseases. *Front Neurosci*, *15*, 618435. https://doi.org/10.3389/fnins.2021.618435

Renkin, E. M. (1985). B. W. Zweifach Award lecture. Regulation of the microcirculation. *Microvasc Res*, *30*(3), 251-263. https://doi.org/10.1016/0026-2862(85)90057-3

Rhodes, C. E., Denault, D., & Varacallo, M. (2023). Physiology, Oxygen Transport. In *StatPearls*. https://www.ncbi.nlm.nih.gov/pubmed/30855920

Robinson, A. P., Harp, C. T., Noronha, A., & Miller, S. D. (2014). The experimental autoimmune encephalomyelitis (EAE) model of MS: utility for understanding disease pathophysiology and treatment. *Handb Clin Neurol*, *122*, 173-189. https://doi.org/10.1016/B978-0-444-52001-2.00008-X

Rocca, M. A., Barkhof, F., De Luca, J., Frisen, J., Geurts, J. J. G., Hulst, H. E., Sastre-Garriga, J., Filippi, M., & Group, M. S. (2018). The hippocampus in multiple sclerosis. *Lancet Neurol*, *17*(10), 918-926. https://doi.org/10.1016/S1474-4422(18)30309-0

Rovaris, M., Confavreux, C., Furlan, R., Kappos, L., Comi, G., & Filippi, M. (2006). Secondary progressive multiple sclerosis: current knowledge and future challenges. *Lancet Neurol*, *5*(4), 343-354. https://doi.org/10.1016/S1474-4422(06)70410-0

Sadovnick, A. D., & Baird, P. A. (1988). The familial nature of multiple sclerosis: age-corrected empiric recurrence risks for children and siblings of patients. *Neurology*, *38*(6), 990-991. https://doi.org/10.1212/wnl.38.6.990

Sankar, S. B., Pybus, A. F., Liew, A., Sanders, B., Shah, K. J., Wood, L. B., & Buckley, E. M. (2019). Low cerebral blood flow is a non-invasive biomarker of neuroinflammation after repetitive mild traumatic brain injury. *Neurobiol Dis*, *124*, 544-554. https://doi.org/10.1016/j.nbd.2018.12.018

Sen, M. K., Almuslehi, M. S. M., Shortland, P. J., Coorssen, J. R., & Mahns, D. A. (2020). Revisiting the Pathoetiology of Multiple Sclerosis: Has the Tail Been Wagging the Mouse? *Front Immunol*, *11*, 572186. https://doi.org/10.3389/fimmu.2020.572186

Silverman, A., & Petersen, N. H. (2023). Physiology, Cerebral Autoregulation. In *StatPearls*. https://www.ncbi.nlm.nih.gov/pubmed/31985976

Sisco, N. J., Borazanci, A., Dortch, R., & Stokes, A. M. (2021). Investigating the relationship between multi-scale perfusion and white matter microstructural integrity in patients

with relapsing-remitting MS. *Mult Scler J Exp Transl Clin*, *7*(3), 20552173211037002. https://doi.org/10.1177/20552173211037002

Soman, S., Dai, W., Dong, L., Hitchner, E., Lee, K., Baughman, B. D., Holdsworth, S. J., Massaband, P., Bhat, J. V., Moseley, M. E., Rosen, A., Zhou, W., & Zaharchuk, G. (2020). Identifying cardiovascular risk factors that impact cerebrovascular reactivity: An ASL MRI study. *J Magn Reson Imaging*, *51*(3), 734-747. https://doi.org/10.1002/jmri.26862

Ssali, T., Anazodo, U. C., Thiessen, J. D., Prato, F. S., & St Lawrence, K. (2018). A Noninvasive Method for Quantifying Cerebral Blood Flow by Hybrid PET/MRI. *J Nucl Med*, *59*(8), 1329-1334. https://doi.org/10.2967/jnumed.117.203414

Stewart, C. R., Stringer, M. S., Shi, Y., Thrippleton, M. J., & Wardlaw, J. M. (2021). Associations Between White Matter Hyperintensity Burden, Cerebral Blood Flow and Transit Time in Small Vessel Disease: An Updated Meta-Analysis. *Front Neurol*, *12*, 647848. https://doi.org/10.3389/fneur.2021.647848

Stromnes, I. M., & Goverman, J. M. (2006a). Active induction of experimental allergic encephalomyelitis. *Nat Protoc*, *1*(4), 1810-1819. https://doi.org/10.1038/nprot.2006.285

Stromnes, I. M., & Goverman, J. M. (2006b). Passive induction of experimental allergic encephalomyelitis. *Nat Protoc*, *1*(4), 1952-1960. https://doi.org/10.1038/nprot.2006.284

Stys, P. K. (2010). Multiple sclerosis: autoimmune disease or autoimmune reaction? *Can J Neurol Sci*, *37 Suppl 2*, S16-23. https://doi.org/10.1017/s0317167100022393

Stys, P. K., Zamponi, G. W., van Minnen, J., & Geurts, J. J. (2012). Will the real multiple sclerosis please stand up? *Nat Rev Neurosci*, *13*(7), 507-514. https://doi.org/10.1038/nrn3275

Sumowski, J. F., Benedict, R., Enzinger, C., Filippi, M., Geurts, J. J., Hamalainen, P., Hulst, H., Inglese, M., Leavitt, V. M., Rocca, M. A., Rosti-Otajarvi, E. M., & Rao, S. (2018). Cognition in multiple sclerosis: State of the field and priorities for the future. *Neurology*, *90*(6), 278-288. https://doi.org/10.1212/WNL.0000000000004977

Sun, Z., Gao, C., Gao, D., Sun, R., Li, W., Wang, F., Wang, Y., Cao, H., Zhou, G., Zhang, J., & Shang, J. (2021). Reduction in pericyte coverage leads to blood-brain barrier dysfunction via endothelial transcytosis following chronic cerebral hypoperfusion. *Fluids Barriers CNS*, *18*(1), 21. https://doi.org/10.1186/s12987-021-00255-2

t Hart, B. A., Vogels, J., Bauer, J., Brok, H. P., & Blezer, E. (2004). Non-invasive measurement of brain damage in a primate model of multiple sclerosis. *Trends Mol Med*, *10*(2), 85-91. https://doi.org/10.1016/j.molmed.2003.12.008

Taylor, R. C., & Webster, C. J. (1987). Methodological problems in evaluating hyperbaric treatment of multiple sclerosis. A case study. *Neuroepidemiology*, *6*(1-2), 77-84. https://doi.org/10.1159/000110101

Thompson, A. J., Banwell, B. L., Barkhof, F., Carroll, W. M., Coetzee, T., Comi, G., Correale, J., Fazekas, F., Filippi, M., Freedman, M. S., Fujihara, K., Galetta, S. L., Hartung, H. P., Kappos, L., Lublin, F. D., Marrie, R. A., Miller, A. E., Miller, D. H., Montalban, X., . . . Cohen, J. A. (2018). Diagnosis of multiple sclerosis: 2017 revisions of the McDonald criteria. *Lancet Neurol*, *17*(2), 162-173. https://doi.org/10.1016/S1474-4422(17)30470-2

Tietz, S. M., & Engelhardt, B. (2019). Visualizing Impairment of the Endothelial and Glial Barriers of the Neurovascular Unit during Experimental Autoimmune Encephalomyelitis In Vivo. *J Vis Exp*(145). https://doi.org/10.3791/59249

Titus, H. E., Chen, Y., Podojil, J. R., Robinson, A. P., Balabanov, R., Popko, B., & Miller, S. D. (2020). Pre-clinical and Clinical Implications of "Inside-Out" vs. "Outside-In" Paradigms in Multiple Sclerosis Etiopathogenesis. *Front Cell Neurosci*, *14*, 599717. https://doi.org/10.3389/fncel.2020.599717

Tokarska, N., Naniong, J. M. A., Johnston, J. M., Salapa, H. E., Muir, G. D., Levin, M. C., Popescu, B. F., & Verge, V. M. K. (2023). Acute intermittent hypoxia alters disease course and promotes CNS repair including resolution of inflammation and remyelination in the experimental autoimmune encephalomyelitis model of MS. *Glia*, *71*(8), 2045-2066. https://doi.org/10.1002/glia.24381

Tolias, C. M., Kumaria, A., & Bullock, M. R. (2009). Hyperoxia and traumatic brain injury. *J Neurosurg*, *110*(3), 607-609; author reply 609-611. https://doi.org/10.3171/JNS.2009.110.3.0607a

Tortora, D., Mattei, P. A., Navarra, R., Panara, V., Salomone, R., Rossi, A., Detre, J. A., & Caulo, M. (2017). Prematurity and brain perfusion: Arterial spin labeling MRI. *Neuroimage Clin*, *15*, 401-407. https://doi.org/10.1016/j.nicl.2017.05.023

van Beek, A. H., Claassen, J. A., Rikkert, M. G., & Jansen, R. W. (2008). Cerebral autoregulation: an overview of current concepts and methodology with special focus on the elderly. *J Cereb Blood Flow Metab*, *28*(6), 1071-1085. https://doi.org/10.1038/jcbfm.2008.13

Wang, C., Foxley, S., Ansorge, O., Bangerter-Christensen, S., Chiew, M., Leonte, A., Menke, R. A., Mollink, J., Pallebage-Gamarallage, M., Turner, M. R., Miller, K. L., & Tendler, B. C. (2020). Methods for quantitative susceptibility and R2* mapping in whole post-mortem brains at 7T applied to amyotrophic lateral sclerosis. *Neuroimage*, *222*, 117216. https://doi.org/10.1016/j.neuroimage.2020.117216

Wang, Y., & Liu, T. (2015). Quantitative susceptibility mapping (QSM): Decoding MRI data for a tissue magnetic biomarker. *Magn Reson Med*, *73*(1), 82-101. https://doi.org/10.1002/mrm.25358

Wardlaw, J. M., Valdes Hernandez, M. C., & Munoz-Maniega, S. (2015). What are white matter hyperintensities made of? Relevance to vascular cognitive impairment. *J Am Heart Assoc*, *4*(6), 001140. https://doi.org/10.1161/JAHA.114.001140

Waubant, E., Lucas, R., Mowry, E., Graves, J., Olsson, T., Alfredsson, L., & Langer-Gould, A. (2019). Environmental and genetic risk factors for MS: an integrated review. *Ann Clin Transl Neurol*, *6*(9), 1905-1922. https://doi.org/10.1002/acn3.50862

Weiner, H. L. (2008). A shift from adaptive to innate immunity: a potential mechanism of disease progression in multiple sclerosis. *J Neurol*, *255 Suppl 1*, 3-11. https://doi.org/10.1007/s00415-008-1002-8

Weissert, R. (2012). Experimental Autoimmune Encephalomyelitis. In *Experimental Autoimmune Encephalomyelitis - Models, Disease Biology and Experimental Therapy*. https://doi.org/10.5772/29792

Willer, C. J., Dyment, D. A., Risch, N. J., Sadovnick, A. D., Ebers, G. C., & Canadian Collaborative Study, G. (2003). Twin concordance and sibling recurrence rates in multiple sclerosis.

Proc Natl Acad Sci U S A, *100*(22), 12877-12882. https://doi.org/10.1073/pnas.1932604100

Wilson, J. R., & Fuchs, P. N. (2022). Oxygen Therapy for the Treatment of Experimental Autoimmune Encephalomyelitis. *Sports and Exercise Medicine – Open Journal*, *8*(1), 15-20. https://doi.org/10.17140/semoj-8-186

Wood, J. C., Enriquez, C., Ghugre, N., Tyzka, J. M., Carson, S., Nelson, M. D., & Coates, T. D. (2005). MRI R2 and R2* mapping accurately estimates hepatic iron concentration in transfusion-dependent thalassemia and sickle cell disease patients. *Blood*, *106*(4), 1460-1465. https://doi.org/10.1182/blood-2004-10-3982

Wood, J. C., Fassler, J. D., & Meade, T. (2004). Mimicking liver iron overload using liposomal ferritin preparations. *Magn Reson Med*, *51*(3), 607-611. https://doi.org/10.1002/mrm.10735

Wood, J. C., & Ghugre, N. (2008). Magnetic resonance imaging assessment of excess iron in thalassemia, sickle cell disease and other iron overload diseases. *Hemoglobin*, *32*(1-2), 85-96. https://doi.org/10.1080/03630260701699912

Wood, J. C., Zhang, P., Rienhoff, H., Abi-Saab, W., & Neufeld, E. (2014). R2 and R2* are equally effective in evaluating chronic response to iron chelation. *American Journal of Hematology*, *89*(5), 505-508. https://doi.org/10.1002/ajh.23673

Yang, R., & Dunn, J. F. (2019). Multiple sclerosis disease progression: Contributions from a hypoxia-inflammation cycle. *Mult Scler*, *25*(13), 1715-1718. https://doi.org/10.1177/1352458518791683

Zhang, Y., Gauthier, S. A., Gupta, A., Chen, W., Comunale, J., Chiang, G. C., Zhou, D., Askin, G., Zhu, W., Pitt, D., & Wang, Y. (2016). Quantitative Susceptibility Mapping and R2* Measured Changes during White Matter Lesion Development in Multiple Sclerosis: Myelin Breakdown, Myelin Debris Degradation and Removal, and Iron Accumulation. *AJNR Am J Neuroradiol*, *37*(9), 1629-1635. https://doi.org/10.3174/ajnr.A4825